SCATTERING OF LASER RADIATION FROM THE OCEAN SURFACE

Kamala S. Krishnan, et al

Stanford Research Institute

Prepared for:

Office of Naval Research
Advanced Research Projects Agency

October 1973

UNCLASSIFIED

SECURITY CLASSIFICATION OF THIS PAGE (When Data Entered)

REPORT DOCUMENTATION PAGE		READ INSTRUCTIONS BEFORE COMPLETING FORM
1. REPORT NUMBER	2. GOVT ACCESSION NO.	3. RECIPIENT'S CATALOG NUMBER AD-772 122
4. TITLE (and Subtitle) SCATTERING OF LASER RADIATION FROM THE OCEAN SURFACE		5. TYPE OF REPORT & PERIOD COVERED Midpoint Technical Report 23 April to 31 August 1973
		6. PERFORMING ORG. REPORT NUMBER SRI Project ISE 2618
7. AUTHOR(s) Kamala S. Krishnan Norman A. Peppers		8. CONTRACT OR GRANT NUMBER(s) N00014-73-C-0445
9. PERFORMING ORGANIZATION NAME AND ADDRESS Stanford Research Institute 333 Ravenswood Avenue Menlo Park, California		10. PROGRAM ELEMENT, PROJECT, TASK AREA & WORK UNIT NUMBERS ARPA Order No. 2185 Amend. 3 Program Code No. 3E20
11. CONTROLLING OFFICE NAME AND ADDRESS Defense Advanced Research Projects Agency 1400 Wilson Boulevard Arlington, Virginia 22217		12. REPORT DATE October 1973 / 13. NO OF PAGES ~~111~~ 105
14. MONITORING AGENCY NAME & ADDRESS (if diff. from Controlling Office) Office of Naval Research, Department of the Navy 800 North Quincy Street Arlington, Virginia 22217		15. SECURITY CLASS. (of this report) Unclassified / 15a. DECLASSIFICATION/DOWNGRADING SCHEDULE

16. DISTRIBUTION STATEMENT (of this report)

Distribution of this document is unlimited.

17. DISTRIBUTION STATEMENT (of the abstract entered in Block 20, if different from report)

18 SUPPLEMENTARY NOTES The views and conclusions contained in this document are those of the authors and should not be interpreted as necessarily representing the official policies, either expressed or implied, of the Advanced Research Projects Agency or the U.S. Government.

19. KEY WORDS (Continue on reverse side if necessary and identify by block number)

Wave statistics
Capillary waves
Diffuse backscatter
Temporal coherence
Power spectrum of ocean waves
Wave slope spectrum
Laser speckle
Remote monitoring

20. ABSTRACT (Continue on reverse side if necessary and identify by block number)

There has been considerable controversy in the optical literature concerning the theory of "speckle patterns" resulting from the diffuse scattering of coherent light and the information about the scatterer obtainable from the speckle pattern. The resolution and reconciliation of these theoretical differences and the application of the theory to scattering from the ocean surface were the objectives of this study.

A brief historical review of some previous theoretical work and a description of the apparent discrepancies which have now been reconciled are given. A more complete

DD FORM 1 JAN 73 1473

EDITION OF 1 NOV 65 IS OBSOLETE

UNCLASSIFIED

SECURITY CLASSIFICATION OF THIS PAGE (When Data Entered)

19. KEY WORDS (Continued)

20 ABSTRACT (Continued)

treatment of these topics, has been presented in an earlier report. Therein it was shown that the surface characteristics of the scatterer can be related to the ensemble average power spectral density of the scattered radiation. However, since the measurement of the power spectral density is difficult and a more practical observable is the ensemble average scattered intensity distribution, an analytical expression for the latter is developed from basic principles and related to some average properties of the scattering surface.

By assuming a Gaussian distribution for the surface elevation, the average intensity distribution is related to the second-order statistics of the surface. It is shown that this relationship is similar to that obtained in the case of high-frequency microwave backscatter. The mathematical parameters related to the covariance function of the surface are shown to lead to the mean square elevation, slope, and curvature of the surface.

In order to apply these theoretical results to the ocean surface, a wind-dependent two-dimensional power spectral density for the ocean surface elevation (based on a large amount of empirical data) is assumed. The surface covariance function is determined and it is shown that the average scattered intensity distribution is determined solely by the slope statistics of the surface for the case of optical illumination. An analytical expression for the scattered intensity distribution is derived for a general geometry. The detailed distribution is calculated for the backscatter geometry and its behavior is examined as a function of wind speed. It is found that as the wind increases, the backscattered intensity is reduced and spread over larger angles. It is inferred that the downwind slopes increase only slightly faster than the crosswind slopes.

A reasonable parametrized form is assumed for the spectral shape of a perturbation. A parametric study was performed and it was found that the effect of the perturbation on the intensity distribution is most pronounced in the capillary region. The energy content of the perturbation required to see significant changes is on the same order as the energy content of the natural spectrum in the capillary region and insignificant compared to the total energy of the waves. The viscous cutoff does not have much effect on the intensity. The angular shape and the orientation of the perturbation affect mainly the symmetry of the intensity pattern with respect to the wind direction. Some mathematical details regarding the surface covariance function are presented in the two appendices.

Midpoint Technical Report

Covering the Period 23 April to 31 August 1973

SCATTERING OF LASER RADIATION FROM THE OCEAN SURFACE

By: K. S. KRISHNAN N. A. PEPPERS

Prepared for:

OFFICE OF NAVAL RESEARCH
DEPARTMENT OF THE NAVY
800 NORTH QUINCY STREET
ARLINGTON, VIRGINIA 22217

Attention: DIRECTOR
UNDERSEA PROGRAMS
NAVAL APPLICATIONS AND ANALYSIS DIVISION

Sponsored by:

DEFENSE ADVANCED RESEARCH
PROJECTS AGENCY
DARPA Order No. 2185, Amendment 3
Contract N00014-73-C-0445
Contract Amount: $62,961.00

Program Code No. 3E20
23 April 1973 - 22 December 1973
SRI Project ISE 2618

Approved by:

EARLE D. JONES, *Director*
Electronics and Bioengineering Laboratory

BONNAR T. COX, *Executive Director*
Information Sciences and Engineering Division

SUMMARY

There has been considerable controversy in the optical literature concerning the theory of "speckle patterns" resulting from the diffuse scattering of coherent light and the information about the scatterer obtainable from the speckle pattern. The resolution and reconciliation of these theoretical differences and the application of the theory to scattering from the ocean surface were the objectives of this study.

A brief historical review of some previous theoretical work and a description of the apparent discrepancies which have now been reconciled are given (Section II). A more complete treatment of these topics, has been presented in an earlier report. Therein it was shown that the surface characteristics of the scatterer can be related to the ensemble average power spectral density of the scattered radiation. However, since the measurement of the power spectral density is difficult and a more practical observable is the ensemble average scattered intensity distribution, an analytical expression for the latter is developed from basic principles and related to some average properties of the scattering surface (Section II-C).

By assuming a Gaussian distribution for the surface elevation, the average intensity distribution is related to the second-order statistics of the surface. It is shown that this relationship is similar to that obtained in the case of high-frequency microwave backscatter (Section II-D). The mathematical parameters related to the covariance function of the surface are shown to lead to the mean square elevation, slope, and curvature of the surface (Section II-E).

In order to apply these theoretical results to the ocean surface, a wind-dependent two-dimensional power spectral density for the ocean surface elevation (based on a large amount of empirical data) is assumed (Section III-B). The surface covariance function is determined and it is shown that the average scattered intensity distribution is determined solely by the slope statistics of the surface for the case of optical illumination (Section III-C). An analytical expression for the scattered intensity distribution is derived for a general geometry. The detailed distribution is calculated for the backscatter geometry and its behavior is examined as a function of wind speed (Section III-D). It is found that as the wind increases, the backscattered intensity is reduced and spread over larger angles. It is inferred that the downwind slopes increase only slightly faster than the crosswind slopes.

A reasonable parametrized form is assumed for the spectral shape of a perturbation (Section III-E). A parametric study was performed and it was found that the effect of the perturbation on the intensity distribution is most pronounced in the capillary region. The energy content of the perturbation required to see significant changes is on the same order as the energy content of the natural spectrum in the capillary region and insignificant compared to the total energy of the waves. The viscous cutoff does not have much effect on the intensity. The angular shape and the orientation of the perturbation affect mainly the symmetry of the intensity pattern with respect to the wind direction (Section III-F). Some mathematical details regarding the surface covariance function are presented in the two appendices.

CONTENTS

ILLUSTRATIONS

TABLES

FOREWORD

This technical report covers the activity during the period 23 April 1973 through 31 August 1973. The principal investigator, Dr. Kamala S. Krishnan, was responsible for the research activity under SRI Project ISE 2618. The technical direction of the program was provided by Dr. Richard F. Hoglund, Chief, Advanced Concepts Division, Strategic Technology Office, Defense Advanced Research Projects Agency, Arlington, Virgina.

The research program discussed in this report was supported by Defense Advanced Research Projects Agency of the Department of Defense and was monitored by the Office of Naval Research under Contract No. N00014-73-C-0445.

ACKNOWLEDGMENTS

The authors acknowledge with gratitude the contributions of Dr. Joseph W. Goodman of Stanford University, who was a consultant during the course of the work. The authors are indebted to Drs. Richard C. Honey and Harold Guthart of SRI for many valuable suggestions. The discussions with Drs. Richard F. Hoglund of ARPA and Philip Selwyn of IDA, Washington, D.C., were of considerable value during the program.

I INTRODUCTION

A. Motivation

Scalar diffraction theory has been applied with considerable quantitative success to numerous microwave and optical problems for which spatial coherence is preserved. However, confidence in theoretical predictions is not high for problems involving scattering from rough surfaces. Often, analytical solutions to scattering problems can be obtained only by invoking simplifying approximations that are known to be rather crude. Moreover, experimental testing of scattering theory is difficult because of the dual problem of not only obtaining a surface for which the theoretical approximations are valid but also specifying the statistical characteristics of the surface. In the case of optical scattering from a rather calm sea, the usual gentle slope and gentle curvature assumptions seem to be reasonably well justified and one would expect quantitative predictions to be moderately accurate provided the Fresnel and Fraunhofer conditions--as well as the small angle conditions--are met. Although experimental testing of these predictions cannot yet be accomplished because there is no technique now available to measure the statistical characteristics of the sea with the accuracy and resolution that is required, such techniques exist in principle, and when available in hardware form could provide the means to perform this important test. The recognition of these facts, and the desire to develop practical methods of utilizing the powerful coherent light sources that are now available for measuring ocean wave statistics, have motivated this research.

B. Outline of the Report

There has been considerable controversy in the optical literature concerning the theory of "speckle patterns" from diffusely scattered coherent light. A brief historical review of some previous theoretical work is included here as well as a description of some of the apparent discrepancies which now have been reconciled. This is done in order to demonstrate the foundation of the theoretical approach taken here.

Starting with the Huygens-Fresnel principle, a principle familiar to optical physicists, we develop an analytical expression for the observed ensemble average scattered intensity, and relate it to statistical characteristics of the scattering surface. This result is compared with the microwave backscatter cross section that is derived from the Helmholtz integral formalism and leads to a new physical interpretation of the backscatter cross section. We place a physical interpretation on the important mathematical parameters that determine the scattered intensity.

Finally, because sufficiently accurate experimental data describing the statistical characteristics of the ocean are not available, we use a recently reported[4] theoretical description of the ocean-wave-height power spectral density to make numerical calculations of the scattered intensity distribution as a function of wind speed and direction. In addition, we calculate the scattered intensity distribution when certain assumed perturbations having arbitrary angular orientation with respect to the wind direction are superimposed.

---

*References are listed at the end of this report.

C. Definition of the Problem

The problem that is addressed in this report can be outlined with the help of Figure 1. A plane monochromatic wave, $E_i(u,v,z)$, is incident on the surface of the ocean at the origin of the coordinate system, (u,v,z). The mean plane of the ocean surface is taken to be the (u,v) plane, and the angles A and B define the plane of incidence and angle of incidence respectively. The observation plane, the (x,y) plane, is parallel to the (u,v) plane and is located a distance h above it. The observation point, Q_o, is defined either by the coordinates (x,y,h), or

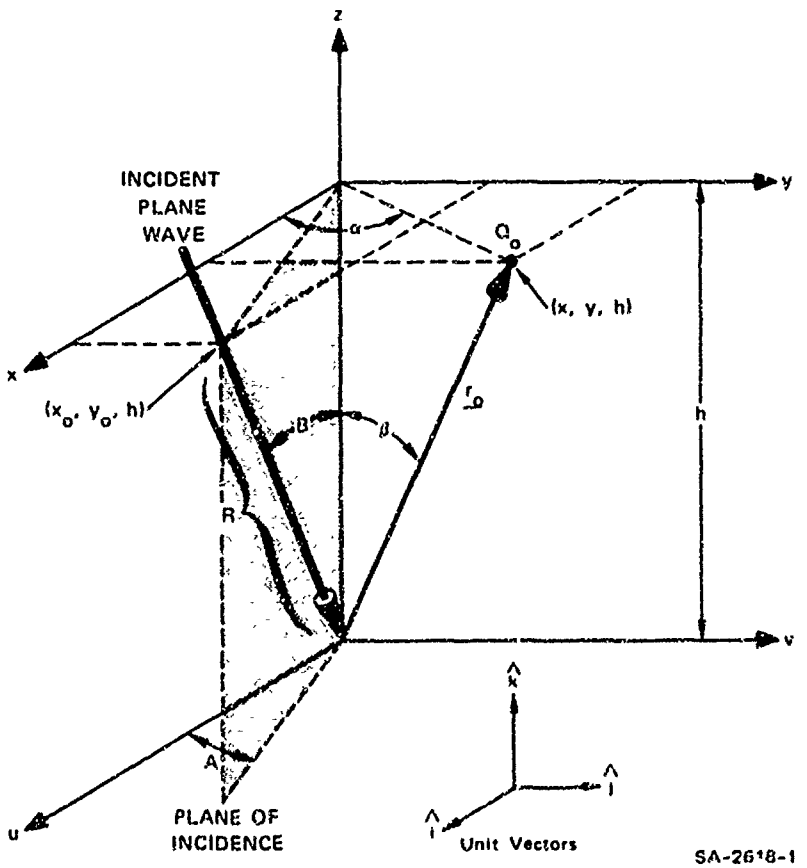

FIGURE 1 COORDINATE SYSTEMS AND GEOMETRY OF SCATTERING PROBLEM

the vector $\underline{r}_o$, and angles α and β. The incident plane wave has the specific form

$$E_i(u,v,z) = g(u,v,z)E_o \exp\left(j \underline{k}_i \cdot \underline{r}\right) \tag{1.1}$$

where g(u,v,z) is an amplitude aperture function limiting the extent of the plane wave and

$$\underline{k}_i = -k[\sin B \cos A \hat{i} + \sin B \sin A \hat{j} + \cos B \hat{k}] \tag{1.2}$$

and

$$\underline{r} = u \hat{i} + v \hat{j} + z \hat{k} \tag{1.3}$$

with $(\hat{i},\hat{j},\hat{k})$ being unit vectors along the (u,v,z) directions respectively.

The arbitrary aperture function g(u,v,o) defines the finite portion of the ocean that is illuminated and permits infinite limits to be used on integrals over the (u,v) plane. For example, the power, P_i, incident on the (u,v) plane is given by

$$P_i = \frac{1}{2Z_o} \int_{-\infty}^{\infty}\int |E_i(u,v,o)|^2 \, dudv = \frac{E_o^2}{2Z_o} \int_{-\infty}^{\infty}\int [g(u,v,o)]^2 \, dudv \tag{1.4}$$

where Z_o is the impedance of free space (120 π ohms). In the specific case for which the incident beam has a Gaussian cross section, the integral Eq. (1.4) has the value πq^2, where E_o^2 is the peak intensity and q is the e^{-1} intensity radius.

Figure 2 will aid in further defining the geometry of the scattering problem. The point Q_s is located on the surface of the ocean within the aperture function g(u,v,o) and has coordinates [u,v,w(u,v)], where w(u,v) is the elevation of the water surface above the mean (u,v) plane. Alternatively, the point Q_s may be defined by the vector $\underline{r}_s$ and the angles a and b.

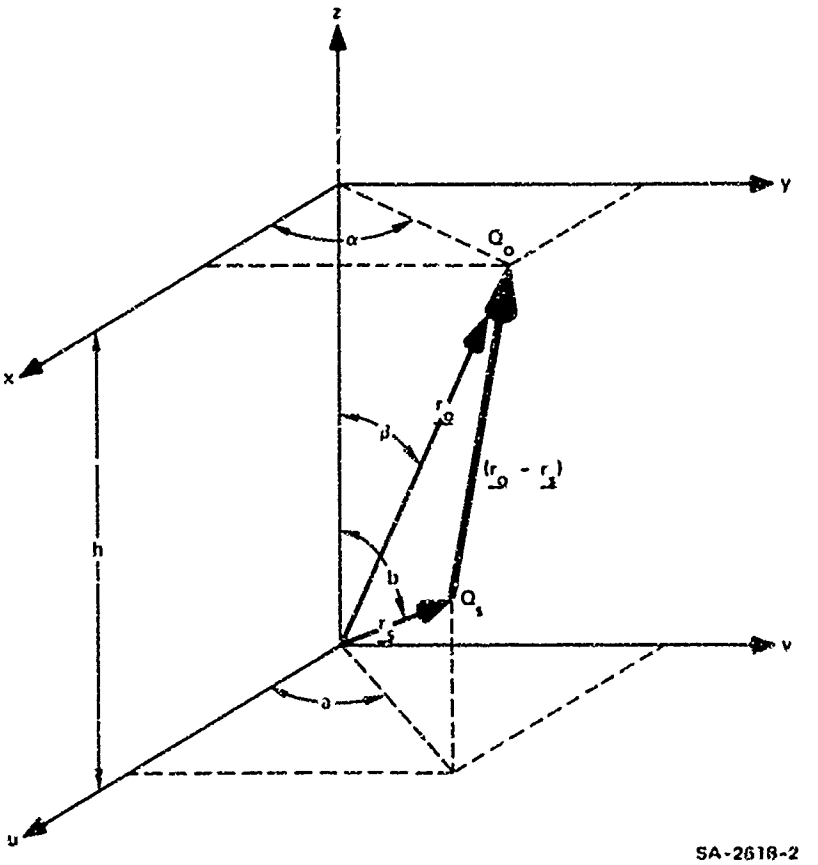

FIGURE 2 VECTOR GEOMETRY

II GENERAL THEORY

A. Historical Background and Review

After the operation of the first CW He-Ne laser, considerable interest arose in the speckled appearance of typical diffuse surfaces illuminated by coherent light. It was soon recognized that the origin of these granular patterns lay in the optical roughness of the surfaces from which the light was scattered.[2,3]

The first detailed statistical treatment of this phenomenon, now known as laser speckle, was that of Goodman.[4] Treating the scattering or reflecting surface as a statistical ensemble of many point-scatterers with independent and uniformly distributed phases on $(0, 2\pi)$, Goodman showed, among other results, that the power spectral density (or Wiener spectrum) of the intensity pattern of reflected light was, up to scaling factors, identical with the autocorrelation function of brightness (i.e., intensity) distribution across the scattering spot.

Goldfischer[5] independently derived the same result using essentially the same model as Goodman.[4] Again the scatterers were assumed to be infinitesimal in size and independent, and were taken to have phases uniformly distributed on $(0,2\pi)$. This assumption is mathematically equivalent to assuming that the spatial coherence of the fields behaves similarly to a δ-function; that is, the spatial coherence has value unity for zero displacement and value zero for finite displacement.

In an extension of his previous results, Goodman[6] later discussed the properties of speckle patterns as they affect the performance of optical radars. In an appendix to this paper, he presented a generalized

theory that allowed a finite correlation area to exist in the fields at the scattering surface. Thus, the assumption of infinitesimal scatterers was removed, but, significantly, the phase of the scattered light at any point on the object was still assumed to be uniformly distributed on $(0,2\pi)$. Hence, the theory applies only for surfaces that are quite rough on the scale of the wavelength of the illumination.

Following this early work that dealt with the intensity patterns existing in the scattered light, other investigators--notably Lowenthal and Arsenault[7]--have studied the properties of similar patterns observed in the images of coherently illuminated diffuse objects. These treatments have assumed that the complex fields in the image plane obey circular Gaussian statistics; i.e., the real and imaginary parts of the field are zero mean, uncorrelated Gaussian random variables, with identical variances. Such an assumption is valid if the correlation area of the diffusely transmitted or reflected wavefront is small compared with the area of the point-spread function of the imaging system and if the phase of the light at each point on the object is approximately uniformly distributed on $(0,2\pi)$. Since the current discussion will be limited to speckle patterns observed by direct measurement of intensity in the scattered light, without any intervening optics, the problem studied by Lowenthal and Arsenault will not be addressed.

The next important piece of work dealing with directly observed speckle patterns is that of Crane.[9] He derives results that appear in various respects to conflict with earlier results of Goodman[4,6] and Goldfischer. Crane's comments are directed at the paper by Goldfischer, but his chief criticism is as follows: Goldfischer assumes that the field produced by a small subsection of a diffuse surface is proportional to the square root of the area of that subsection; but for coherent light, the field must be directly proportional to the area because the

field contributions add on an amplitude basis. Thus, Crane concludes that Goldfischer used a physically incorrect model and that this is the reason for the apparent differences between the results of the two theories. It should be mentioned that Crane's theory has the merit of allowing for a finite correlation area of the diffuse surface. Of the work preceding Crane's, only that of Goodman[3] allowed for this possibility.

Crane's criticism of Goldfischer's work was answered in a letter by Arsenault.[8] Arsenault asserts that the differences between Goldfischer's and Crane's results arise because the former theory derives statistical average results while the latter is entirely a deterministic theory. Arsenault addresses his comments only to the early part of Crane's paper and in particular, to that portion through Crane's Eq. (16). In a later portion of his paper leading to his Eqs. (38) and (39), Crane has derived expressions for the statistical average power spectral density, the same quantity derived by Goldfischer. The important differences between these two expressions were not reconciled by Arsenault's comments. However, in 1973 Goodman[10] showed that the discrepancies are only apparent and not real, and that they have resulted from improper interpretation of results rather than improper development of the theory. Specifically, Crane's result as expressed by his Eq. (39) can only be applied to relatively smooth surfaces, that is, surfaces for which the rms surface roughness is much less than one wavelength of the scattered radiation. On the other hand, the results of Goodman's and Goldfischer's analysis can only be applied to truly rough surfaces, that is, to surfaces for which the rms surface roughness is much greater than one wavelength of the scattered radiation. Moreover, Goodman[10]--starting with Crane's Eq. (38)--derived an approximate expression for the statistical average power spectral density, valid for truly rough surfaces, that is entirely consistent with all previous theoretical work. Thus, the apparent discrepancies

have been reconciled and all theories are mutually consistent when properly applied to their regions of validity.

B. Approximations and Assumptions

The mathematical statement of the Huygens-Fresnel principle is

$$E(x,y) = \frac{1}{j\lambda} \int_S \frac{E_s(u,v,w) \exp\left[jk|\underline{r}_o - \underline{r}_s|\right] \cos\left[\underline{n},\left(\underline{r}_o - \underline{r}_s\right)\right] dS_s}{|\underline{r}_o - \underline{r}_s|} \quad . \quad (2.1)$$

Implicit in the use of this principle are approximations and assumptions similar to those used in the Helmholtz integral formalism--the usual starting point for microwave scattering calculations. A more complete discussion of these approximations and assumptions will be found in Beckmann and Spizzichino.[2]

As in the case of all scalar theories, the results obtained here are valid only for small angles of incidence and small bistatic angles. We make the approximation that the field $E_s(u,v,w)$ reflected from the surface can be represented by the product $\eta(u,v)\, E_i(u,v,w)$, where $\eta(u,v)$ is the surface reflectance. This is a reasonable approximation since the minimum water wavelength λ_{min} is known to be much larger than the optical wavelength λ. The amplitude reflectance, $\eta(u,v)$, is taken to be $-|\eta(B)|$, where $\eta(B)$ is the Fresnel amplitude reflectance at the incidence angle B; the surface elemental area, dS_s, is taken to be the same as the elemental area dudv in the (u,v) plane. The obliquity factor is taken to be cos β. The preceding three approximations are reasonable for a rath calm sea with gentle slopes. Finally, the factor $|\underline{r}_o - \underline{r}_s|$ is approximated by r_o in the denominator of Eq. (2.1), and also by the first few terms of its binomial expansion

$$|\underline{r}_o - \underline{r}_s| \approx r_o - \frac{xu + yv}{r_o} + \frac{u^2 + v^2}{2r_o} - w \cos\beta \quad (2.2)$$

in the exponent of Eq. (2.1). In this regard it should be noted that there are different ways of grouping the terms in the binomial expansion that result in slightly different approximations. In one case, the small angle is approximated by its tangent while in the other case it is approximated by its sine. The Huygens-Fresnel principle, in its approximate form, is stated here as Eq. (2.3).

$$E(x,y) = \frac{\cos^2 \beta \, e^{jkr_o}}{j\lambda h} \iint_{-\infty}^{\infty} E_s(u,v,w) \exp\{jk[\psi(u,v) - w \cos \beta]\} \, du\,dv \qquad (2.3)$$

with

$$\psi(u,v) = \frac{u^2 + v^2}{2r_o} - \frac{xu + yv}{r_o} \quad . \qquad (2.4)$$

The basic statistical assumption is made here that the ocean wave height statistics are wide-sense stationary, at least over the patch of ocean illuminated, and the wave heights are Gaussian distributed.[12,13] The effects associated with sampling only a finite patch of the ocean both in the wave height statistics and the optical field statistics are accounted for. The statistics of the scattered fields at the observation point are taken to be circular complex Gaussian. Such statistics arise only when the scattered field components generate a complex random walk, with approximate uniform phase associated with the various field contributions. This amounts to assuming that the rms surface roughness is comparable with or greater than the wavelength of the scattered radiation, an assumption that is well justified even for a calm ocean. It does mean, however, that the present results cannot be applied to perfectly smooth surfaces, such as polished mirrors.

C. Ensemble Average Scattered Intensity

In this section an expression is derived for the ensemble average scattered intensity distribution, $\langle I(x,y)\rangle$, as a function of the normalized ensemble average spatial coherence function of the fields in the (u,v) plane. Subsequently it is shown how the spatial coherence can be expressed in terms of physically observable ensemble average surface characteristics.

An explicit expression for the field $E_s(u,v,w)$ can be written with the help of Eqs. (1.1), (1.2), and (1.3).

$$E_s(u,v,w) \sim E(u,v) \exp\left\{-jk\left[\psi_o(u,v) + w \cos B\right]\right\} \quad , \tag{2.5}$$

with

$$\psi_o(u,v) = u \sin B \cos A + v \sin B \sin A = \frac{1}{R}\left(ux_o + vy_o\right) \tag{2.6}$$

and

$$E(u,v) \triangleq -\left|\eta(B)\right| g(u,v,o)\, E_o \quad . \tag{2.7}$$

Equation (2.3) now may be restated as

$$E(x,y) = \frac{\cos^2 \beta\, e^{jkr_o}}{\quad} \iint_{-\infty}^{\infty} E(u,v) \exp\left\{jk\left[\psi(u,v) - \psi_o(u,v) - w(\cos B + \cos \beta)\right]\right\} dudv \quad . \tag{2.8}$$

As an aid to interpreting these results, note that the Huygens-Fresnel principle may be stated in the equivalent form[6]

$$E(x,y) = \frac{\cos^2 \beta \; e^{jkr_o}}{j\lambda h} \iint_{-\infty}^{\infty} E_p(u,v) \exp[jk\psi_o(u,v)] \, dudv \qquad (2.9)$$

where $E_p(u,v)$ is the mathematically equivalent field in the (u,v) plane as opposed to the field on the scattering surface. The terminology "mathematically equivalent" field is used here to emphasize the fact that $E_p(u,v)$ is not the physical field in the (u,v) plane but, rather, it is equivalent to a physical field which, if present in the (u,v) plane, would produce the field E(x,y). A comparison of Eq. (2.9) with Eq. (2.8) yields the result

$$E_p(u,v) = E(u,v) \exp\left\{-jk\left[\psi_o(u,v) - w(\cos B + \cos \beta)\right]\right\} \quad . \qquad (2.10)$$

The ensemble average scattered intensity, $\langle I(x,y) \rangle$, is, by definition

$$\langle I(x,y) \rangle \triangleq \langle E(x,y) E^*(x,y) \rangle \qquad (2.11)$$

where the carets are used to indicate that an ensemble average is to be performed. Equation (2.9) may be used in Eq. (2.11) to yield

$$\langle I(x,y) \rangle = \frac{\cos^4 \beta}{(\lambda h)^2} \iiint_{-\infty}^{\infty} \left\langle E_p(u_1,v_1) E_p^*(u_2,v_2) \right\rangle \times \exp\left\{jk\left[\psi(u_1,v_1) - \psi(u_2,v_2)\right]\right\} du_1 dv_1 du_2 dv_2 \quad . \qquad (2.12)$$

The quantity in carets in the integrand will be recognized as the mutual intensity $J(u_1,v_1,u_2,v_2)$ of the equivalent fields in the (u,v) plane, and from Eq. (2.10) is given by

$$\left\langle J(u_1,v_1,u_2,v_2) \right\rangle = E(u_1,v_1) E^*(u_2,v_2) \exp\left\{-jk\left[\psi_o(u_1,v_1) - \psi_o(u_2,v_2)\right]\right\} \left\langle \exp\left[jk(w_1 - w_2)(\cos B + \cos \beta)\right] \right\rangle \quad . \qquad (2.13)$$

Using the new variables

$$u_1 = u_o + \frac{\Delta u}{2} \quad , \quad u_2 = u_o - \frac{\Delta u}{2} \quad ,$$
$$v_1 = v_o + \frac{\Delta v}{2} \quad , \quad v_2 = v_o - \frac{\Delta v}{2} \quad , \tag{2.14}$$

Eq. (2.13) becomes

$$\left\langle J\left(u_o, v_o; \Delta u, \Delta v\right)\right\rangle = J_o\left(u_o, v_o; \Delta u, \Delta v\right)\langle \gamma(\Delta u, \Delta v)\rangle \tag{2.15}$$

with

$$J_o\left(u_o, v_o; \Delta u, \Delta v\right) \triangleq E\left(u_o + \frac{\Delta u}{2}, v_o + \frac{\Delta v}{2}\right) E^*\left(u_o - \frac{\Delta u}{2}, v_o - \frac{\Delta v}{2}\right) \tag{2.16}$$

and

$$\langle \gamma(\Delta u, \Delta v)\rangle \triangleq \exp[-jk(\Delta u \sin B \cos A + \Delta v \sin B \sin A)]$$
$$\times \left\langle \exp jk\left(w_1 - w_2\right)(\cos B + \cos \hat{\beta})\right\rangle \quad . \tag{2.17}$$

Equation (2.12) now takes the form

$$\langle I(x,y)\rangle = \frac{\cos^4 \hat{\beta}}{(\lambda h)^2} \int\int_{-\infty}^{\infty} J_o\left(u_o, v_o; \Delta u, \Delta v\right)\langle \gamma(\Delta u, \Delta v)\rangle$$
$$\times \exp\left[jk\left(\frac{u_o \Delta u}{r_o} + \frac{v_o \Delta v}{r_o} - \frac{x\Delta u}{r_o} - \frac{y\Delta v}{r_o}\right)\right] du_o dv_o d\Delta u d\Delta v \quad . \tag{2.18}$$

It will be demonstrated subsequently (see Appendix B) that the function $\langle \gamma(\Delta u, \Delta v)\rangle$ has a nonnegligible value only for displacements $(\Delta u, \Delta v)$ less than a few wavelengths of the scattered radiation. Using this

knowledge and the approximation

$$\exp\left[j\,\frac{k}{r_o}\left(u_o\Delta u + v_o\Delta v\right)\right] \simeq 1 \quad , \tag{2.19}$$

Eq. (2.18) now can be written as

$$\langle I(x,y)\rangle \simeq \frac{\cos^4\beta}{(\lambda h)^2}\left[\iint_{-\infty}^{\infty} I_o\left(u_o,v_o\right)\,du_o dv_o\right]\cdot \underset{\frac{x}{\lambda r_o},\frac{y}{\lambda r_o}}{\overset{\Delta u,\Delta v}{\mathfrak{F}}}\left\{\langle\gamma(\Delta u,\Delta v)\rangle\right\} \tag{2.20}$$

where

$$I_o\left(u_o,v_o\right) \triangleq J_o\left(u_o,v_o;0,0\right) \tag{2.21}$$

and the notation $\overset{c,d}{\underset{a,b}{\mathfrak{F}}}$ is used to indicate a two-dimensional Fourier transform with respect to spatial frequencies (a,b) and spatial coordinates (c,d).

The approximation indicated by Eq. (2.19) is reasonable as long as the angle subtended by the aperture function at the observation point is smaller than about one degree.

The integral in square brackets in Eq. (2.20) may be evaluated with the help of Eqs. (2.21), (2.16), (2.7), and (1.4).

$$\iint_{-\infty}^{\infty} I_o\left(u_o,v_o\right)\,du_o dv_o = 2Z_o\left|\eta(B)\right|^2 P_1 = 2Z_o P_r \tag{2.22}$$

where P_r is used to indicate the reflected power. Finally, Eq. (2.20) may be rewritten as

$$\langle I(x,y)\rangle = \frac{\cos^2\beta}{\left(\lambda r_o\right)^2}\left(2Z_o P_r\right)\underset{\frac{x}{\lambda r_o},\frac{y}{\lambda r_o}}{\overset{\Delta u,\Delta v}{\mathfrak{F}}}\left\{\langle\gamma(\Delta u,\Delta v)\rangle\right\} \quad . \tag{2.23}$$

There is an interesting interpretation of Eq. (2.23) that is consistent with the understanding of the propagation of spatial coherence. For the case of an infinite aperture, Eq. (2.15) reduces to

$$\left\langle J\left(u_o, v_o; \Delta u, \Delta v\right)\right\rangle_\infty = \left|\eta(B)\right|^2 E_o^2 \langle \gamma(\Delta u, \Delta v)\rangle \quad .$$

In this form, $\langle \gamma(\Delta u, \Delta v)\rangle$ will be recognized as the space invariant, normalized, ensemble average spatial coherence function. Thus, Eq. (2.23) indicates that it is the spatial coherence that primarily determines the distribution of scattered intensity. It is therefore important to be able to relate the spatial coherence to surface characteristics in a manner that will enable numerical calculations to be made.

It is possible to derive expressions for other ensemble average observables, such as spatial coherence and power spectral density.[14] The ensemble average spatial coherence in the observation plane can be shown to be the Fourier transform of the aperture function on the scattering surface and is therefore not related to surface characteristics. Moreover, while the ensemble average power spectral density of the scattered radiation can be related to surface characteristics, the experimental technique of measuring this quantity would be intensity interferometry and therefore, in a practical sense, it would be more difficult to measure than the ensemble average scattered intensity distribution. Finally, it should be mentioned that since the intensity averaged over many "speckles" is equivalent to the intensity for temporally incoherent light, the expressions derived here are valid for incoherent quasi-monochromatic light sources, such as filtered sunlight.

D. Spatial Coherence as a Function of Surface Characteristics

The probability distribution function p[w(u,v)] for the surface heights w(u,v) must be known in order to perform ensemble averages. An assumption that is in reasonable agreement with experimental evidence[12] is that the surface height is a stationary zero-mean Gaussian random variable with distribution

$$p[w(u,v)] = (\sigma\sqrt{2\pi})^{-1} \exp\left\{-\frac{[w(u,v)]^2}{2\sigma^2}\right\} \tag{2.24}$$

where

$$\sigma^2 \triangleq \int_{-\infty}^{\infty} [w(u,v)]^2 p[w(u,v)]\, dw(u,v) = \left\langle [w(u,v)]^2 \right\rangle \quad . \tag{2.25}$$

The covariance function $R(\Delta u,\Delta v)$ and the normalized covariance function $\rho(\Delta u,\Delta v)$ for homogeneous (stationary) processes are defined by

$$R(\Delta u,\Delta v) \triangleq \langle w(u,v)w(u+\Delta u, v+\Delta v)\rangle \tag{2.26}$$

and

$$\rho(\Delta u,\Delta v) \triangleq \frac{R(\Delta u,\Delta v)}{\sigma^2} \quad . \tag{2.27}$$

The joint probability distribution function $p[w_1,w_2]$ is given by

$$p[w_1,w_2] = \left[2\pi\sigma^2\sqrt{1-\rho^2}\right]^{-1} \exp\left[-\frac{w_1^2 - 2\rho w_1 w_2 + w_2^2}{2\sigma^2(1-\rho^2)}\right] \tag{2.28}$$

where, for convenience, the following notation has been adopted:

$$w_1 \triangleq w(u,v) \qquad w_2 \triangleq w(u+\Delta u, v+\Delta v) \quad . \tag{2.29}$$

The quantity in ensemble brackets in Eq. (2.17) can be interpreted as the characteristic function for the distribution $p\{w_1,w_2\}$ and thus Eq. (2.17) can be written

$$\langle \gamma(\Delta u,\Delta v)\rangle = \exp[-jk(\Delta u \sin B \cos A + \Delta v \sin B \sin A)]$$

$$\times \exp\left\{-k^2(\cos B + \cos\beta)^2[R(0,0) - R(\Delta u,\Delta v)]\right\}$$

$$= \exp\left[-j\frac{k}{R}\left(\Delta u x_o + \Delta v y_o\right)\right]$$

$$\times \exp\left\{-k^2(\cos B + \cos\beta)^2[R(0,0) - R(\Delta u,\Delta v)]\right\} \quad . \quad (2.30)$$

Through Eq. (2.30) the spatial coherence function is related to the surface height covariance function which, with the known (or assumed) probability distribution, completely characterizes the surface. Finally, using Eq. (2.30) in Eq. (2.23), we get

$$\langle I(x,y)\rangle = \frac{\cos^2\beta}{\left(\lambda r_o\right)^2}\left(2Z_o P_r\right)$$

$$\times \underset{\frac{1}{\lambda}\left(\frac{x}{r_o}+\frac{x_o}{R}\right),\frac{1}{\lambda}\left(\frac{y}{r_o}+\frac{y_o}{R}\right)}{\overset{\Delta u,\Delta v}{\mathcal{F}}} \left(\exp\left\{-k^2(\cos B+\cos\beta)^2[R(0,0)-R(\Delta u,\Delta v)]\right\}\right) \quad . \quad (2.31)$$

It is of some interest to compare this result with the high frequency microwave backscatter cross section σ^o. In our notation the backscattered (monostatic) intensity, I, is given by Frost and Jackson:[15]

$$I = \frac{2Z_o P_i}{4\pi r_o^2}\sigma^o \quad (2.32)$$

where

$$\sigma^o = |\eta(\beta)|^2\left(\frac{4\pi}{\lambda^2}\right)\int\int_{-\infty}^{\infty} \cos(2k\Delta u \sin\beta)$$

$$\times \exp\left\{-4k^2 \cos^2\beta[R(0,0) - R(\Delta u,\Delta v)]\right\} d\Delta u d\Delta v \quad . \qquad (2.33)$$

When the backscatter conditions, $B = \beta$, $A = 0$, $x = r_o \sin\beta$, $y = 0$, are used in Eq. (2.23), the result is

$$\left\langle I\left(r_o \sin\beta, 0\right)\right\rangle = \frac{\cos^2\beta\left(2Z_o p_r\right)}{\left(\lambda r_o\right)^2} \underset{\frac{\sin\beta}{\lambda},0}{\overset{\Delta u,\Delta v}{\mathfrak{F}}} [\langle\gamma(\Delta u,\Delta v)\rangle] \quad . \qquad (2.34)$$

We may construct a backscatter cross section σ' using Eq. (2.32) for the definition and Eq. (2.34) for the backscattered intensity

$$\sigma' = \cos^2\beta|\eta(\beta)|^2\left(\frac{4\pi}{\lambda^2}\right) \underset{\frac{\sin\beta}{\lambda},0}{\overset{\Delta u,\Delta v}{\mathfrak{F}}} [\langle\gamma(\Delta u,\Delta v)\rangle] \quad . \qquad (2.35)$$

Since the covariance function is even in Δu (for $\Delta v = 0$), the Fourier cosine transform can be used in place of the Fourier transform, to obtain from Eq. (2.35)

$$\sigma' = \cos^2\beta|\eta(\beta)|^2\left(\frac{4\pi}{\lambda^2}\right)\int\int_{-\infty}^{\infty} \cos(2k\Delta u \sin\beta)$$

$$\times \exp\left\{-4k^2 \cos^2\beta[R(0,0) - R(\Delta u\ \Delta v)]\right\} d\Delta u d\Delta v \qquad (2.36)$$

which is identical with Eq. (2.33) except for a factor of $\cos^2\beta$. This factor, which is approximately unity for small angles, arises from the obliquity factor in the Huygens-Fresnel principle, and appears to be the

only difference between our results and the results of more rigorous scalar diffraction theory.[16]

E. The Surface Covariance Function

Let w(u,v) be a realization of the random process representing the elevation of the ocean surface. Evidently w(u,v) is a real zero-mean random variable. The surface covariance function $R(\Delta u,\Delta v)$ of the random surface elevation is defined by

$$R(u,v,\Delta u,\Delta v) \triangleq \langle w(u,v)w(u+\Delta u,v+\Delta v)\rangle \quad . \tag{2.37}$$

When the process is assumed to be homogeneous (stationary) in the wide sense, R depends only on the displacements $(\Delta u,\Delta v)$ and not on the coordinates (u,v); i.e.:

$$\langle w(u,v)w(u+\Delta u,v+\Delta v)\rangle = R(\Delta u,\Delta v) \quad . \tag{2.38}$$

Further, R must be symmetric about zero displacement; i.e.:

$$R(\Delta u,\Delta v) = R(-\Delta u,-\Delta v) \quad . \tag{2.39}$$

Or, in polar coordinates

$$R(\Delta r,\theta) = R(\Delta r,\theta+\pi) \quad . \tag{2.40}$$

Since the measurement of the surface elevation is feasible over only a finite area of the ocean, it implies the presence of an aperture $g_a(u,v)$, so that the measured surface elevation is given by

$$w_g(u,v) = w(u,v)g_a(u,v) \tag{2.41}$$

where $g_a(0,0) = 1$, $g_a(\infty,\infty) = 0$, and $[\lim(a \to \infty) g_a(u,v)] = 1$, so that $w_g(u,v) = w(u,v)$ as $a \to \infty$. If $W_g(\ell_u, \ell_v)$ is the Fourier transform of $w_g(u,v)$,

$$W_g(\ell_u, \ell_v) = \iint_{-\infty}^{\infty} w_g(u,v) \exp\left[-j\left(u\ell_u + v\ell_v\right)\right] dudv \quad . \tag{2.42}$$

The ensemble average power spectral density of the functions $w_g(u,v)$ is defined as

$$S_g^*(\ell_u, \ell_v) \triangleq \frac{\left\langle \left| W_g(\ell_u, \ell_v) \right|^2 \right\rangle}{\iint_{-\infty}^{\infty} \left| g_a(u,v) \right|^2 dudv} \quad . \tag{2.43}$$

If R is continuous, then by the use of the Wiener-Khintchine theorem, it follows that

$$R(\Delta u, \Delta v) = \frac{1}{(2\pi)^2} \iint_{-\infty}^{\infty} S^*(\ell_u, \ell_v) \exp\left[j\left(\Delta u \ell_u + \Delta v \ell_v\right)\right] d\ell_u d\ell_v \tag{2.44}$$

and

$$S^*(\ell_u, \ell_v) = \iint_{-\infty}^{\infty} R(\Delta u, \Delta v) \exp\left[-j\left(\Delta u \ell_u + \Delta v \ell_v\right)\right] d\Delta u d\Delta v \tag{2.45}$$

where

$$S^*(\ell_u, \ell_v) = \lim_{a \to \infty} S_g^*(\ell_u, \ell_v) \tag{2.46}$$

and $S^*(\ell_u, \ell_v)$ is known as the power spectral density of the random process $w(u,v)$. It may also be shown that

$$\mathfrak{F}^{-1}\left[S_g^*(\ell_u, \ell_v)\right] = R(\Delta u, \Delta v) \frac{\bar{g}_a \overset{*}{*} g_a}{\iint \left| g_a(u,v) \right|^2 dudv} \triangleq \overline{R_g} \quad . \tag{2.47}$$

If the covariance of the apertured functions $w_g(u,v)$ is defined as

$$R_g(u,v,\Delta u,\Delta v) \triangleq \left\langle w_g(u,v) w_g(u - \Delta u, v + \Delta v) \right\rangle \quad , \tag{2.48}$$

then

$$\overline{R_g}(\Delta u,\Delta v) = \frac{\displaystyle\iint_{-\infty}^{\infty} R_g(u,v,\Delta u,\Delta v)\, du\,dv}{\displaystyle\iint_{-\infty}^{\infty} |g_a(u,v)|^2\, du\,dv} \quad . \tag{2.49}$$

These equations express the result that the covariance function $R(\Delta u,\Delta v)$ and the power spectral density $S^*(\ell_u,\ell_v)$ of the random process $w(u,v)$ form a Fourier transform pair. The covariance function R_g is not the Fourier transform of $S_g^*(\ell_u,\ell_v)$. However, the space average of R_g forms a Fourier transform pair with $S_g^*(\ell_u,\ell_v)$. It is to be noted that R_g is not homogeneous and that $[\lim(a \to \infty) R_g] = R(\Delta u,\Delta v)$. Figure 3 shows the geometrical relationship between the several domains between which the transforms are defined.

Frequently, the surface covariance function cannot be obtained from the power spectral density since the Fourier transformation indicated in Eq. (2.44) is difficult to perform. For this reason, as well as to obtain a more direct physical insight into the various operations, we develop R in a Taylor series about the origin.

$$R(\Delta u,\Delta v) = \sum_{n=0}^{\infty} \frac{1}{n!} \left\{ \left[\Delta u \frac{\partial}{\partial p} + \Delta v \frac{\partial}{\partial q} \right]^n R(p,q) \right\}_{p=q=0} \quad . \tag{2.50}$$

Because of the symmetry implied by Eq. (2.39), it can be shown that in Eq. (2.50), the terms for which n is odd are identically zero. In other words, all odd order partial derivatives of R are zero at the origin.

Domain			Functions Defined
Cartesian	Polar	Vector	
(u, v)	(, a)		w, w_g, g_a
(ξ_u, ξ_v)	(ξ, ϕ)	$\underline{\xi}$	S_g^*, S^*, S
(Δu, Δv)	(Δr, θ)	$\underline{\Delta r}$	$\bar{R}_g$, R, $\langle\gamma\rangle$
(x, y)	(, α)		$\langle\,!\,\rangle$

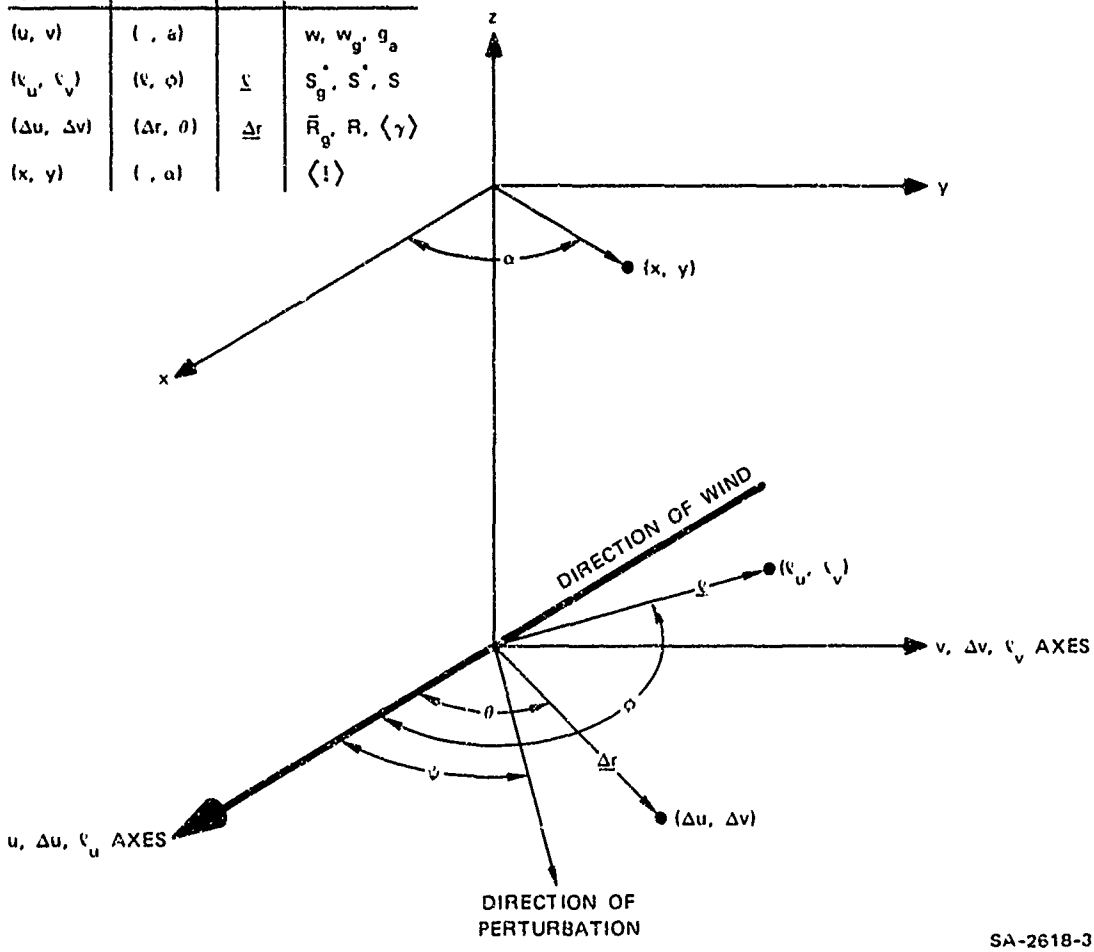

FIGURE 3 GEOMETRICAL RELATIONSHIPS BETWEEN TRANSFORM DOMAINS

$$\left[\frac{\partial^n}{\partial p^\alpha \partial q^{n-\alpha}} R(p,q)\right]_{p=q=0} = 0 \quad \text{for } n \text{ odd} \quad . \tag{2.51}$$

Thus Eq. (2.50) becomes

$$R(\Delta u, \Delta v) = \sum_{n=0}^{\infty} \frac{1}{2n!} \left\{\left[\Delta u \frac{\partial}{\partial p} + \Delta v \frac{\partial}{\partial q}\right]^{2n} R(p,q)\right\}_{p=q=0} \quad . \tag{2.52}$$

Using vector notation, we may write Eq. (2.52) as

$$R(\underline{\Delta r}) = \sum_{0}^{\infty} \frac{1}{2n!} \left[\left(\underline{\Delta r} \cdot \nabla_p\right)^{2n} R(\underline{p})\right]_{\underline{p}=0} \tag{2.53}$$

where

$$\underline{\Delta r} = \hat{i}\, \Delta u + \hat{j}\, \Delta v \tag{2.54}$$

and

$$\nabla_p = \hat{i} \frac{\partial}{\partial p} + \hat{j} \frac{\partial}{\partial q} \quad . \tag{2.55}$$

The investigation of the region of convergence of the above series requires much more information about the partial derivatives and has not been pursued in detail. However, it can be shown that the maximum value of R occurs at the origin. Further, with the help of the Taylor formula with remainder, we may write

$$R(\underline{\Delta r}) = \sum_{n=0}^{m} \frac{1}{2n!} \left[\left(\underline{\Delta r} \cdot \nabla_p\right)^{2n} R(\underline{p})\right]_{\underline{p}=0}$$

$$+ \frac{1}{(2m+2)!} \left[\left(\underline{\Delta r} \cdot \nabla_p\right)^{2m+2} R(\underline{p})\right]_{\underline{p}=\underline{p}_o} \tag{2.56}$$

where $\underline{p}_o = t\, \underline{\Delta r}$ and $0 \leq t \leq 1$.

Writing Eq. (2.44) in vector notation, and using the definition

$$S(\underline{\ell}) = S^{*}(\underline{\ell})/(2\pi)^{2} \quad , \tag{2.57}$$

we get

$$R(\underline{\Delta r}) = \int_{\text{plane}} S(\underline{\ell}) \exp(j\, \underline{\Delta r} \cdot \underline{\ell})\, d\underline{\ell} \quad . \tag{2.58}$$

Substituting in the right hand side of Eq. (2.53), we get

$$R(\underline{\Delta r}) = \sum_{n=0}^{m} \frac{(j)^{2n}}{2n!} \int_{\text{plane}} S(\underline{\ell})(\underline{\Delta r} \cdot \underline{\ell})^{2n}\, d\underline{\ell}$$

$$+ \frac{(j)^{2m+2}}{(2m+2)!} \int_{\text{plane}} S(\underline{\ell})(\underline{\Delta r} \cdot \underline{\ell})^{2m+2} \exp\left(j\, \underline{p}_{o} \cdot \underline{\ell}\right) d\underline{\ell} \quad . \tag{2.59}$$

If we use polar coordinates to describe both $R(\Delta r,\theta)$ and $S(\ell,\Phi)$, we have

$$\underline{\Delta r} \cdot \underline{\ell} = \Delta r\, \ell \cos(\theta - \Phi)$$

and

$$R(\Delta r,\theta) = \sum_{n=0}^{m} (-1)^{n}\left(\Delta r^{2n}/2n!\right) \int_{0}^{\infty}\int_{-\pi}^{\pi} S(\ell,\Phi)[\ell \cos(\theta - \Phi)]^{2n}\, \ell\, d\ell d\Phi$$

$$+ (-1)^{m+1}\left[\Delta r^{2m+2}/(2m+2)!\right] \int_{0}^{\infty}\int_{-\pi}^{\pi} S(\ell,\Phi)[\ell \cos(\theta - \Phi)]^{2m+2}$$

$$\times \exp\left(j\, p_{o}\, \ell \cos\theta\right) \ell\, d\ell d\Phi \tag{2.60}$$

or

$$R(\Delta r,\theta) \triangleq \sum_{n=0}^{m} \frac{(-1)^n}{2n!} M_{2n}(0)\Delta r^{2n} + \frac{(-1)^{m+1}}{2m+2!} M_{2m+2}(p)\Delta r^{2m+2} \qquad (2.61a)$$

where

$$M_{2n}(0) = \int_0^{\infty}\int_{-\pi}^{\pi} S(\ell,\phi)[\ell \cos(\theta - \phi)]^{2n}\, \ell\, d\ell d\phi \quad . \qquad (2.61b)$$

It is thus seen that the various terms in the expansion of Eq. (2.56) correspond to various moments of the power spectral density. These moments may also be related to the ensemble average properties of the random process w(u,v). The first term of the expansion, or the zeroth moment, is

$$M_o = \int_0^{\infty}\int_{-\pi}^{\pi} S(\ell,\phi)\, \ell\, d\ell d\phi \quad , \qquad (2.62)$$

using Eqs. (2.61a) and 60). From Eq. (2.38) it is seen that

$$R(0,0) = \left\langle [w(u,v)]^2 \right\rangle \quad . \qquad (2.63)$$

Thus the zeroth moment gives the mean square elevation.

The second moment is given by

$$M_2 = \int_0^{\infty}\int_{-\pi}^{\pi} S(\ell,\phi)\, \ell^3 \cos^2(\theta - \phi)\, d\ell d\phi \quad , \qquad (2.64)$$

and the second term of the expansion is

$$-\frac{1}{2} M_2 \Delta r^2 = \frac{1}{2}\left[\left(\underline{\Delta r} \cdot \underline{\nabla}_p\right)^2 R(\underline{p})\right]_{\underline{p}=0} \quad . \qquad (2.65)$$

From Eq. (2.38) it can be shown that,

$$\left[\left(\Delta r \cdot \nabla_p\right)^2 R(\underline{p})\right]_{\underline{p}=0} = -\Delta r^2 \left\langle \left[(\underline{\Delta r}/\Delta r) \cdot \nabla_u w\right]^2 \right\rangle \qquad (2.66)$$

or

$$M_2 = \left\langle \left[(\underline{\Delta r}/\Delta r \cdot \nabla_u w(u,v)\right]^2 \right\rangle \quad . \qquad (2.67)$$

$[(\underline{\Delta r}/\Delta r) \cdot \nabla_u w]$ is the component of the gradient in the direction of the unit vector $(\underline{\Delta r}/\Delta r)$. Since

$$(\underline{\Delta r}/\Delta r) \cdot \nabla_u w = \left[\frac{\partial w}{\partial u} \cos\theta \cdot \left(\frac{\partial w}{\partial v}\right) \sin\theta\right] \quad , \qquad (2.68)$$

M_2 may also be expressed as

$$M_2 = \left[\left\langle\left(\frac{\partial w}{\partial u}\right)^2\right\rangle \cos^2\theta + 2\left\langle\left(\frac{\partial w}{\partial u}\right)\left(\frac{\partial w}{\partial v}\right)\right\rangle \sin\theta\cos\theta + \left\langle\left(\frac{\partial w}{\partial v}\right)^2\right\rangle \sin^2\theta\right] \quad . \quad (2.69)$$

Thus the second moment, M_2, is seen to be equal to the mean square of the slope component in the direction θ.

The fourth moment, M_4, may be similarly related to the partial derivatives of $w(u,v)$, which are related to the curvature of the surface. Thus,

$$\begin{aligned} M_4 &= \left\{\left[(\underline{\Delta r}/\Delta r) \cdot \nabla_p\right]^4 R(\underline{p})\right\}_{\underline{p}=0} \\ &= \left\langle \left\{\left[(\underline{\Delta r}/\Delta r) \cdot \nabla_u\right]^2 w(u,v)\right\}^2 \right\rangle \\ &= \left\langle \left[\frac{\partial^2 w}{\partial u^2}\cos^2\theta + 2\sin\theta\cos\theta \frac{\partial^2 w}{\partial u \partial v} + \frac{\partial^2 w}{\partial v^2}\sin^2\theta\right]^2 \right\rangle \quad . \quad (2.70) \end{aligned}$$

III CALCULATION OF THE SCATTERED INTENSITY DISTRIBUTION

A. General

The theoretical relationships developed in the foregoing are applied in this chapter to the scattering of optical radiation from the surface of the ocean. A specific power spectral density is assumed for the surface elevation of the natural sea surface, and an expression is obtained for the scattered intensity. Subsequently, a specific form is assumed for the power spectral density of a perturbation on the ocean surface. An expression is obtained for the intensity distribution due to the perturbed ocean surface. Numerical calculations are made to evaluate the effects of the various parameters of the perturbation.

B. The Power Spectrum of Ocean Surface Elevation

In a recent report a large amount of experimental data were digested to develop an analytic representation of the spectrum of a wind roughened sea. This spectrum, which is a function of wind velocity, has been used in the present study as the power spectral density of the surface elevation of ocean waves.

For a friction velocity u_* greater than a minimum value $u_{*_m} = 12$ cm/s, the spectrum has been defined by the following equations.

$$\frac{S^*(\ell,\phi)}{(2\pi)^2} = S(\ell,\phi)$$

$$= S(\ell)F(\ell,\phi) \qquad \text{for } \begin{matrix} 0 < \ell < \infty \\ -\pi < \phi < \pi \end{matrix} \qquad (3.1)$$

$$F(\ell,\phi) = (1/3\pi)\cos^4\phi\left\{1 - \exp\left[-g^2/2\ell^2U^4\right]\right\}$$

$$\cdot \frac{1}{2\pi}\left[1 + a_1(u_*)\cos 2\phi\right]\exp\left[-g^2/2\ell^2U^4\right] \qquad (3.2)$$

and

$$S(\ell) = \begin{cases} S_1 = \left(a/2\ell^4\right)\exp\left[-\beta g^2/\ell^2U^4\right] & 0 \le \ell \le \ell_1 & (3.3a) \\ S_2 = a'\left(2\ell_1^{1/2}\ell^{7/2}\right) & \ell_1 \le \ell \le \ell_2 & (3.3b) \\ S_3 = aD'\left(2\ell_3^{p}\ell^{4-p}\right) & \ell_2 \le \ell \le \ell_3 & (3.3c) \\ S_4 = aD'\left(2\ell^4\right) & \ell_3 \le \ell \le \ell_4 & (3.3d) \\ S_5 = aD\ell^6/\left(2\ell^{10}\right) & \ell_4 \le \ell < \infty & (3.3e) \end{cases}$$

where $a = 8.1 \times 10^{-3}$, $\beta = 0.74$, $\ell_2 = 0.3588\ \text{cm}^{-1}$, $\ell_3 = 0.9437\ \text{cm}^{-1}$, and

U = the wind velocity at an altitude of 19.5 meters

$$= -2.5\,u_*\left\{\ln\left[\left(0.684/u_*\right) + 4.28 \times 10^{-5}\,u_*^2 - 0.0443\right] - \ln 1950\right\} \qquad (3.4)$$

$$\ell_1 = \ell_2\left(u_{*m}/u_*\right)^2 \qquad (3.5)$$

$$\ell_4 = 0.5726\,u^{1/2}\ell_m/D^{1/6} \qquad (3.6)$$

$$\ell_m = (g\rho/\tau)^{1/2}$$

$$= 3.672\ \text{cm}^{-1} \qquad (3.7)$$

$$D = \left(1.274 + 0.0268\,u_* + 6.03 \times 10^{-5}\,u_*^2\right)^2 \qquad (3.8)$$

$$p = \log_{10}\left(D u_{*_m} u_*\right) \log_{10}\left(\ell_3 \ell_2\right) \tag{3.9}$$

$$a_1 = 0.214 \log_{10} u_* \quad 0.036 \quad .^* \tag{3.10}$$

Thus it is seen that $S(\ell,\phi)$ is dependent on the friction velocity, or indirectly on the wind speed.

In this description of the spectrum, the direction of the wind has been assumed to coincide with the u-axis or the direction $\phi = \psi = 0$.

We note that

$$\int_{-\pi}^{\pi} F(\ell,\phi)\, d\phi = 1 \quad . \tag{3.11}$$

In Figure 4, $\ell\, S(\ell)$ is plotted against ℓ. The area under the curve is equal to the mean square elevation according to Eq. (2.62). Figure 5 presents the proven spectral density on a log-log plot, accentuating the dependence on wind speed in regions of interest to this study. It is to be noted that a negligible contribution is made to surface roughness from wave numbers larger than 0.01 cm^{-1}. Figure 6 shows the factor $\exp[-g^2/2\ell^2U^4]$ as a function of ℓ, as well as ℓ_1 as a function of u_*. It is seen that the factor is almost unity for $\ell > \ell_1$. Figures 7 and 8 present the angular dependence of the power spectral density for $\ell < \ell_1$ and $\ell > \ell_1$, for various values of the parameter a_1.

C. Covariance Function of the Ocean Surface

The surface covariance function $R(\Delta r,\vartheta)$ is given by the Fourier transform of the power spectrum of the wave elevation as given by Eq.

---

*This relation for a_1 is an approximate analytic expression for the wind speed dependence of a_1 obtained from the data in Pierson's report. Though a_1 could depend on ℓ, this dependence is ignored.

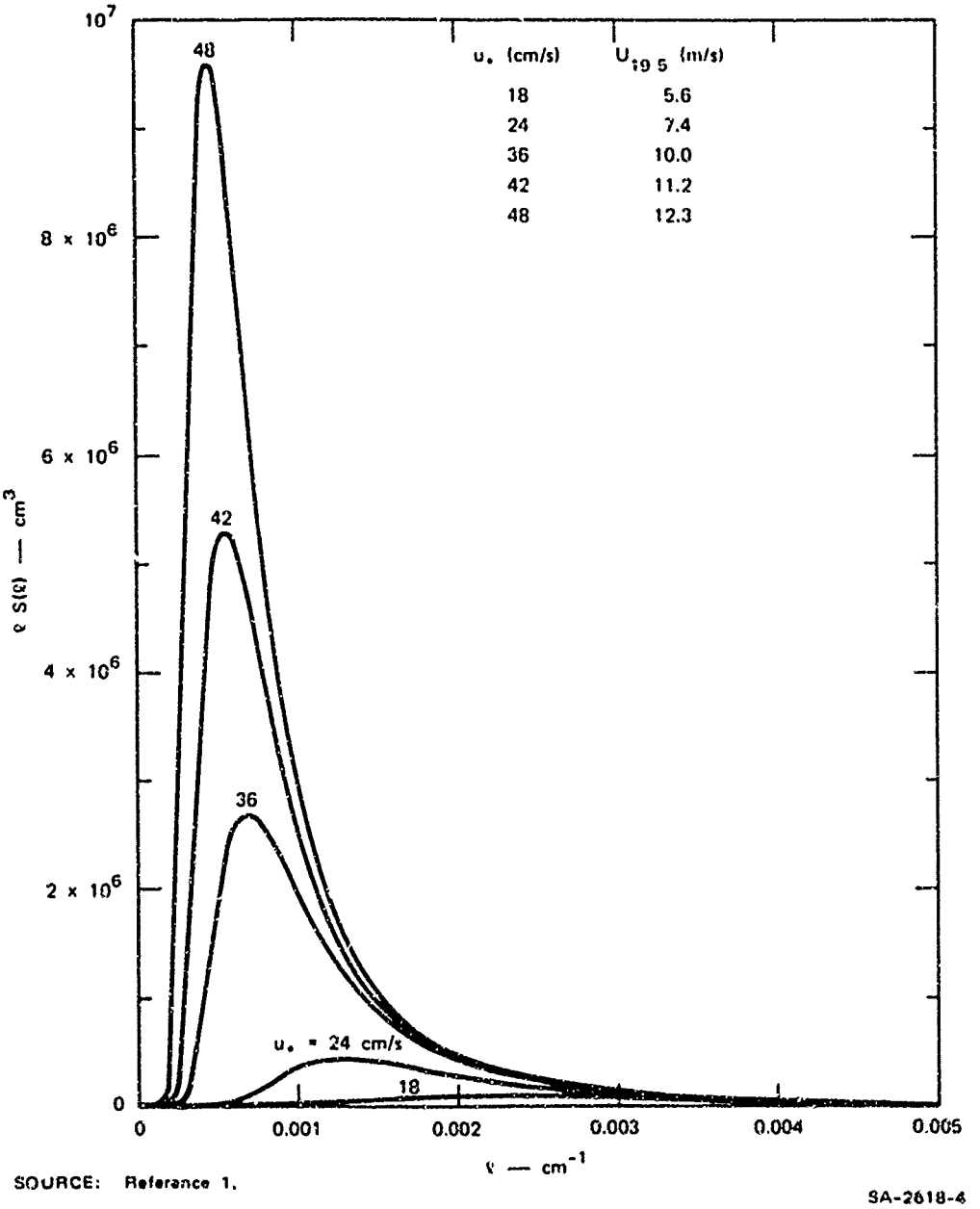

FIGURE 4 POWER SPECTRAL DENSITY OF OCEAN SURFACE ELEVATION FOR A RANGE OF WIND SPEEDS

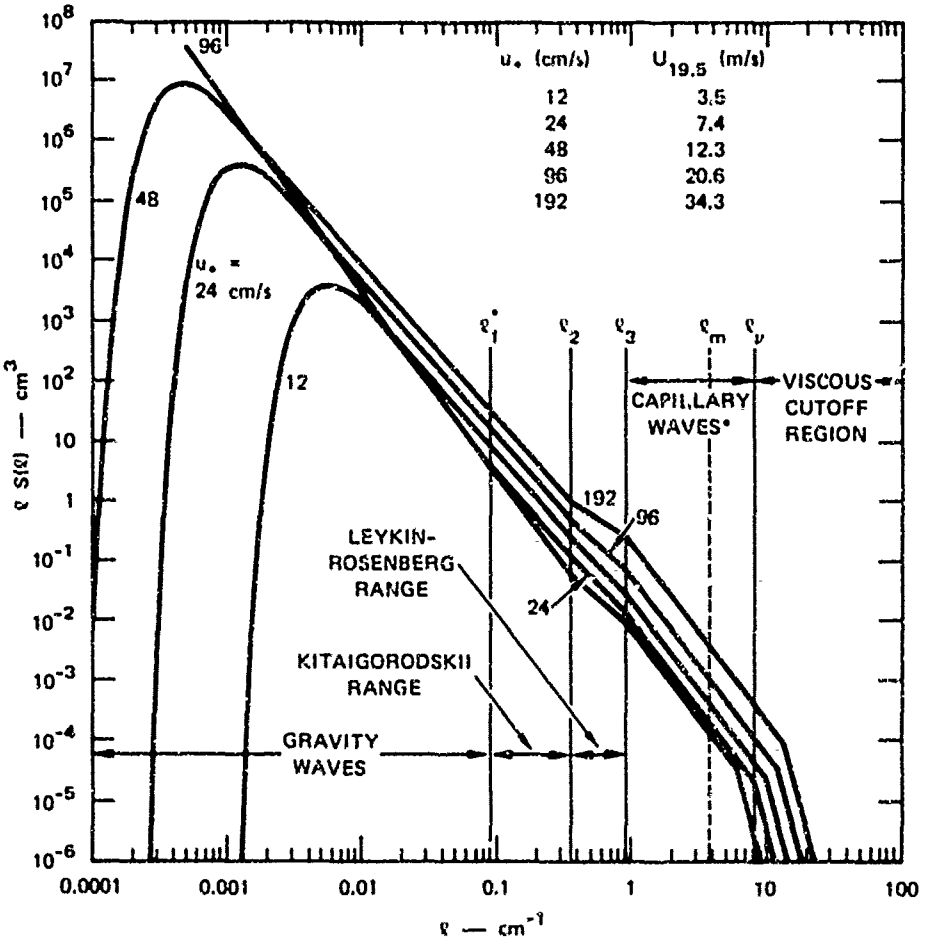

*The ranges shown and the values of ℓ_1^* and ℓ_ν are for $u_* = 24$ cm/s.

SOURCE Reference 1.

SA-2618-5

FIGURE 5 POWER SPECTRAL DENSITY OF OCEAN SURFACE WAVE ELEVATION FOR A RANGE OF WIND SPEEDS

(2.58). Thus,

$$R(\Delta r,\theta) = \int_0^\infty \ell\, S(\ell)\left\{\int_{-\pi}^{\pi} F(\ell,\phi)\, \exp[j\ell\Delta r\, \cos(\phi - \theta)]\, d\phi\right\} d\ell \quad . \quad (3.12)$$

The integral over ϕ may be performed analytically and expressed in terms of Bessel functions of even order, J_{2m}. The details of the integration are presented in Appendix A.

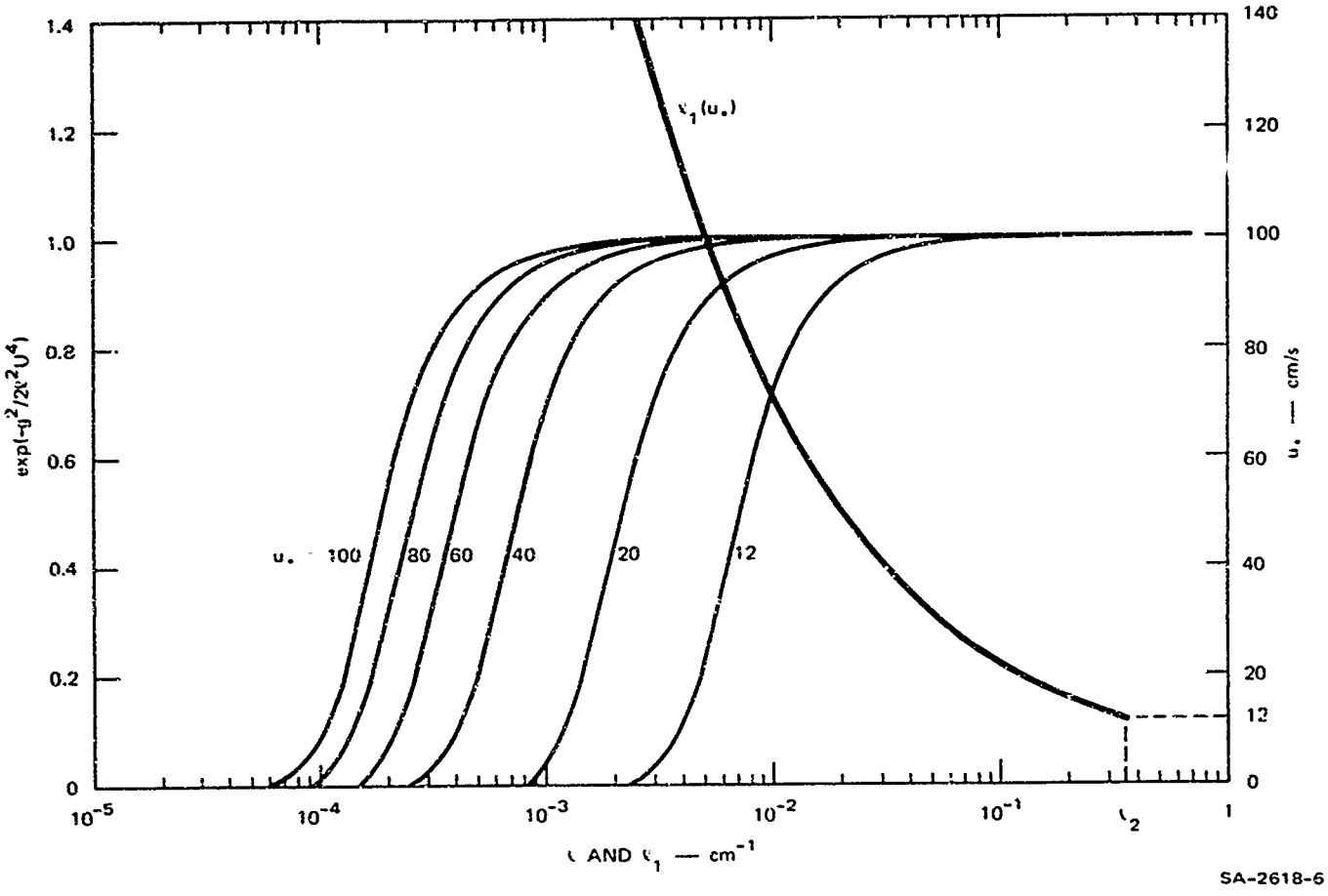

FIGURE 6 PLOTS OF $\exp[-g^2/2\ell^2U^4]$ AS A FUNCTION OF ℓ AND $\ell_1(u_*)$ AS A FUNCTION OF u_*.

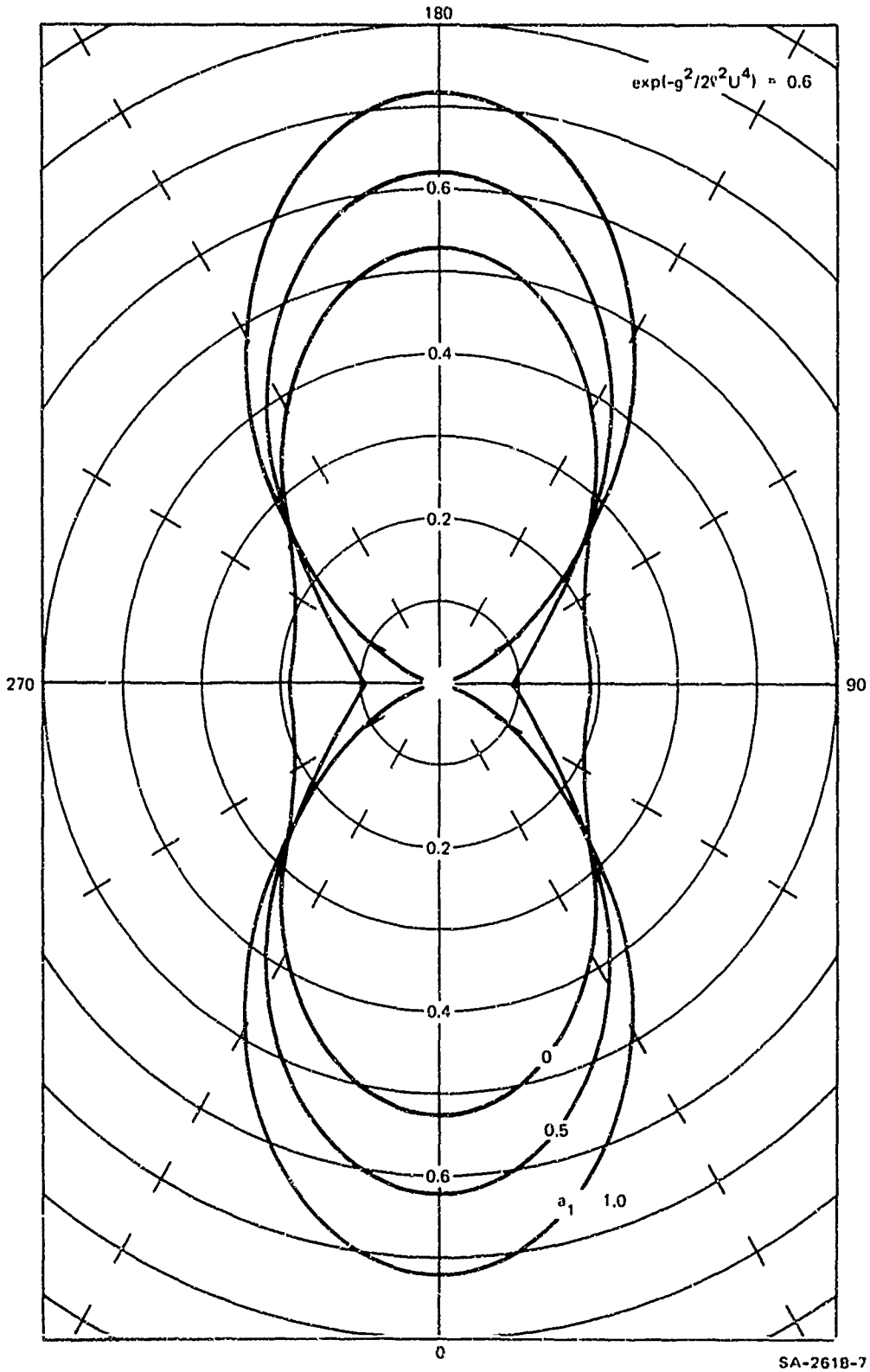

FIGURE 7 ANGULAR DEPENDENCE OF $S(\ell, \phi)$ FOR $\ell < \ell_1$

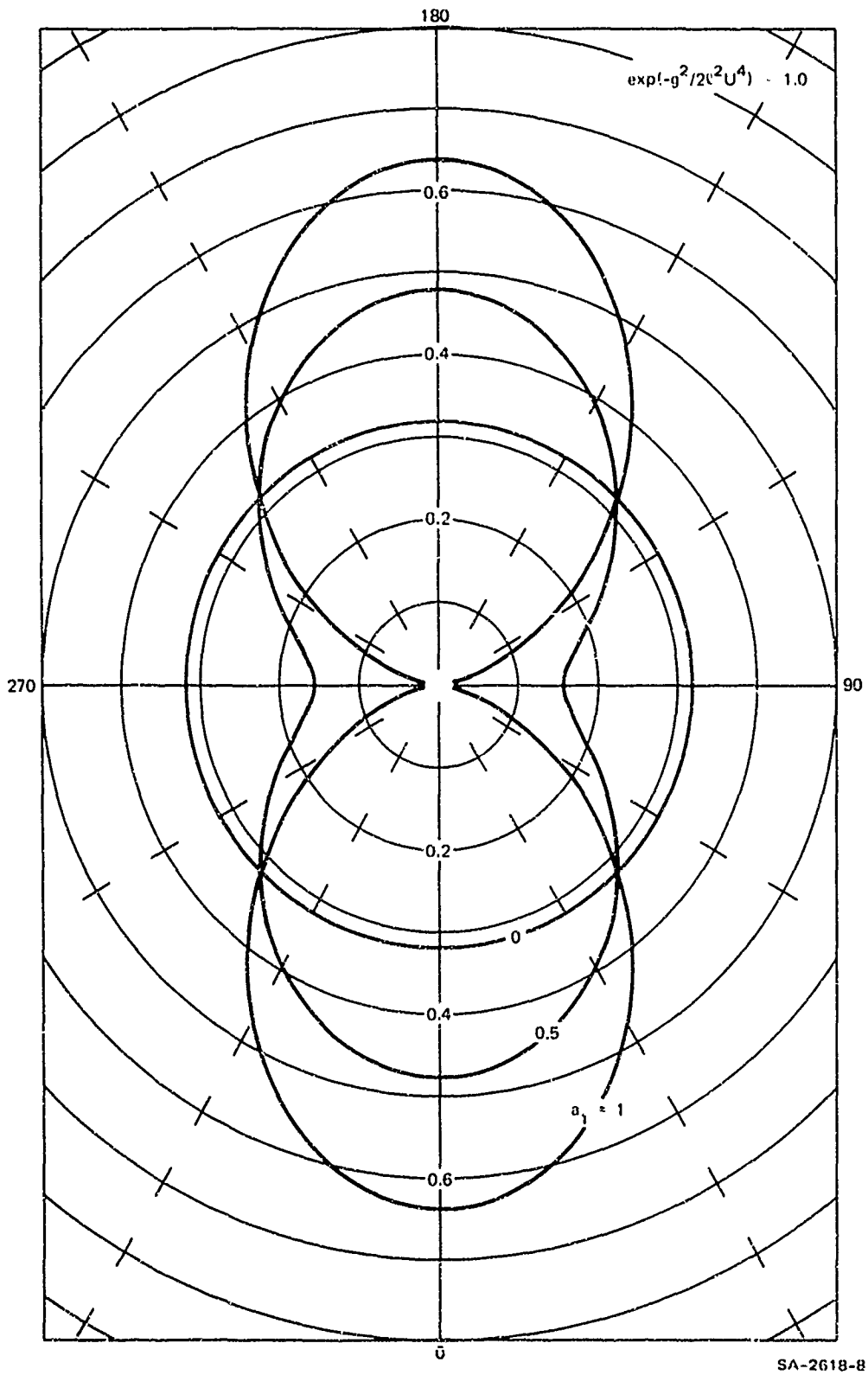

FIGURE 8 ANGULAR DEPENDENCE OF $S(\ell, \phi)$ FOR $\ell > \ell_1$

$$R(\Delta r,\theta) = \int_0^\infty \ell\, S(\ell)\left[J_o - (4/3)\cos 2\theta\, J_2 + (1/3)\cos 4\theta\, J_4\right] d\ell$$

$$+ \int_0^\infty \ell\, S(\ell)E(\ell)\left[(1/3)\left(4 - 3a_1\right)\cos 2\theta\, J_2 - (1/3)\cos 4\theta\, J_4\right] d\ell \qquad (3.13)$$

where

$$E(\ell) = \exp\left[-g^2/2\ell^2U^4\right] \qquad (3.14)$$

for $\Delta r = 0$, $J_o = 1$, and $J_2 = J_4 = 0$. Thus

$$R(0,\theta) = \int_0^\infty \ell\, S(\ell)\, d\ell = M_o \quad . \qquad (3.15)$$

For larger values of Δr, R undergoes oscillatory behavior governed by the particular combination of the almost periodic Bessel functions.

Examination of the θ dependence of R as given by Eq. (3.13) shows that R is periodic in θ with a period of $\pi/2$. In other words, R is symmetric about both cartesian axes. It should be emphasized that this is not a general property of covariance functions but derives from the chosen power spectral density, which was chosen with the same symmetry.

Although analytic integration of Eq. (3.13) to obtain an expression for $R(\Delta r,\theta)$ is difficult, numerical evaluation is possible. However, for the purposes of this study, the method of moments described in Chapter II turns out to be more fruitful. From Eqs. (2.60), (2.61), and (3.1) we get

$$M_{2n} = \int_0^\infty \int_{-\pi}^{\pi} S(\ell)r(\ell,\phi)\ell^{2n+1}\cos^{2n}(\theta - \phi)\, d\ell d\phi \quad . \qquad (3.16)$$

In the further development, we shall need only the second moment, which has the form

$$M_2 = F_o(u_*) \cos^2 \theta + G_o(u_*)$$

$$= \left(F_o + G_o\right) \cos^2 \theta + G_o \sin^2 \theta \quad . \tag{3.17}$$

The details of the evaluation of the spectral moments as well as the forms of $F_o(u_*)$ and $G_o(u_*)$ are also given in Appendix A. On comparison with Eq. (2.69) it is evident that

$$\left\langle \left(\frac{\partial w}{\partial u}\right)^2 \right\rangle = F_o + G_o \tag{3.18}$$

$$\left\langle \left(\frac{\partial w}{\partial v}\right)^2 \right\rangle = G_o \tag{3.19}$$

and

$$\left\langle \left(\frac{\partial w}{\partial u}\right)\left(\frac{\partial w}{\partial v}\right) \right\rangle = 0 \quad . \tag{3.20}$$

Equation (3.20) is the result of the choice of wind direction made in the definition of the power spectral density. The values of M_o, M_2, M_4, M_6, as well as G_o for $\theta = 0$ are plotted in Figure 9 as a function of friction velocity and wind speed. (Note that $F_o + G_o = M_2$ for $\theta = 0$.) Of course, M_o is independent of angle θ. The angular dependence of M_2 is seen from Eq. (3.17). The angular dependence of M_4 and M_6 is complicated; however, they all have maximum values at $\theta = 0$.

It is of significance to consider these numerical values for the moments, along with the Taylor's formula for $R(\Delta r, \theta)$ given by Eqs. (2.56) and (2.61).

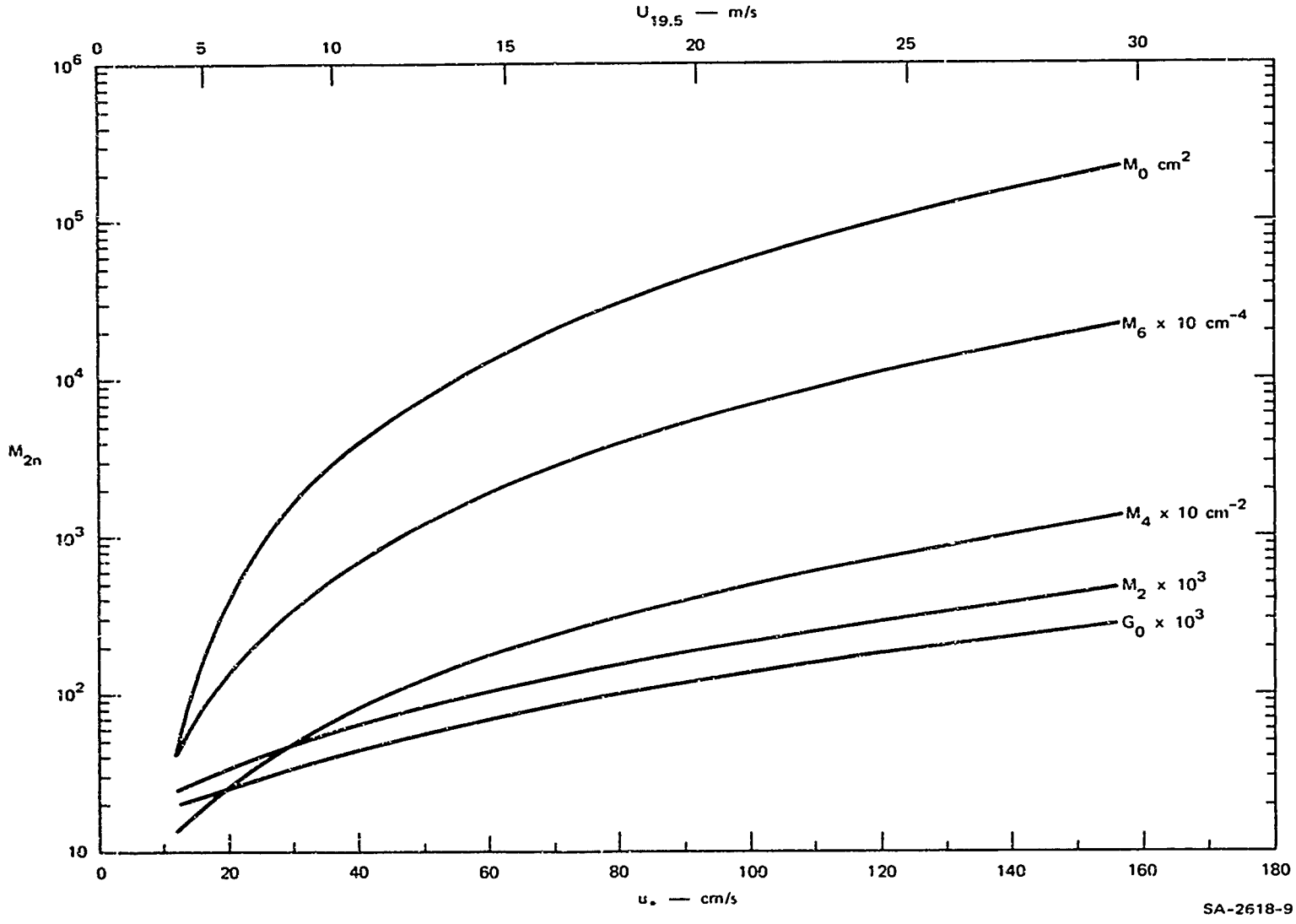

FIGURE 9 WIND SPEED DEPENDENCE OF SPECTRAL MOMENTS

$$R(\Delta r,\theta) = M_o - \frac{1}{2} M_2 \Delta r^2 + \frac{1}{24} M_4 \Delta r^4 - \frac{1}{120} M_6\left(p_o\right)\Delta r^6 \quad . \quad (3.21)$$

Consider the approximate representation of $R(\Delta r,\theta)$ by only the first two terms of Eq. (3.21). Taylor's remainder theorem indicates that the maximum error resulting from this truncation is given by the next term after the truncation. For $u_* = 192$ cm/s and $\Delta r = 0.1$ cm, the terms in the series are numerically given by

$$\frac{1}{2} M_2 \Delta r^2 = 3.64 \times 10^{-3}$$

$$\frac{1}{24} M_4 \Delta r^2 = 9.63 \times 10^{-5}$$

$$\frac{1}{120} M_6 \Delta r^6 = 3.34 \times 10^{-5} \quad .$$

Thus, $M_o - (1/2) M_2 \Delta r^2$ appears to be a very accurate representation of $R(\Delta r,\theta)$ for displacements Δr up to 0.1 cm.

D. Intensity Distribution of Optical Radiation Scattered by the Sea

The ensemble average spatial coherence function is given by Eq. (2.30) as

$$\langle \gamma(\Delta u,\Delta v)\rangle = \exp[-jk(\Delta u \sin B \cos A + \Delta v \sin \beta \sin A)]$$

$$\times \exp\left\{-k^2(\cos \beta + \cos B)^2[R(0,0) - R(\Delta u,\Delta v)]\right\} \quad . \quad (3.22)$$

It is argued in Appendix B that the factor $[R(0,0) - R(\Delta u,\Delta v)]$ in the exponent in Eq. (3.22) may be replaced by $(1/2)M_2\Delta r^2$ when k is the wave vector of optical radiation. Thus

$$\langle \gamma(\Delta u,\Delta v)\rangle = \exp\left[-j\,\frac{k}{R}\left(\Delta u x_o + \Delta v y_o\right)\right]$$

$$\times \exp\left[\frac{-k^2}{2}\,(\cos\beta + \cos B)^2\, M_2 \Delta r^2\right] \quad . \qquad (3.23)$$

From Eq. (3.17),

$$M_2 \Delta r^2 = \left(F_o + G_o\right)\Delta u^2 + G_o \Delta v^2 \quad . \qquad (3.24)$$

From Eqs. (2.31), (3.23), and (3.24) the average intensity distribution of optical radiation scattered by the surface of the ocean is given by

$$\langle I(\xi,\eta)\rangle = \frac{2Z_o P_r \cos^2\beta}{\left(\lambda r_o\right)^2}$$

$$\times \int\int_{-\infty}^{\infty} \exp\left\{-\frac{k^2}{2}\,(\cos\beta + \cos B)^2\left[\left(F_o + G_o\right)\Delta u^2 + G_o \Delta v^2\right]\right\}$$

$$\times \exp[-jk(\Delta u\xi + \Delta v\eta)]\, d\Delta u d\Delta v \qquad (3.25)$$

where

$$\xi = \left(\frac{x_o}{R} + \frac{x}{r_o}\right) = \frac{1}{h}\left(x\cos\beta + x_o \cos B\right) \qquad (3.26a)$$

and

$$\eta = \left(\frac{y_o}{R} + \frac{y}{r_o}\right) = \frac{1}{h}\left(y\cos\beta + y_o \cos B\right) \quad . \qquad (3.26b)$$

We note that x_o and y_o are the coordinates of the laser beam at the target plane. Performing the Fourier transformation, we get

$$\langle I(\xi,\eta)\rangle = \frac{Z_o P_r}{\pi r_o^2} \frac{\cos^2 \beta}{(\cos \beta + \cos B)^2} \frac{1}{\sqrt{\left(F_o + G_o\right)G_o}}$$

$$\times \exp\left[-\frac{G_o \xi^2 + \left(F_o + G_o\right)\eta^2}{2(\cos \beta + \cos B)^2 G_o\left(F_o + G_o\right)}\right] \qquad (3.27)$$

or

$$\langle I(x,y)\rangle = \frac{Z_o P_r}{\pi h^2} \frac{\cos^4 \beta}{(\cos \beta + \cos B)^2} \frac{1}{\sqrt{\left(F_o + G_o\right)G_o}}$$

$$\times \exp\left[-\frac{G_o\left(x \cos \beta + x_o \cos B\right)^2 + \left(F_o + G_o\right)\left(y \cos \beta + y_o \cos B\right)^2}{2h^2 G_o\left(F_o + G_o\right)(\cos \beta + \cos B)^2}\right] \qquad (3.28)$$

This general expression for the intensity distribution, may be specialized for the backscatter case by making the substitutions $x = x_o$, $y = y_o$, and $\beta = B$.

$$\langle I(x,y)\rangle_B = \frac{Z_o P_r \cos^2 \beta}{4\pi h^2 \sqrt{\left(G_o + F_o\right)G_o}} \exp\left[-\frac{G_o x^2 + \left(F_o + G_o\right)y^2}{2h^2 G_o\left(F_o + G_o\right)}\right] \qquad (3.29)$$

or

$$\langle I(\alpha,\beta)\rangle_B = \frac{Z_o P_r \cos^2 \beta}{4\pi h^2 \sqrt{\left(G_o + F_o\right)G_o}} \exp\left[-\frac{\tan^2 \beta}{2}\left(\frac{\cos^2 \alpha}{F_o + G_o} + \frac{\sin^2 \alpha}{G_o}\right)\right] \qquad (3.30)$$

where the substitutions $h^2/(x^2 + y^2) = \tan^2 \beta$, $x^2/(x^2 + y^2) = \cos^2 \alpha$, and $y^2/(x^2 + y^2) = \sin^2 \alpha$ as evident from Figure 1 have been made. From Figure 1 it is also seen that the same expression results if the laser transmitter and receiver are situated at the origin in the receiver plane and the position of the illuminated spot on the ocean is described by the spherical coordinates $(r_o, \alpha, \pi - \beta)$.

For normal incidence ($\beta = 0$), Eq. (3.30) leads to

$$\langle I(0,0)\rangle_B \triangleq I_{peak}(u_*)$$

$$= Z_o P_r / \left[4\pi h^2 \sqrt{G_o(F_o + G_o)}\right] \quad . \tag{3.31}$$

We note that I_{peak} is a function of the wind speed, since F_o and G_o are functions of u_*. For a moderate wind speed of 7.4 m/s, corresponding to $u_* = 24$ cm/s, $\sqrt{G_o(F_o + G_o)} = 3.47 \times 10^{-2}$. Assuming a range of one km, a laser power of one watt, and a reflectivity (of the water) of one percent, the factor $(Z_o P_r / 4\pi h^2)$ has a value of 3×10^{-7} volts^{2}m^{-2}. Thus, the peak backscattered intensity under these conditions is 8.66×10^{-6} volt^{2}m^{-2}, or 1.15×10^{-8} watts per square meter.

At any other wind speed we may write

$$\frac{I_{peak}(u_*)}{I_{peak}(24)} = \left\{\frac{G_o(24)\left[F_o(24) + G_o(24)\right]}{G_o(u_*)\left[F_o(u_*) + G_o(u_*)\right]}\right\}^{1/2} \quad . \tag{3.32}$$

In Figure 10, this ratio of the peak intensity to the peak intensity at an arbitrarily chosen friction velocity ($u_* = 24$ cm/s) is plotted against u_* and $U_{19.5}$. It is noted that with increasing wind, or increasing roughness of the surface, the peak intensity decreases.

If we approximate $\cos^2\beta$ by unity in Eq. (3.30), it can be seen that contours of constant backscattered intensity are ellipses described by

$$\left[\frac{\cos^2\alpha}{(F_o + G_o)} + \frac{\sin^2\alpha}{G_o}\right] \tan^2\beta = \text{constant} \tag{3.33}$$

or

$$\frac{x^2}{(F_o + G_o)} + \frac{y^2}{G_o} = \text{constant} \quad . \tag{3.34}$$

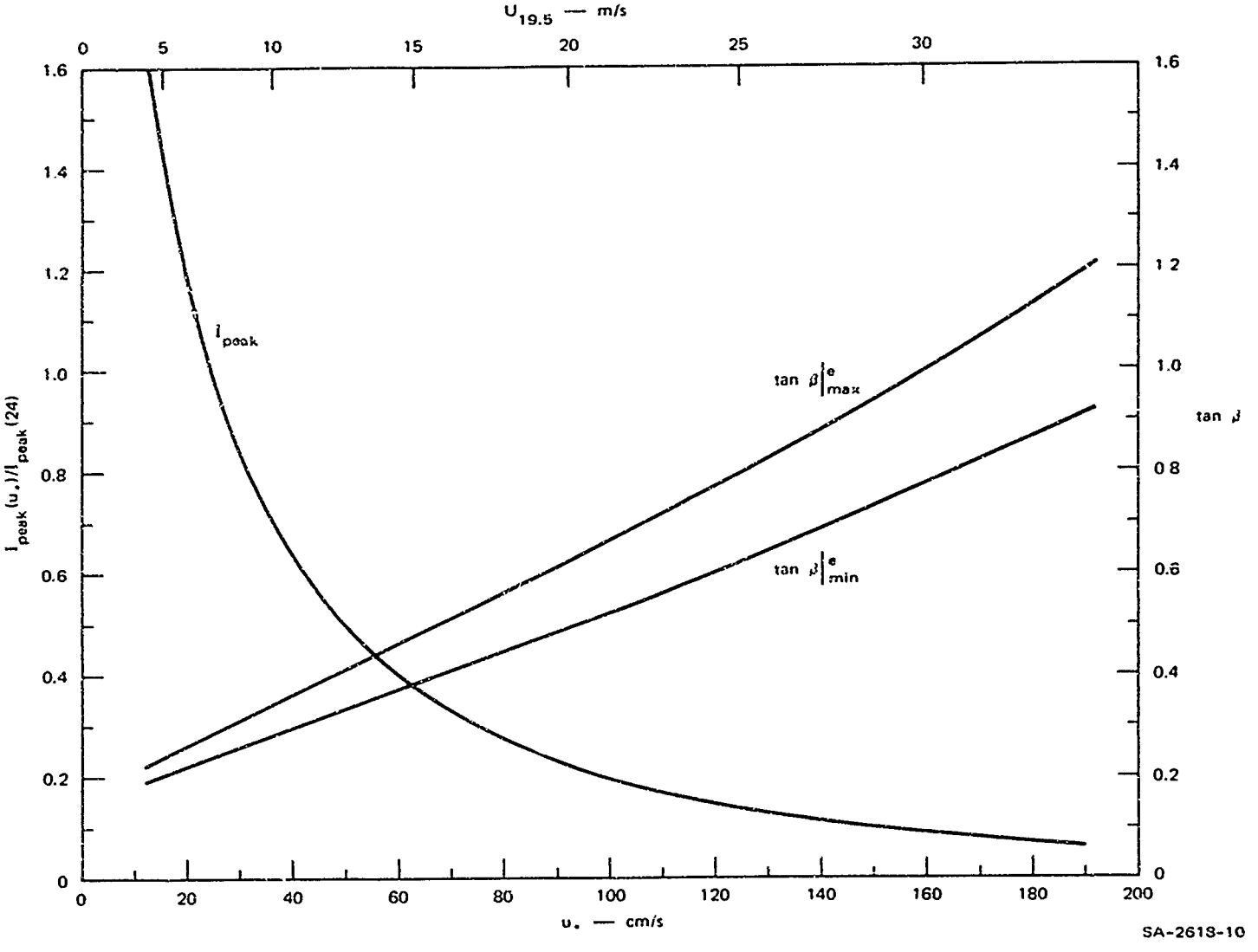

FIGURE 10 WIND DEPENDENCE OF THE PEAK INTENSITY AND ANGULAR SPREAD OF BACKSCATTERED OPTICAL RADIATION

Such lines of constant backscattered intensity--or isophotes--are shown in Figures 11 to 15 for various wind speeds. In each figure, the isophotes are shown in a polar plot against α, for values of $(I/I_{peak}) = 0.8$, 0.6, $1/e$, and 0.2. The $1/e$ isophote is shown dotted. The value $(I/I_{peak}) = 1$ corresponds to the origin in each case. The radial distance to the isophote at the azimuthal angle α is proportional to tan β, the tangent of the angle of incidence at which the intensity is the shown fraction of the peak intensity at the same wind speed. The absolute intensities at the isophotes may be compared by using the ratio $[I_{peak}(u_*)/I_{peak}(24)]$ shown on each figure.

The semimajor and semiminor axes of the ellipse of the $1/e$ isophote are characteristic of each wind speed. In Figure 10, these values are also plotted as $\tan \beta|^e_{max}$ and $\tan \beta|^e_{min}$ against wind speed. From these figures, it is evident that as the wind speed increases, the intensity distribution becomes broader as well as lower in absolute value. This is consistent with the intuitive notion that as the wind increases, the mean slope increases, spreading the incident energy over a larger angular spread. We note that the $\tan \beta|^e_{max}$ and $\tan \beta|^e_{min}$ curves have approximately the same slope. In other words, the eccentricity of the ellipses changes only to a small degree with increasing wind speed. This implies that with increasing wind the downwind slope increases only slightly faster than the crosswind slope.

At low wind speeds, the values of tan β are small even at small values of (I/I_{peak}). So for these cases, the approximation $\cos^2 \beta = 1$ is valid. However, at higher wind speeds, tan β becomes appreciable even for $(I/I_{peak}) = 0.8$, and the approximation is no longer valid. Thus, in these cases the isophotes will be ellipses only near the origin (small β), and at larger values of tan β the curves in Figures 11 to 15 do not represent isophotes. The qualitative observations about the backscattered intensity made above are still valid.

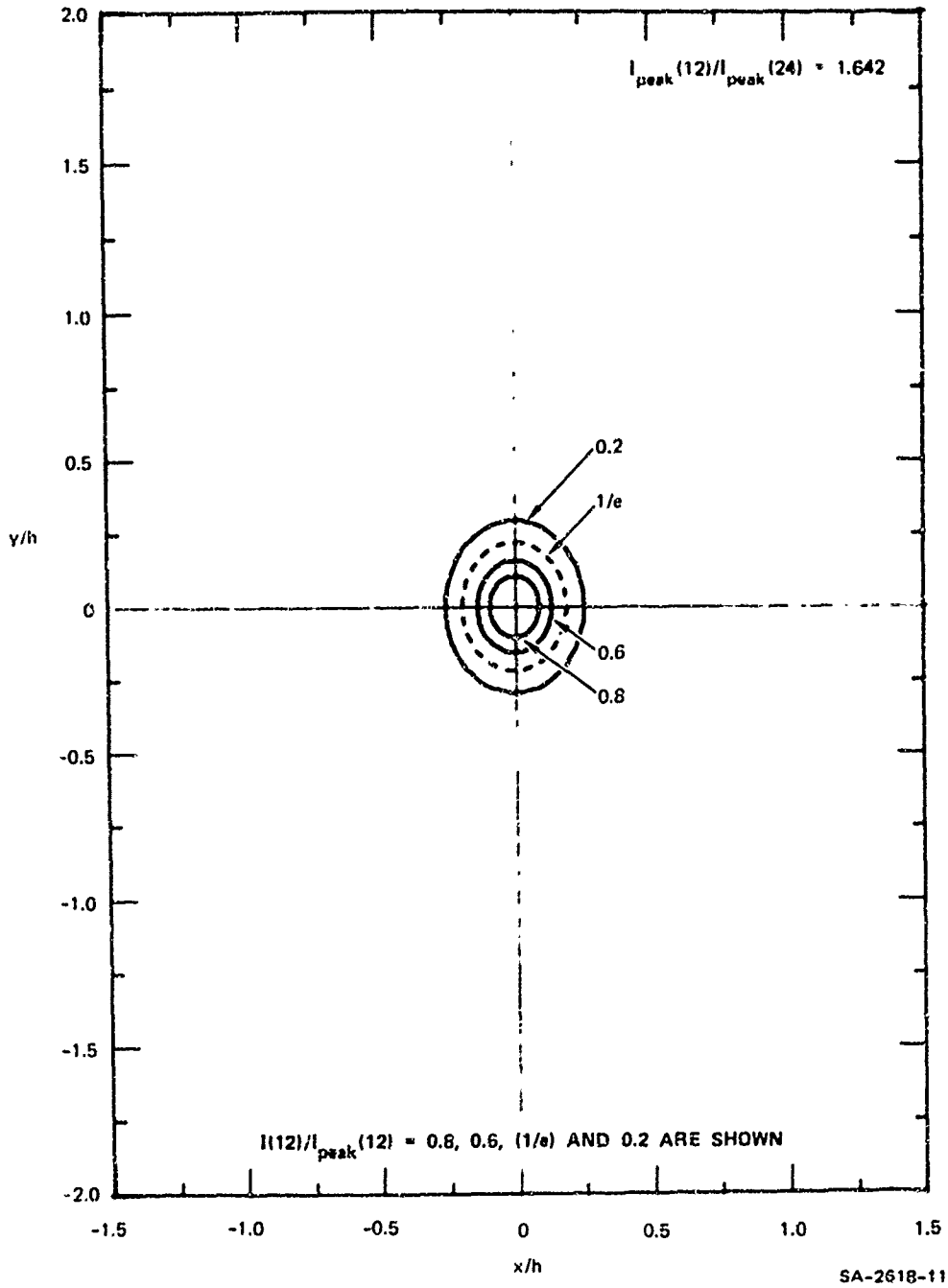

FIGURE 11 ISOPHOTES OF BACKSCATTERED INTENSITY AT $u_* = 12$ cm/s

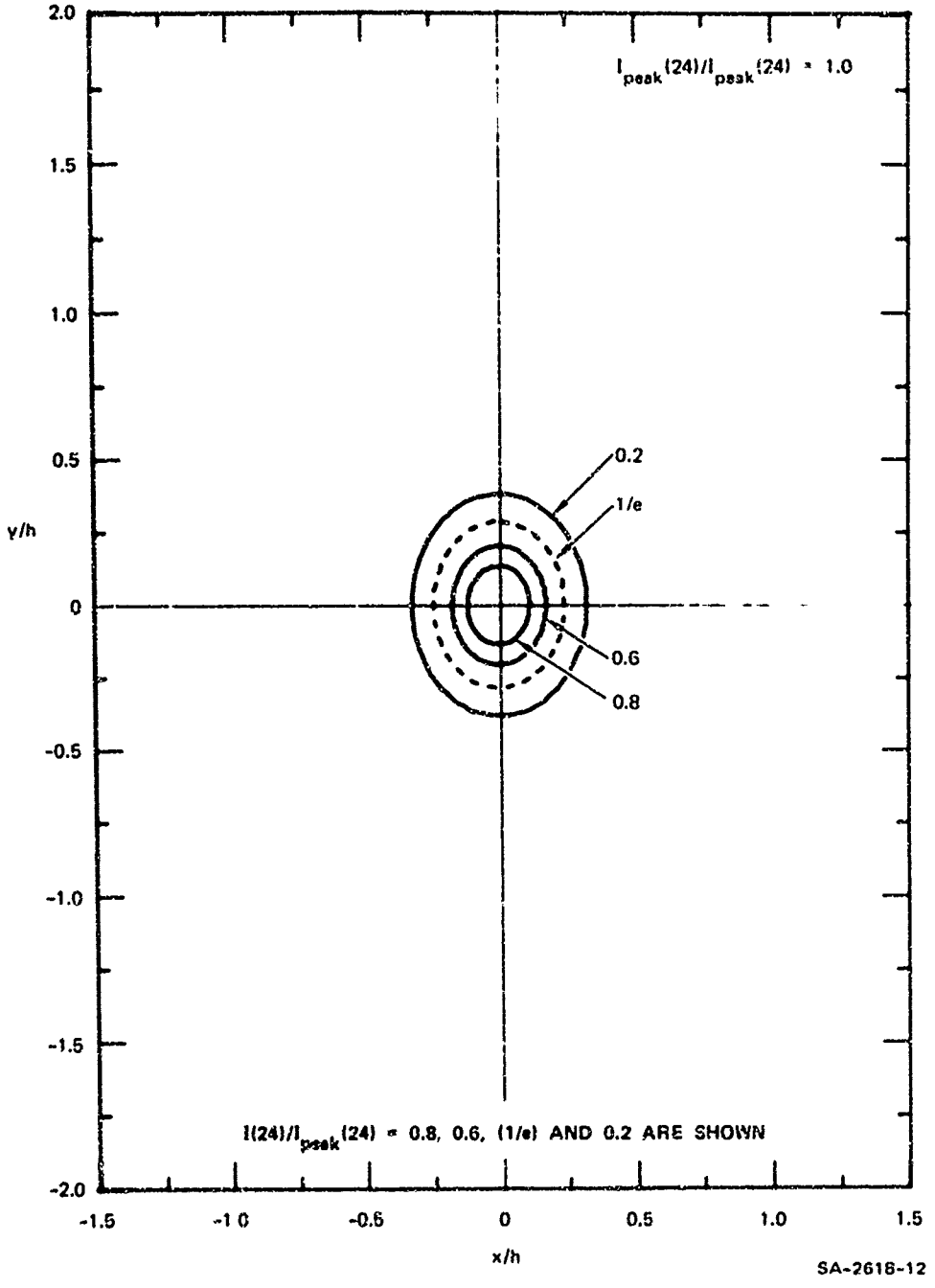

FIGURE 12 ISOPHOTES OF BACKSCATTERED INTENSITY AT $u_* = 24$ cm/s

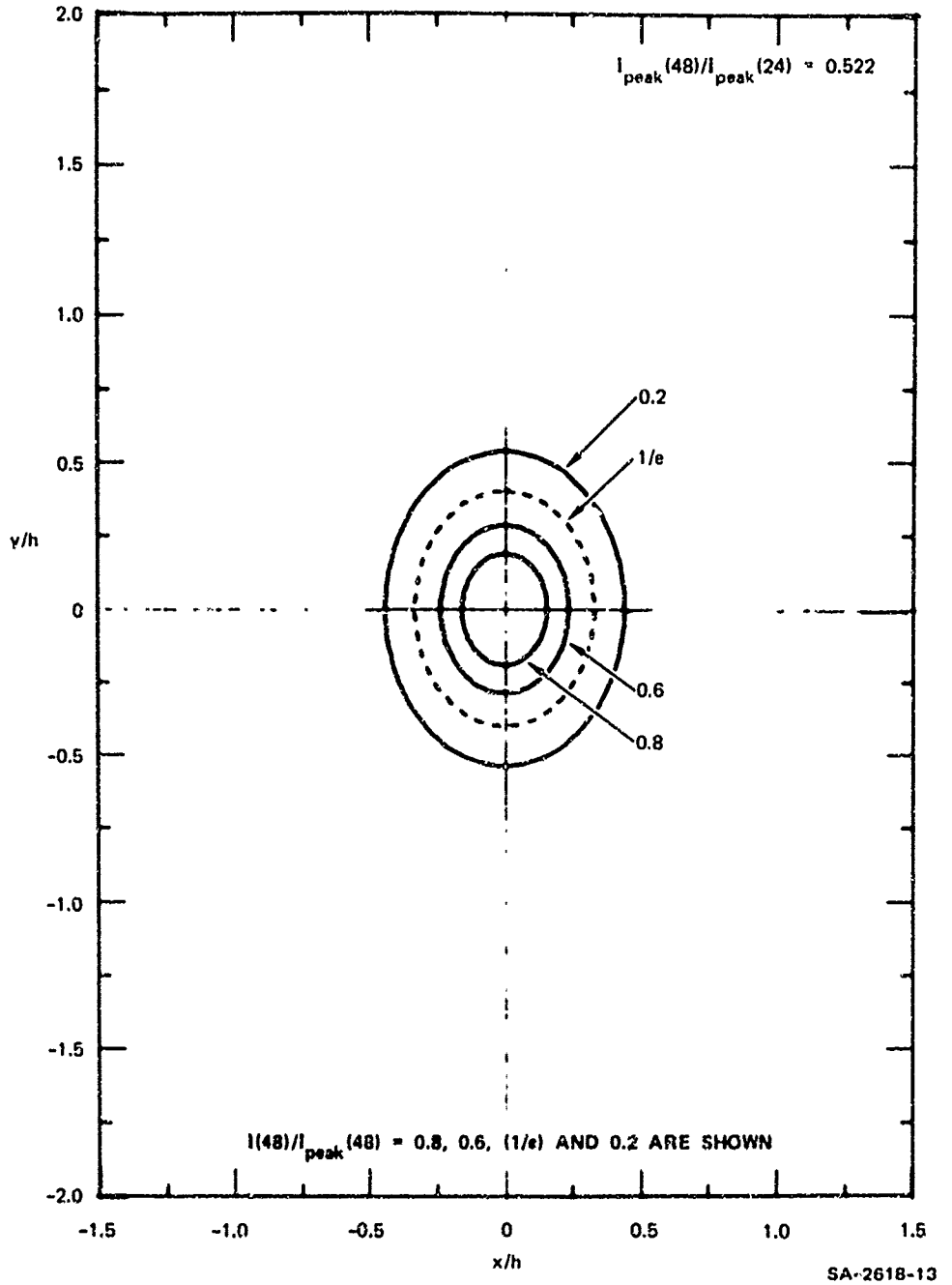

FIGURE 13 ISOPHOTES OF BACKSCATTERED INTENSITY AT $u_* = 48$ cm/s

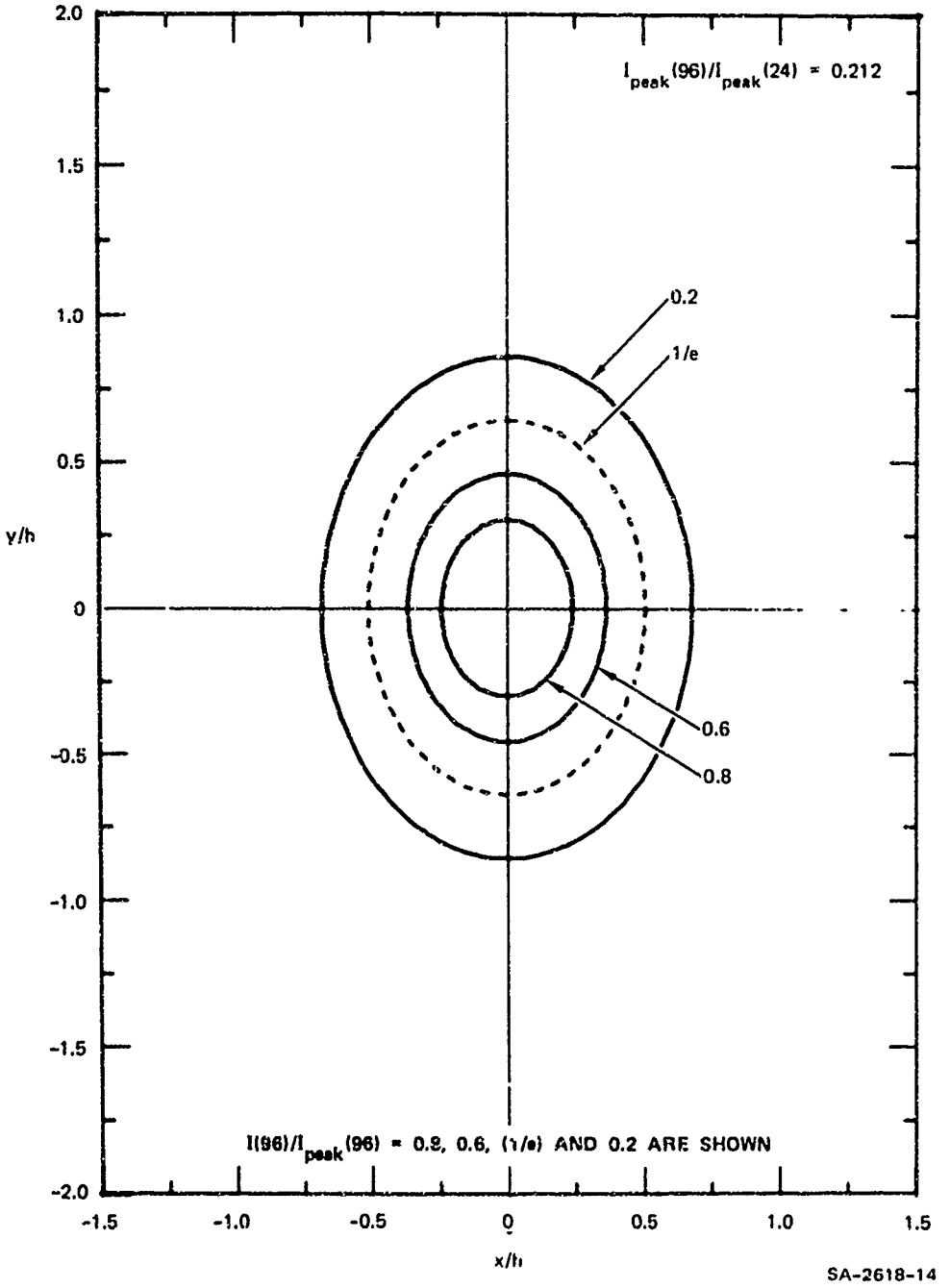

FIGURE 14 ISOPHOTES OF BACKSCATTERED INTENSITY AT $u_* = 96$ cm/s

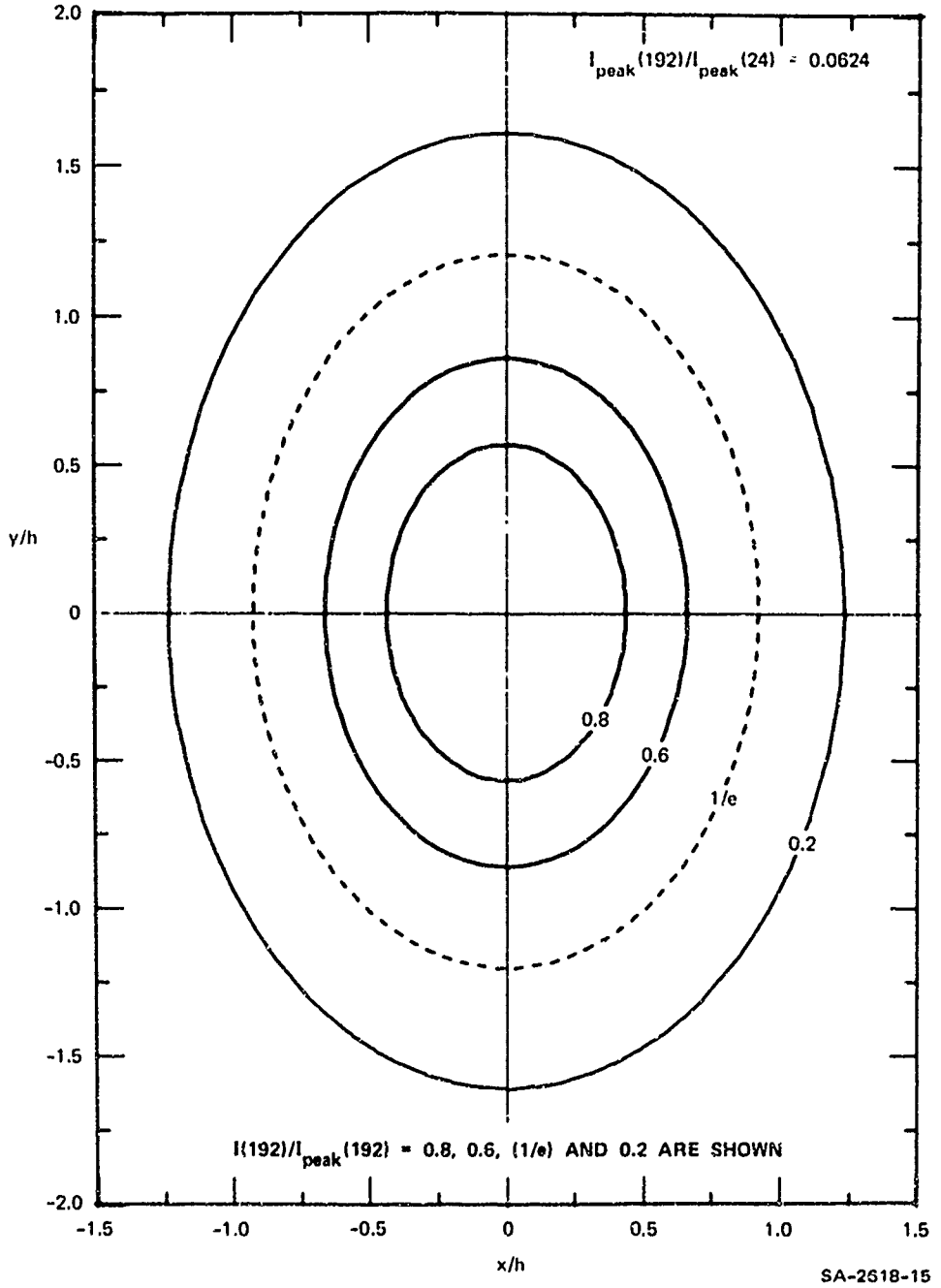

FIGURE 15 ISOPHOTES OF BACKSCATTERED INTENSITY AT $u_* = 152$ cm/s

When $\cos^2 \beta$ can no longer be approximated by unity, and to the extent that the theory developed is applicable at such angles of incidence, the curves shown in Figures 11 to 15 may still be used to determine the backscattered intensity as a function of α and β.

Equation (3.30) may be rewritten as

$$\left[\frac{\cos^2 \alpha}{\left(F_o + G_o\right)} + \frac{\sin^2 \alpha}{G_o}\right] \tan^2 \beta = -2 \ln\left(\frac{I}{I_{peak} \cos^2 \beta}\right) \quad . \quad (3.35)$$

For a constant value of the right-hand side, this equation still describes the ellipses of Figures 11 to 15, with α equal to the polar angle and $\tan \beta$ equal to the radial distance. In Figure 16,

$$I/\left[I_{peak} \cdot \cos^2 \beta\right] = \text{constant}$$

is plotted for the same values of the constants that are plotted in Figures 11 to 15. Tan β is also shown as a function of β. Thus at any point on the curves shown in Figures 11 to 15, we can determine α and $\tan \beta$, and from Figure 16, the values of β and I/I_{peak} may be read off. It should be emphasized that the validity of the theory is questionable when the small angle approximation is no longer valid.

E. Power Spectral Density of Assumed Perturbation

In order to investigate the possible effects of various types of changes at the surface that might occur as a result of various ill-defined and possibly unknown interactions, the following power spectral density was assumed for a perturbation to be superimposed on the natural "Pierson spectrum" discussed earlier.

$$S'(\ell,\phi) \triangleq S'(\ell)F'(\phi) \quad (3.36)$$

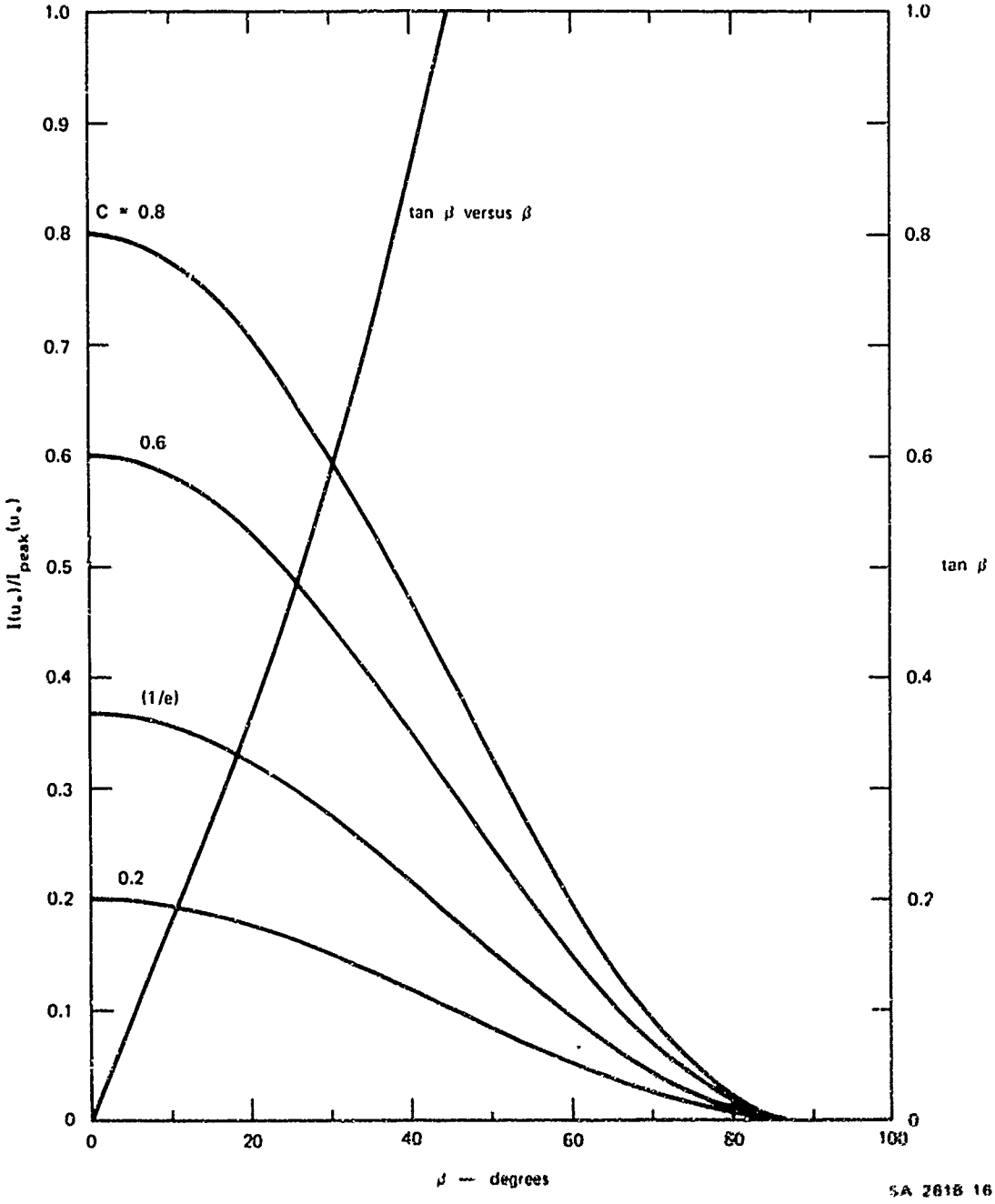

FIGURE 16 PLOTS OF $I(u_\bullet)/I_{peak}(u_\bullet) = C \cos^2 \beta$ (FOR VARIOUS VALUES OF C) AND tan β AS A FUNCTION OF β

$$F'(\phi) = \frac{1}{2\pi}\left[1 + a_1' \cos 2(\phi - \psi)\right] \qquad \text{for } -\pi < \phi < \pi \qquad (3.37)$$

$$S'(\ell) = \begin{cases} \dfrac{EGaD}{2} \exp\left\{\dfrac{3}{2}\left[\left(\dfrac{\ell_{max}}{\ell_\nu'}\right)^2 - \left(\dfrac{\ell_{max}}{\ell}\right)^2\right]\right\} \dfrac{1}{\ell^4} & \text{for } 0 < \ell < \ell_\nu' \\ \dfrac{EGaD}{2} \ell_\nu'^6 \dfrac{1}{\ell^{10}} & \text{for } \ell_\nu' < \ell < \infty \end{cases} \qquad (3.38)$$

where

$$G \triangleq \left(\frac{\ell_{max}^2 \ell_\nu'^2}{\ell_3^2 \ell_{\nu o}^2}\right)\left(\frac{8\ell_{\nu o}'^2 + 3\ell_3^2}{8\ell_\nu'^2 + 3\ell_{max}^2}\right) \qquad (3.39)$$

and $a = 8.1 \times 10^{-3}$, $D = 3.81$, $\ell_3 = 0.944\ cm^{-1}$, and $\ell_{\nu o} = 8.24\ cm^{-1}$. ℓ_{max}, E, ℓ_ν', a_1', and ψ are the variable parameters of the perturbation whose reference values are chosen to be: $\ell_{max} = \ell_3$, $E = 1$, $\ell_\nu' = \ell_{\nu o}$, $a_1' = 0.5$, and $\psi = 45°$. The reference perturbation is thus

$$S_o'(\ell,\phi) \triangleq S_o'(\ell) F_o'(\phi) \qquad (3.40)$$

$$F_o'(\phi) = \frac{1}{2\pi}\left[1 + \sin\phi \cos\phi\right] \qquad \text{for } -\pi < \phi < \pi \qquad (3.41)$$

$$S_o'(\ell) = \begin{cases} \dfrac{aD}{2} \exp\left\{\dfrac{3}{2}\left[\left(\dfrac{\ell_3}{\ell_{\nu o}}\right)^2 - \left(\dfrac{\ell_3}{\ell}\right)^2\right]\right\} \dfrac{1}{\ell^4} & \text{for } 0 < \ell < \ell_{\nu o} \\ \dfrac{aD}{2} \dfrac{\ell_{\nu o}^6}{\ell^{10}} & \text{for } \ell_{\nu o} < \ell < \infty \end{cases} \qquad (3.42)$$

The following general considerations were used to guide this choice. The general shape was chosen to be essentially similar to the Pierson spectrum. However, since the capillary range (ℓ = 1 to 10 cm^{-1}) is believed to be influenced by internal wave and other interactions with the surface, the spectral peak of the perturbation was chosen to be at the beginning of the capillary region at $\ell_3 = 0.944\ cm^{-1}$, whereas the gravity range is dominant in the Pierson spectrum. In order to obtain a few finite initial moments, the spectrum was assumed to have a power law behavior similar to the Pierson spectrum for the viscous cutoff. The spectrum was chosen to coincide for E = 1 at $\ell = \ell'_\nu = \ell_{\nu o} = 8.24\ cm^{-1}$ with the Pierson spectrum for (an arbitrarily chosen but moderate) friction velocity of $u_* = 24$ cm/s. The angular dependence chosen was again suggested by Pierson's report,[1] except that the direction of the maximum wave energy has been chosen at an angle $\circ = \pm$; i.e., at an angle $\pm$ with the wind direction. (See Figure 3.)

The integrated "energy" under the reference perturbation spectrum is calculated to be $5.804 \times 10^{-3}\ cm^2$, composed of $1.314 \times 10^{-3}\ cm^2$ in the range 0 to ℓ_3, $4.161 \times 10^{-3}\ cm^2$ in the range ℓ_3 to $\ell_{\nu o}$, and 2.84 $2.84 \times 10^{-5}\ cm^2$ in the range $\ell_{\nu o}$ to ∞. For comparison, the Pierson spectrum for a friction velocity $u_* = 24$ cm/s contains an "energy" of $8.55 \times 10^{-3}\ cm^2$ in the range ℓ_3 to $\ell_{\nu o}$, $2.84 \times 10^{-5}\ cm^2$ in the range $\ell_{\nu o}$ to ∞, and $844.5\ cm^2$ over the entire range.

Let us now consider the various parameters and their effects on the power spectrum of the perturbation. The defining equations have been arranged so that a change in one parameter does not change any of the others. The value of E determines the energy content of the perturbation with respect to the reference perturbation. The value of ℓ_{max} determines the position of the peak of $\ell S'(\ell)$. ℓ'_ν determines the location of the cutoff. (ℓ_{max} should always be less than ℓ'_ν.) The range of 0 to

1 in the value of the parameter a_1' changes the angular dependence from an isotropic behavior to a cosine behavior (see Figure 8). It has no effect on energy content. The range of ψ is evidently from $-\pi/2$ to $\pi/2$. However, due to the symmetry inherent in the Pierson spectrum, it is adequate to investigate the range 0 to $\pi/2$.

We now consider the perturbed power spectral density

$$S_T(\ell,\phi) \triangleq S(\ell,\phi) + S'(\ell,\phi) \quad . \tag{3.43}$$

The perturbed covariance function resulting from the Fourier transformation of S_T is evidently

$$R_T(\Delta r,\theta) = R(\Delta r,\theta) + R'(\Delta r,\theta) \tag{3.44}$$

where

$$R'(\Delta r,\theta) = \int_0^\infty \ell\, S'(\ell) \left\{ \int_{-\pi}^{\pi} F'(\phi)\, \exp[j\ell\Delta r \cos(\theta - \phi)]\, d\phi \right\} d\ell \quad . \tag{3.45}$$

In a manner analogous to the method for Eq. (3.13) explained in Appendix A

$$R'(\Delta r,\theta) = \int_0^\infty \ell\, S'(\ell) \left[J_o(\ell\Delta r) - a_1' \cos 2(\theta - \psi) J_2(\ell\Delta r) \right] d\ell \quad . \tag{3.46}$$

Once again we note that as long as a_1' is less than unity R' is also monotonically decreasing near the origin, and the relative maxima do not approach the value at $\Delta r = 0$. It is, however, interesting to note that for a value of $a_1' = 1$, the first relative maximum of R' will occur at $\Delta r = 6.9$ cm. Whether R_T has a maximum at this position depends on the relative values of R and R'.

The second moment of $S'(\ell,\phi)$ has the form (see Appendix A)

$$M_2' = F_1 \cos^2 \theta + 2H_1 \sin \theta \cos \theta + G_1 \quad . \tag{3.47}$$

Using Eq. (3.17), we may write

$$M_2 + M_2' = \left(F_o + F_1 + G_o + G_1\right) \cos^2 \theta + 2H_1 \sin \theta \cos \theta + \left(G_o + G_1\right) \sin^2 \theta \quad . \tag{3.48}$$

Using arguments similar to those employed in the unperturbed case, we write

$$\begin{aligned} \left\langle \gamma_T(\Delta u,\Delta v) \right\rangle &= \exp\left[-j \frac{k}{R} \left(\Delta u x_o \quad \Delta v y_o\right)\right] \\ &\quad \times \exp\left\{-k^2(\cos \beta + \cos B)^2 \left[R_T(0,0) - R_T(\Delta u,\Delta v)\right]\right\} \\ &= \exp\left[-j \frac{k}{R} \left(\Delta u x_o + \Delta v y_o\right)\right] \\ &\quad \times \exp\left[-\left(k^2/2\right)(\cos \beta + \cos B)^2 \left(M_2 + M_2'\right) \Delta r^2\right] \end{aligned} \tag{3.49}$$

where we have neglected terms in Δr of order higher than 2 for reasons based on the behavior of $\langle \gamma_T \rangle$ and R_T, as discussed in Appendix B. It is noted that the expression for $[R_T(0,0) - R_T(\Delta u,\Delta v)]$ is a quadratic form which may be diagonalized by a suitable coordinate transformation. Using Eqs. (2.31), (3.49), and (3.26), the scattered intensity distribution is given by

$$\left\langle I_T(\xi,\eta)\right\rangle = \frac{2Z_o P_r \cos^4\beta}{(\lambda h)^2}$$

$$\times\iint_{-\infty}^{\infty}\exp\left\{-\frac{k^2}{2}(\cos\theta+\cos B)^2\left[\left(F_o+F_1+G_o+G_1\right)\Delta u^2+2H_1\Delta u\Delta v+\left(G_o+G_1\right)\Delta v^2\right]\right\}$$

$$\times\exp[-jk(\xi\Delta u+\eta\Delta v)]\,d\Delta u d\Delta v \quad . \tag{3.50}$$

The quadratic form in the exponent may be diagonalized using the rotations

$$\xi' = \xi\cos\delta+\eta\sin\delta \quad , \quad \Delta u' = \Delta u\cos\delta+\Delta v\sin\delta$$

$$\eta' = -\xi\sin\delta+\eta\cos\delta \quad , \quad \Delta v' = -\Delta u\sin\delta+\Delta v\cos\delta \tag{3.51}$$

to obtain

$$\left\langle I_T(\xi',\eta')\right\rangle = \frac{2Z_o P_r \cos^4\beta}{(\lambda h)^2}\iint_{-\infty}^{\infty}\exp\left\{-\frac{k^2}{2}(\cos\theta+\cos B)^2\left[C\Delta u'^2+D\Delta v'^2\right]\right\}$$

$$\times\exp[-jk(\xi'\Delta u'+\eta'\Delta v')]\,d\Delta u' d\Delta v' \tag{3.52}$$

where

$$C = \frac{1}{2}\left[\left(F_o+F_1+2G_o+2G_1\right)+\sqrt{\left(F_o+F_1\right)^2+4H_1^2}\right] \tag{3.53}$$

$$D = \frac{1}{2}\left[\left(F_o+F_1+2G_o+2G_1\right)-\sqrt{\left(F_o+F_1\right)^2+4H_1^2}\right] \tag{3.54}$$

$$\cos \gamma = \left(\frac{2H_1^2}{\left\{ \left[\left(F_o + F_1 \right)^2 + 4H_1^2 \right]^{1/2} - \left(F_o + F_1 \right) \right\} \left[\left(F_o + F_1 \right)^2 + 4H_1^2 \right]^{1/2}} \right)^{1/2} \qquad (3.55)$$

$$\sin \delta = \left\{ \frac{\left[\left(F_o + F_1 \right)^2 + 4H_1^2 \right]^{1/2} - \left(F_o + F_1 \right)}{2 \left[\left(F_o + F_1 \right)^2 + 4H_1^2 \right]} \right\}^{1/2} . \qquad (3.56)$$

We note that C, D, and δ are functions of u_*, ℓ_{max}, ℓ_o', E, a_1', and ψ. Performing the Fourier transformation, we get

$$\left\langle I_T(\xi', \eta') \right\rangle = \frac{Z_o P_r}{\pi h^2 \sqrt{CD}} \frac{\cos^4 \beta}{(\cos \beta + \cos B)^2} \times \exp\left[- \frac{1}{2(\cos \beta + \cos B)^2} \left(\frac{\xi'^2}{C} + \frac{\eta'^2}{D} \right) \right] . \qquad (3.57)$$

For the backscatter case, it may be shown that

$$\xi' = 2 \sin \beta \cdot \cos(\alpha - \delta) \quad , \quad \eta' = 2 \sin \beta \cdot \sin(\alpha - \delta) \qquad (3.58)$$

and

$$\langle I_T(\alpha, \beta) \rangle_B = \frac{Z_o P_r \cos^2 \beta}{4\pi h^2 \sqrt{CD}} \times \exp\left\{ - \frac{\tan^2 \beta}{2} \left[\frac{\cos^2(\alpha - \delta)}{C} + \frac{\sin^2(\alpha - \delta)}{D} \right] \right\} . \qquad (3.59)$$

On comparison with Eq. (3.30) for the intensity in the unperturbed case, it is seen that the major change is a rotation of the distribution by an angle δ.

Once again we make the approximation $\cos^2 \theta = 1$ to rewrite Eq. (3.59)

$$\left[\frac{\cos^2(\alpha - \xi)}{C} + \frac{\sin^2(\alpha - \xi)}{D}\right]\tan^2 \beta = \text{constant} \qquad (3.60)$$

and, as for the unperturbed case, the isophotes are ellipses but tilted to the coordinate axes by the angle ξ. (When the approximation $\cos^2 \theta = 1$ is no longer valid, considerations similar to those in the unperturbed case apply.) The effect of the various parameters are considered in the next section.

It is of interest to rewrite Eq. (3.49), using Eq. (3.23), as

$$\left\langle \gamma_T(\Delta u, \Delta v)\right\rangle = \langle \gamma(\Delta u, \Delta v)\rangle \cdot \exp\left[-\left(k^2 2\right)(\cos \theta + \cos B)^2 M_2' \Delta r^2\right]$$

$$\triangleq \langle \gamma\rangle \langle \gamma'\rangle \quad . \qquad (3.61)$$

From the convolution theorem, it follows that

$$\left\langle I_T\right\rangle = \langle I\rangle * \mathfrak{F}\{\langle \gamma'\rangle\} \qquad (3.62)$$

where * denotes a convolution in the space domain.

From the form of the functions γ and γ', both γ and γ' are seen to be two-dimensional Gaussians, even though it is not immediately obvious from the expression for $\langle \gamma'\rangle$ since a coordinate rotation is required to cast it in the standard form. Their Fourier transforms $\langle I\rangle$ and $\mathfrak{F}\{\langle \gamma'\rangle\}$ then must also be Gaussian. The convolution of a two-dimensional Gaussian with another results in yet another Gaussian $\langle I_T\rangle$. In this case, it turns out to be analytically more convenient to perform the Fourier transformation directly than the convolution.

F. Parametric Analysis of the Effect of Perturbations

As indicated in the previous section, a parametrized power spectral density was chosen for the perturbation, largely on heuristic grounds, and an analytical expression was developed for the average backscattered intensity. The variable parameters of the perturbation spectrum are:

- ℓ_{max}, the position of the maximum.
- ℓ', the position of the short-wavelength cutoff.
- E, the energy parameter of the perturbation.
- a_1', the factor controlling the angular dependence of the power spectrum.
- γ, the angle the perturbation makes with the wind direction.

Since these parameters can be varied independently of each other, it is evident that an infinite variety of conditions is possible. To limit this variety to a reasonable number, it was decided to choose a standard condition and vary each of the parameters about this condition. Table 1 summarizes the conditions studied.

In Figure 17, $\ell S'(\ell)$ is plotted against log ℓ for various values of ℓ_{max} and E to show the spectral shape of the perturbations. For purposes of comparison, the Pierson spectrum is also shown for several values of u_*. Since it is difficult to appreciate from this log-log plot, that the energy is held constant while the parameters are changed, $\ell^2 S'(\ell)$ is plotted against log ℓ in Figure 18. In this case the area under the curve, equal to the energy, is the same as the area under the curve of $\ell S'(\ell)$ versus ℓ, even though the spectral maximum is shifted. Note that a_1' and γ have no influence on this plot of the power spectrum; i.e., for all values of a_1' and γ, the power spectrum of the perturbation is the same as the standard. Figure 8 conveys the effect of a_1' on the spectrum.

Table 1

PARAMETERS OF THE PERTURBATION

Parameter			
Description	Symbol	Standard Value	Range of Variation
Peak position	ℓ_{max}	0.944 cm^{-1}	0.01-10 cm^{-1}
Energy parameter	E	1	0-10
Short-wavelength cutoff	ℓ'_{ν}	8.24 cm^{-1}	1-20 cm^{-1}
Angular dependence	a'_1	0.5	0-2
Orientation with respect to wind	ψ	45°	0°-90°

ψ rotates this pattern about the origin of the angle ψ. Note also that for E = 0, the perturbation is identically zero, and the results correspond to the unperturbed case.

Figures 19 to 28 show the effects of changing the various parameters on the quantities entailed in determining the backscattered intensity distribution. In Figures 19, 21, 23, 25, and 27, I_{peak} refers to the backscattered intensity at normal incidence ($\beta = 0$), relative to the value for the standard perturbation. Tan $\beta|^{e}_{max}$ and tan $\beta|^{e}_{min}$ respectively refer to the semimajor and semiminor axes of the (1/e) isophote. In other words, they correspond to the value of β when the intensity has fallen to (1/e) of the value at $\beta = 0$. The angle δ is the angle by which the symmetry axes of the isophotes are rotated from the direction of the wind.

The effect of the various parameters is portrayed in a different manner in Figures 20, 22, 24, 26, and 28, where isophotes for which $I = (1/e)\, I^{standard}_{peak}$ derived from Eq. (3.60) are shown for two selected values of the parameters, in addition to the standard. The intensity on

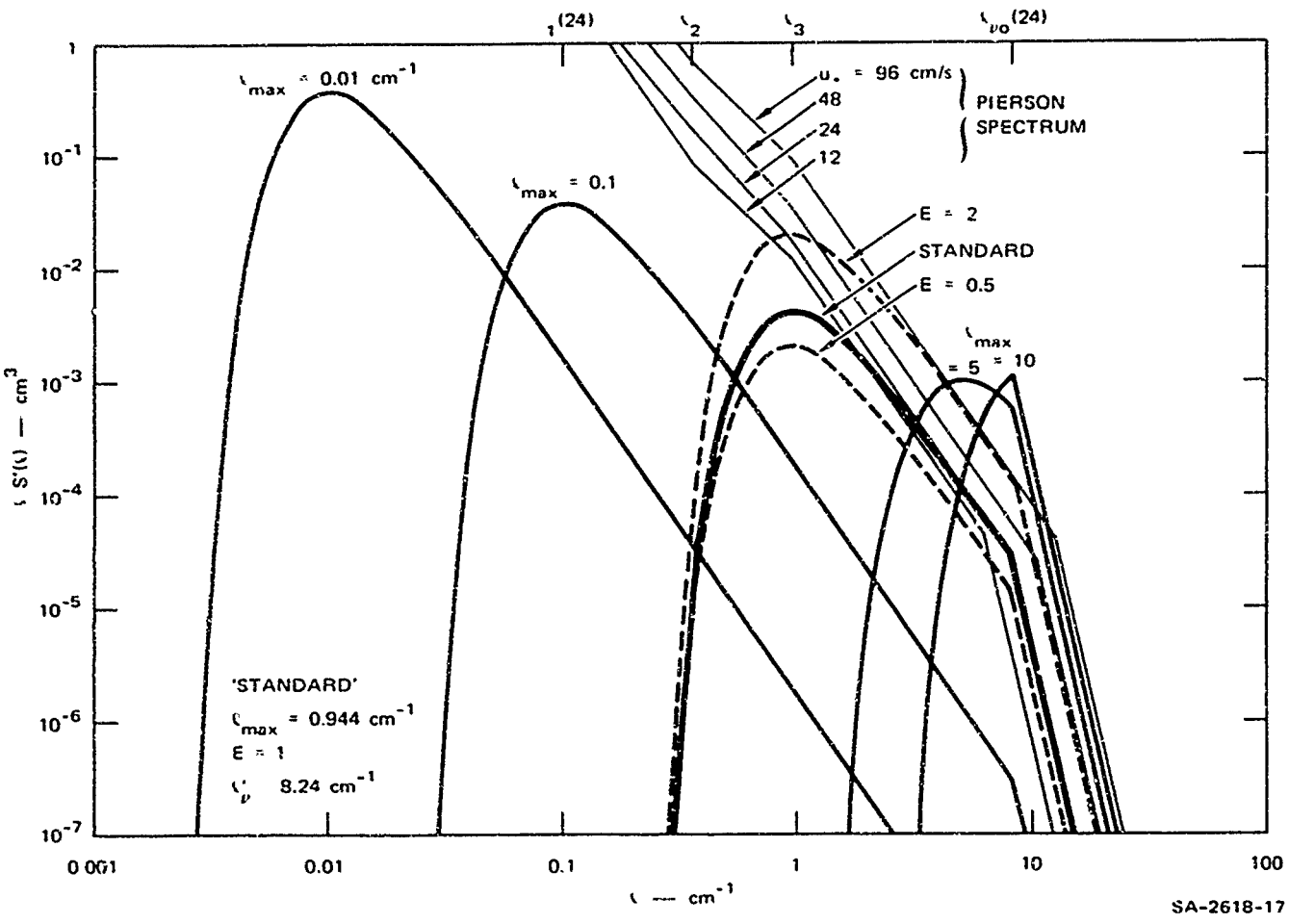

FIGURE 17 POWER SPECTRAL DENSITY OF THE PERTURBATION FOR VARIOUS VALUES OF THE PARAMETERS

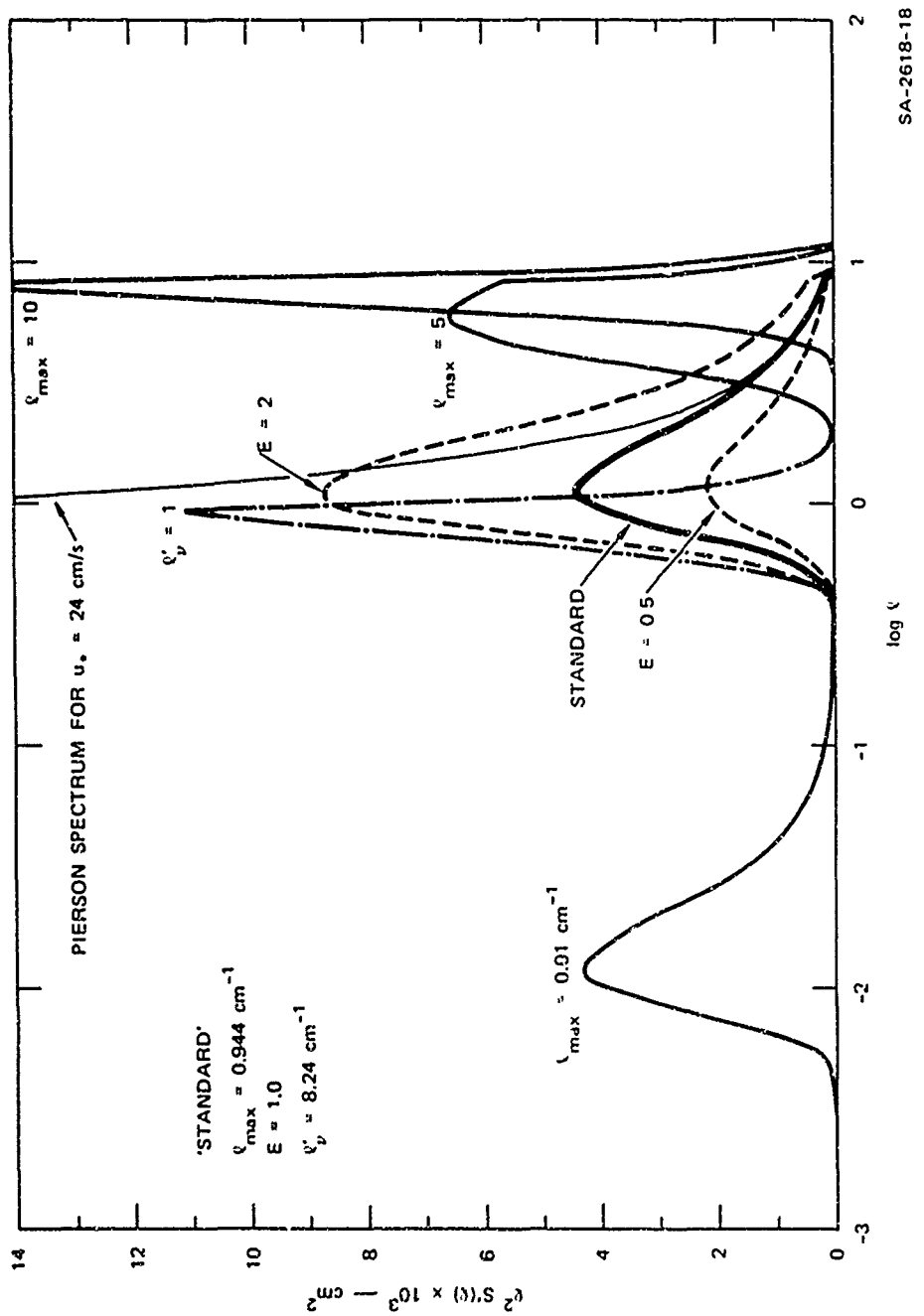

FIGURE 18 ENERGY PRESERVING PLOT OF ℓ^2 S'(ℓ) AS A FUNCTION OF log ℓ FOR THE PERTURBATION FOR VARIOUS VALUES OF THE PARAMETERS

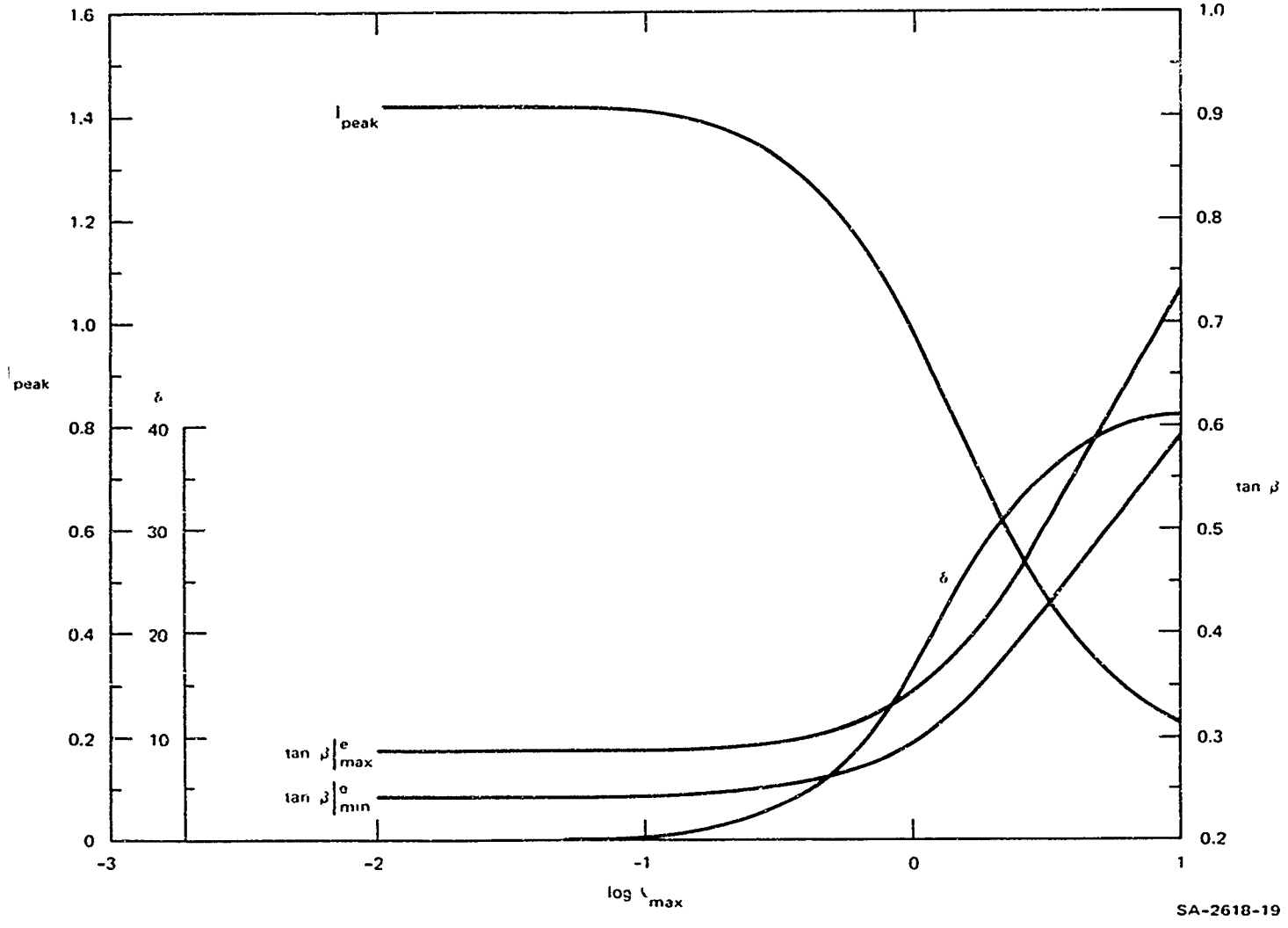

FIGURE 19 EFFECT OF THE SPECTRAL POSITION OF THE PERTURBATION

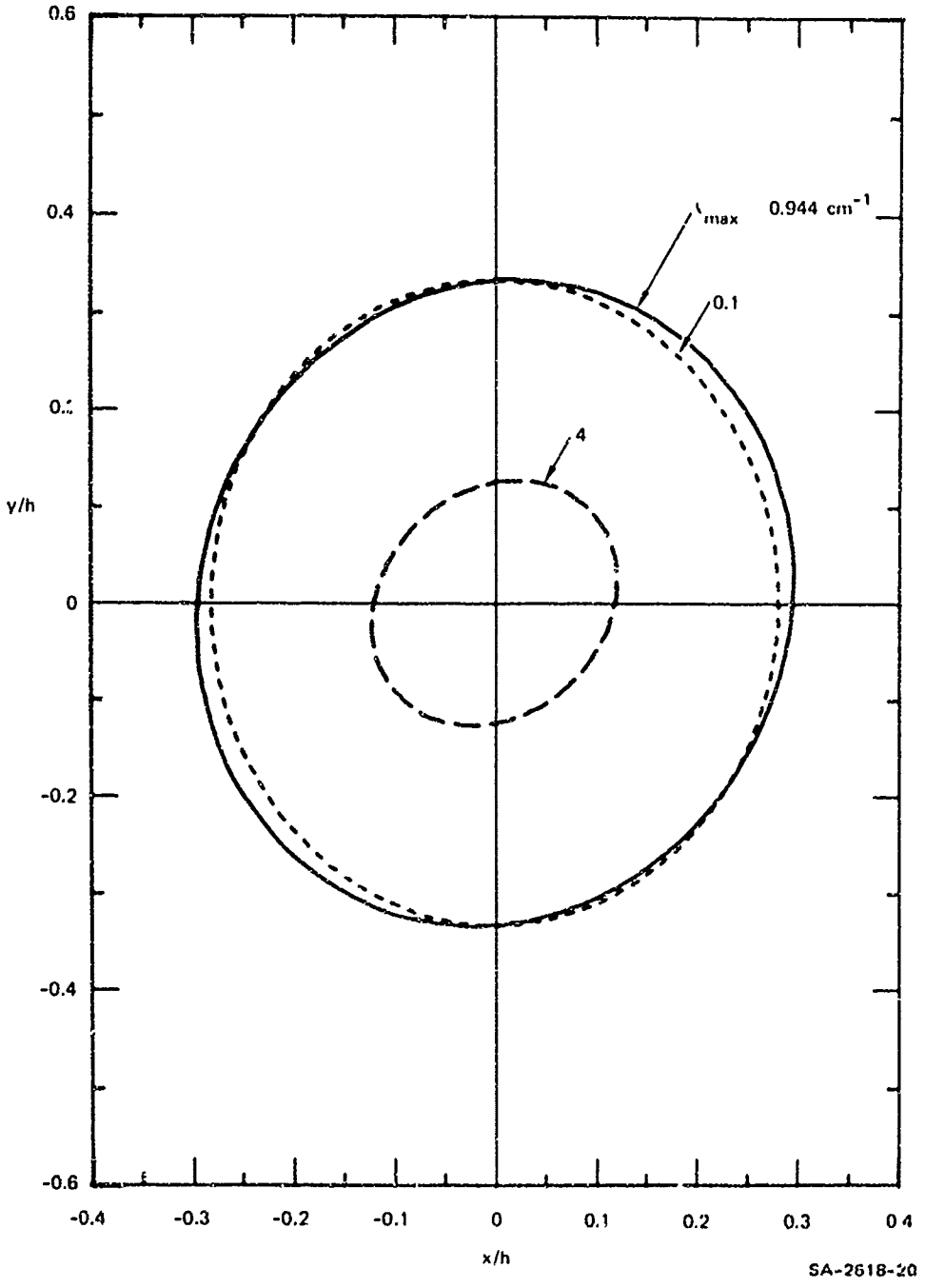

FIGURE 20 EFFECT OF THE SPECTRAL POSITION OF THE PERTURBATION: (1/e) ISOPHOTES FOR SELECTED PARAMETER VALUES

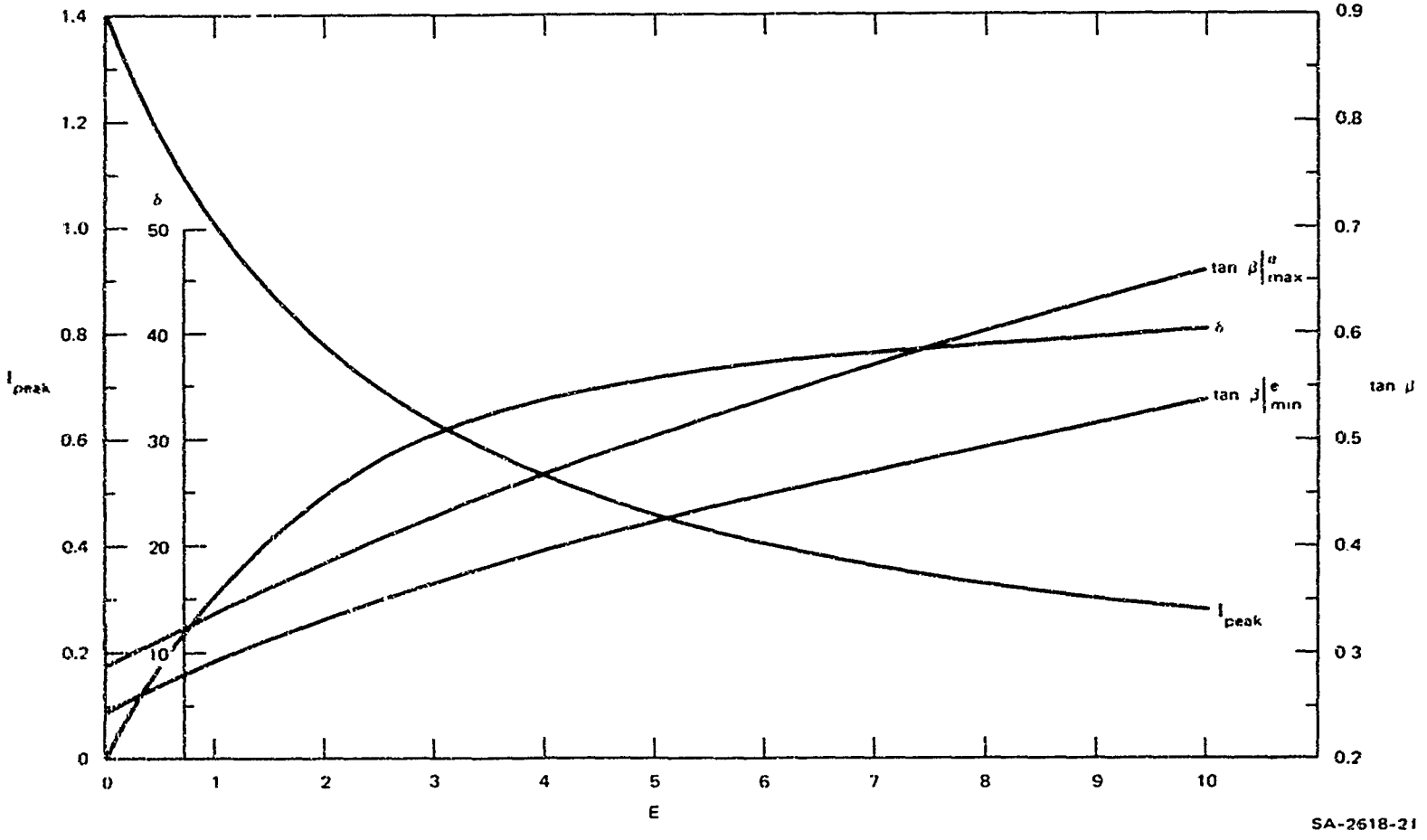

FIGURE 21 EFFECT OF THE ENERGY CONTENT OF THE PERTURBATION

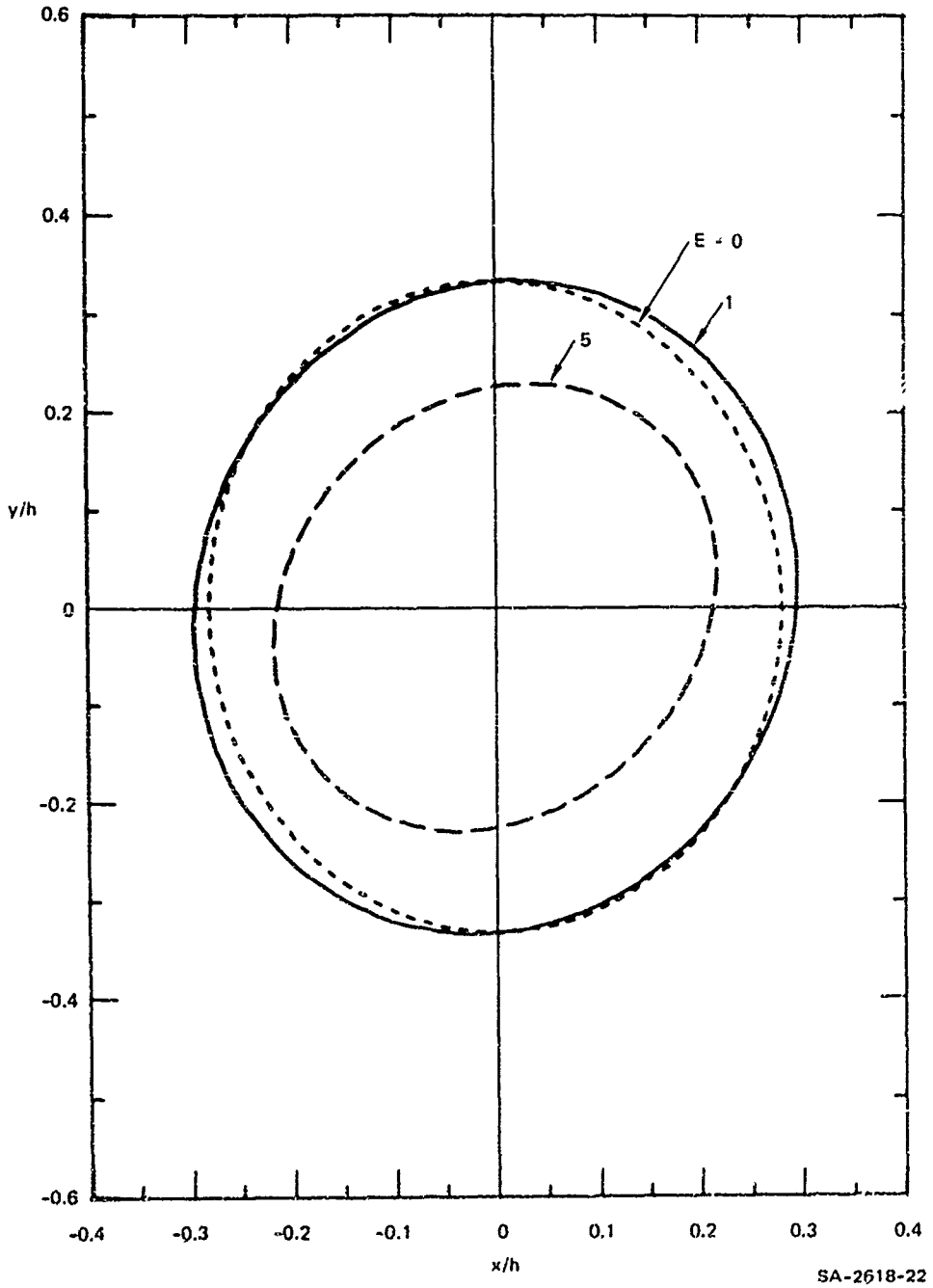

FIGURE 22 EFFECT OF THE ENERGY CONTENT OF THE PERTURBATION: (1/e) ISOPHOTES FOR SELECTED PARAMETER VALUES

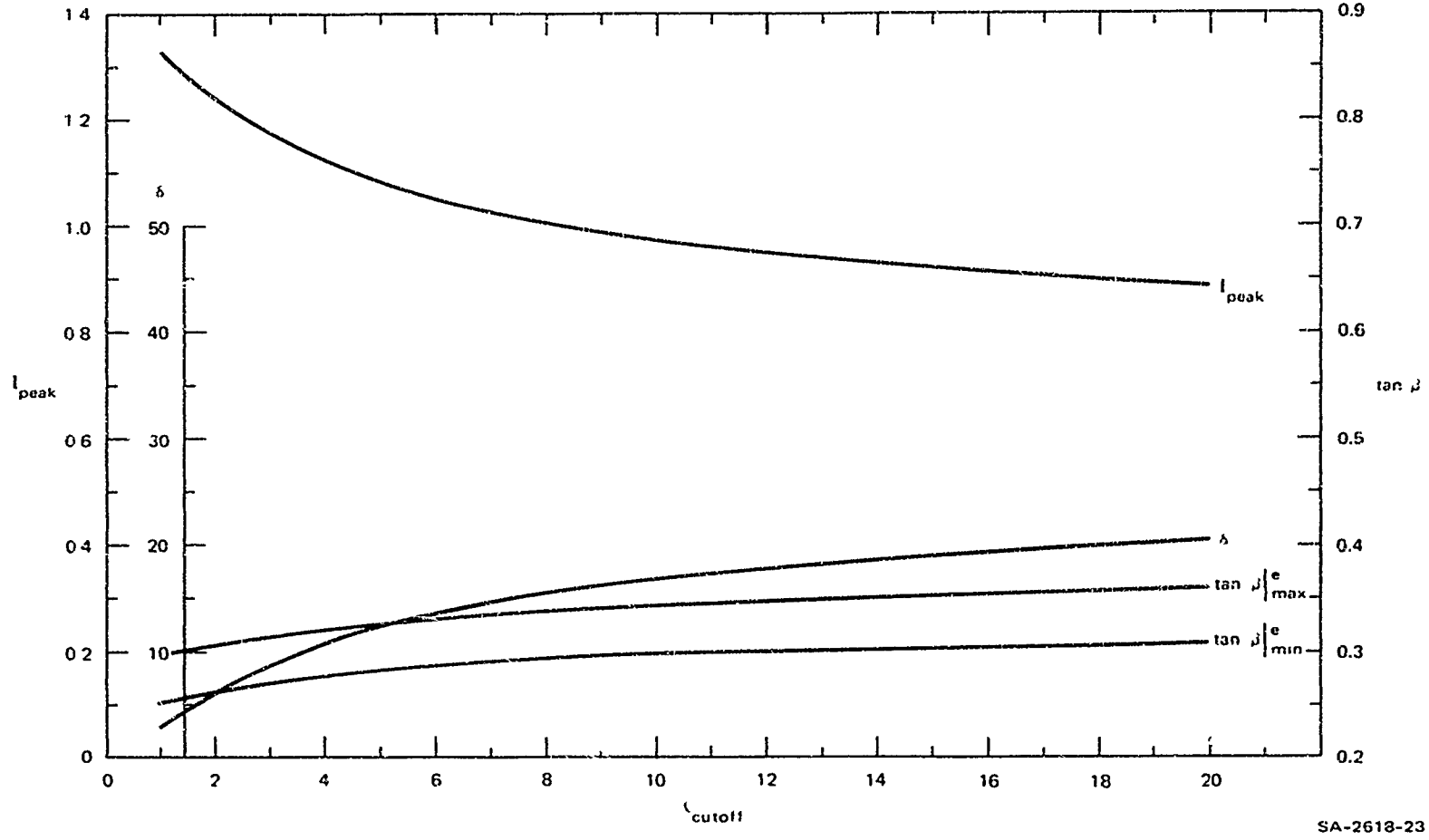

FIGURE 23 EFFECT OF THE POSITION OF THE VISCOUS CUT-OFF

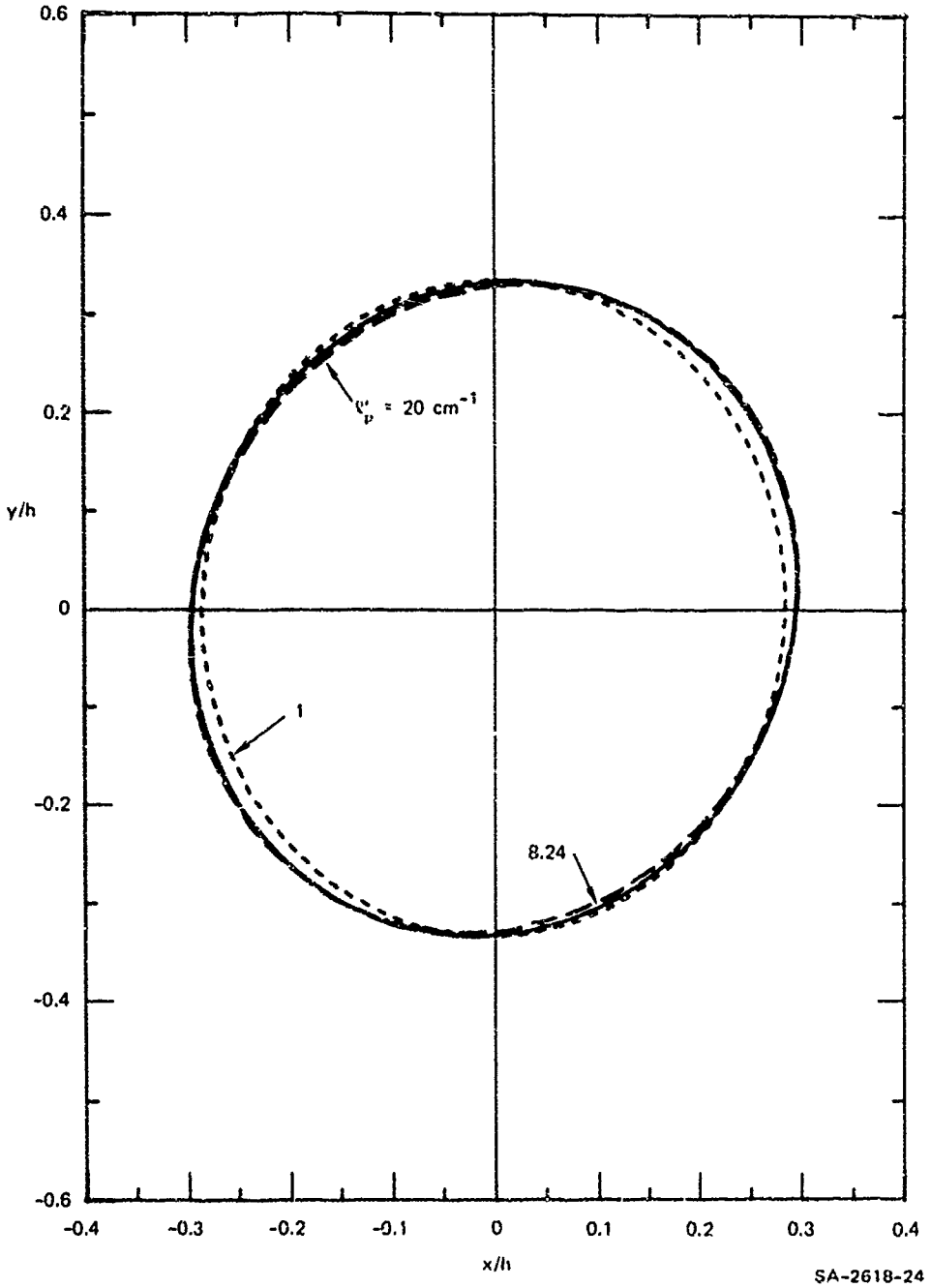

FIGURE 24 EFFECT OF THE POSITION OF THE VISCOUS CUT-OFF: (1/e) ISOPHOTES FOR SELECTED PARAMETER VALUES

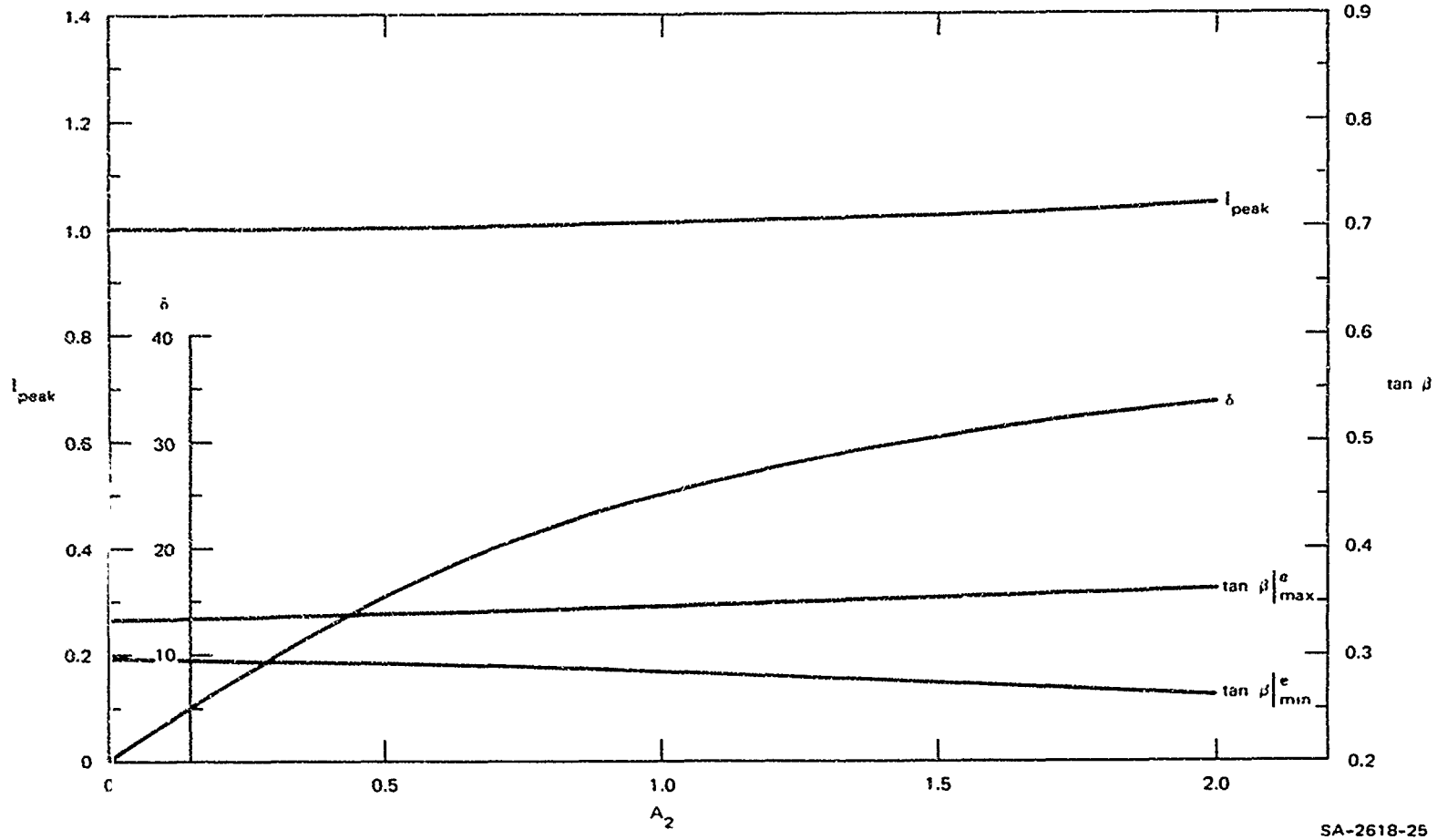

FIGURE 25 EFFECT OF THE ANGULAR DISTRIBUTION

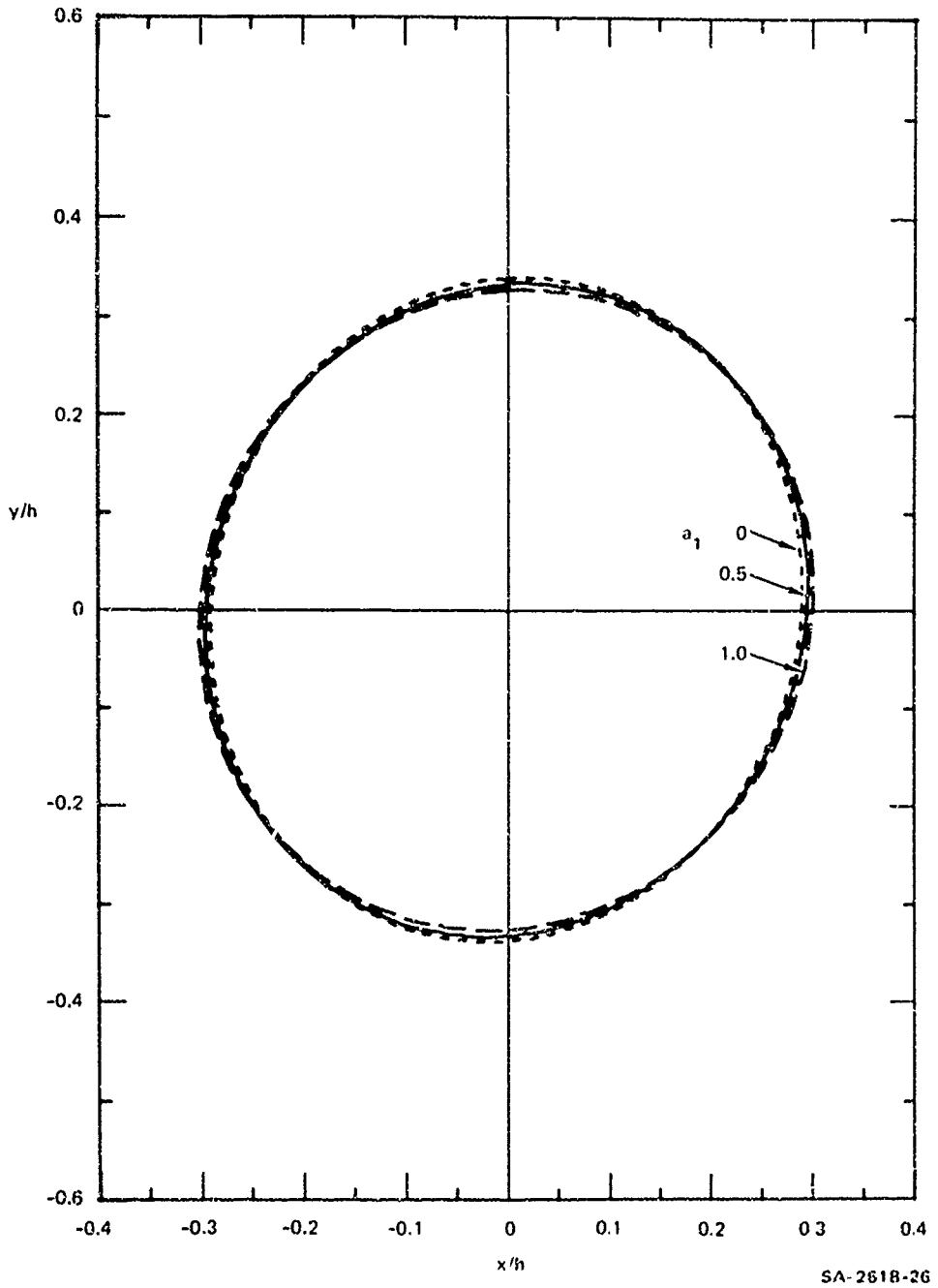

FIGURE 26 EFFECT OF THE ANGULAR DISTRIBUTION: (1/e) ISOPHOTES FOR SELECTED PARAMETER VALUES

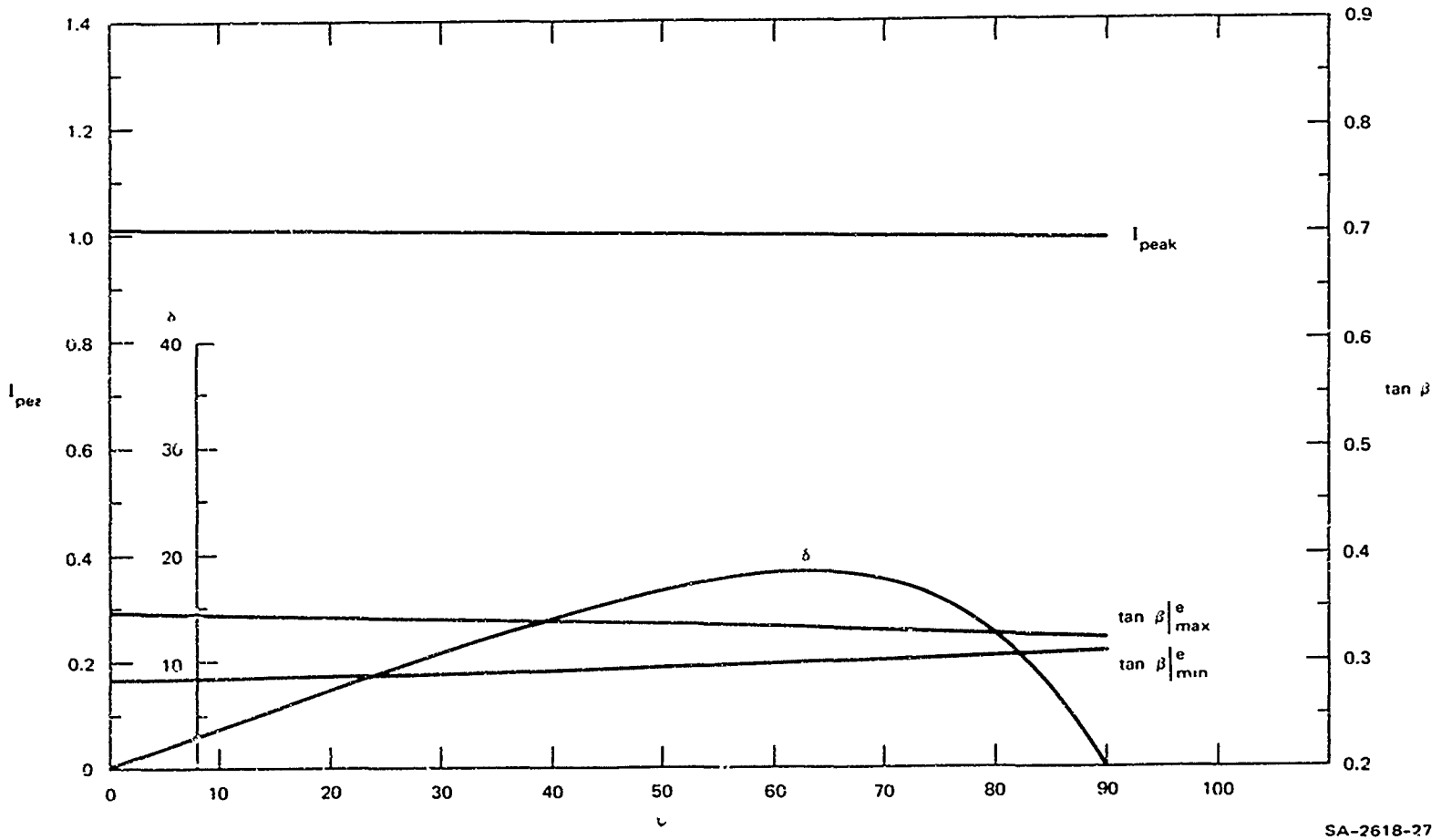

FIGURE 27 EFFECT OF THE ORIENTATION OF THE PERTURBATION

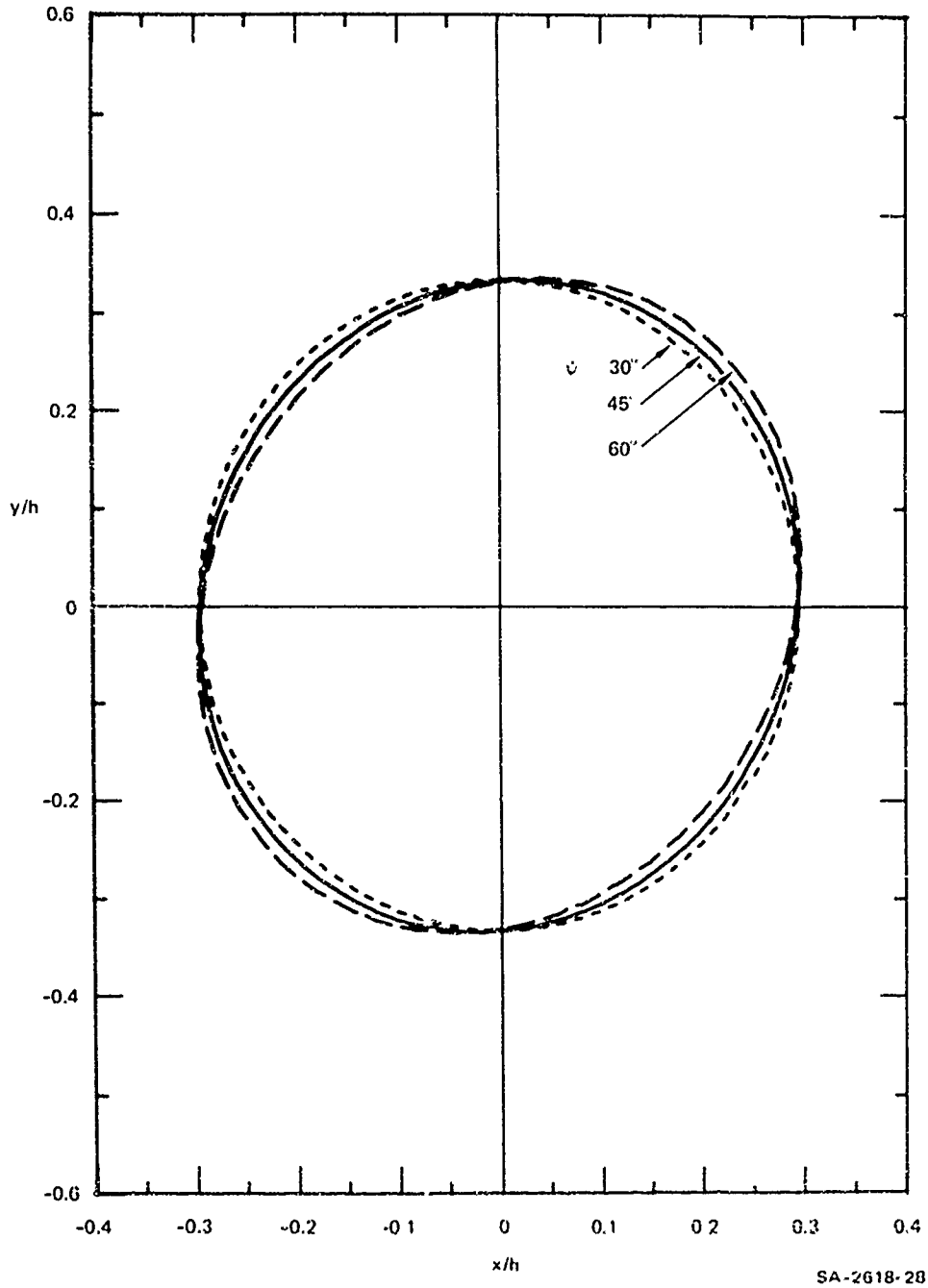

FIGURE 28 EFFECT OF THE ORIENTATION OF THE PERTURBATION: (1/e) ISOPHOTES FOR SELECTED PARAMETER VALUES

all the isophotes is (1/e) of the value of the peak intensity (normal incidence, $\beta = 0$) when the standard perturbation is superimposed on the Pierson spectrum ($E = 0$). The change in the angular spread and the rotation of the symmetry axes are to be noted.

While each of these perturbing functions contain an almost insignificant amount of energy when compared to the total energy contained in the Pierson spectrum for $u_* = 24$ cm/s, it is clear from these figures that some of these perturbations can greatly alter the scattered intensity distribution, especially when they are situated in the capillary region.

For example, in Figure 19 as the peak of the perturbing function is moved from outside the capillary region to well within the capillary region, the peak of the scattered intensity drops rapidly, and there is a corresponding broadening of the distribution as indicated by $\tan \beta|^{e}_{max}$ and $\tan \beta|^{e}_{min}$. Moreover, while a perturbation outside the capillary region has little effect on the symmetry of the scattered radiation, a perturbation well within the capillary region can rotate the symmetry axes of the scattered radiation by a large angle δ. Thus, it can be concluded that, at least for the perturbations assumed here, the scattered intensity distribution is more sensitive to perturbations within the capillary region than to perturbations at lower wave numbers.

On the other hand, Figure 23 indicates that moving the high wavenumber cutoff to even higher wave numbers has relatively little effect on the scattered intensity. However, moving this cutoff to lower wave numbers does affect the scattered intensity, particularly for $\ell'_2 \lesssim 1$ cm^{-1}. However, this may be due to the large contribution made to the perturbation by the spectral region near 1 cm^{-1}.

Increasing the [illegible]th (amount of energy) of the standard perturbation also greatly a[illegible] the scattered intensity distribution, as

indicated by Figure 21. Again it is clear that adding energy to the capillary region of the spectrum causes more scattering, as evidenced by the peak intensity falling and $\tan \beta|^{e}_{max}$ and $\tan \beta|^{e}_{min}$ increasing.

We note from Figure 25 that changing the angular shape of the perturbation from isotropic behavior ($a_1' = 0$) to cosine-square behavior ($a_1' = 1$) essentially leaves the peak scattered intensity unchanged but affects the symmetry axes of the scattered intensity indicated by δ and makes the distribution more elliptical.

Similarly, Figure 27 shows that changing the orientation of the perturbation relative to the wind direction has essentially no effect on the peak scattered intensity but does affect the eccentricity of the elliptical intensity distribution (causing it to be more circular) and the orientation of the symmetry axes.

The change of δ with ψ in Figure 27 is interesting. It shows a maximum and decreases toward zero. In other words, even though the direction of the perturbation continues to greater angles, the intensity distribution returns to orientation along the wind. On closer examination, it is found that the behavior of δ at $\psi > 45$ is dependent on the relative values of F_o and F_1 in Eqs. (3.48) and (3.53)-(3.56), which is governed by the value of the energy content of the perturbation. It is found that δ returns to zero at $\psi = 90$, when $E < 1.675$, and that δ continues on to 90° at $\psi = 90$, when $E > 1.675$. At $E = 1.675$, $F_o = F_1$. It should be noted, however, that $\tan \beta|^{e}_{max}$ and $\tan \beta|^{e}_{min}$ are approaching each other, meaning that the intensity distribution is very nearly circular. For this reason quite possibly, no great practical significance could be attached to this observation.

Comparison of these results with those accompanying Figures 10-15, shows that, except for symmetry, the changes in intensity distribution

brought about as a result of perturbations are similar to those brought about by changes in wind speed and therefore these two causes cannot be distinguished by measurements of intensity alone.

It has been assumed, of course, that the ocean surface is homogeneous under the "scan" in both cases. In other words, the ocean surface has been assumed to present the same statistical behavior over the entire scan area, which is much larger than the spot size. This, however, will rarely be the case. Local fluctuations will always be present. Changes of interest in the natural ocean surface due to internal wave, current, or other interactions would of necessity be inhomogeneous. While the technique will be insensitive, unreliable, or inapplicable to inhomogeneities smaller than a spot size, the variations on scanning over an inhomogeneity will be significant and interpretable given appropriate additional environmental data. With the development presented here, it is difficult to assess these effects quantitatively, lacking empirical data on the spatial and temporal variations in the ideal spectra assumed in this study.

The results of the parametric study can be summarized as follows. The effect of the perturbation on the intensity is most pronounced in the capillary region. The energy content of the perturbation required to see significant changes is on the same order as the energy content of the natural spectrum in the capillary region and insignificant compared to the total energy of the waves. The viscous cutoff does not have much effect on the intensity. The angular shape and the orientation of the perturbation affect mainly the symmetry of the intensity pattern with respect to the wind direction.

IV SUMMARY AND CONCLUSIONS

The theory of "speckle patterns" from diffusely scattered coherent light has been examined and extended to apply to scattering by the surface of the sea. We have determined that the surface characteristics can be related to the ensemble average power spectral density of the scattered radiation. However, since measurement of the latter quantity is difficult, it would be more practical to measure the ensemble average scattered intensity distribution. It turns out that the expression obtained for that distribution is similar to that for high frequency radar backscatter.

Assuming a natural power spectral density for the ocean surface elevation, the average scattered intensity distribution is determined solely by the slope statistics of the surface in the case of optical illumination. The detailed distribution was calculated and its behavior at different wind speeds was examined. We found that as the wind increases, the backscattered intensity is reduced and spread over larger angles. We also found that the downwind slopes increase only slightly faster than the crosswind slopes with measuring wind.

A reasonable parametrized form was assumed for the spectral shape of a perturbation, and a parametric study was performed. The effect of the perturbation on the intensity distribution is most pronounced in the capillary region. The energy content of the perturbation required to see significant changes is on the same order as the energy content of the natural spectrum in the capillary region, and is insignificant compared to the total energy of the waves. The viscous cutoff does not have much effect on the intensity. The angular shape and the orientation of the

perturbation affect mainly the symmetry of the intensity pattern with respect to the wind direction.

Appendix A

EVALUATION OF SOME INTEGRALS

1. Integration of the Angular Part of the Fourier Transform of $S(\ell,\phi)$

The Fourier transform of the power spectral density of surface elevation $S(\ell,\phi)$ gives the surface covariance function according to Eq. (2.58)

$$R(\underline{\Delta r}) = \int_{\text{plane}} S(\underline{\ell}) \exp(j\underline{\Delta r} \cdot \underline{\ell})\, d\underline{\ell} \quad . \tag{A.1}$$

Using Eq. (3.1), Eq. (2.58) becomes in polar coordinates

$$R(\Delta r,\theta) = \int_0^\infty \ell S(\ell) \left\{ \int_{-\pi}^{\pi} F(\ell,\phi) \exp[j\Delta r \ell \cos(\phi - \theta)]\, d\phi \right\} d\ell \quad . \tag{A.2}$$

If we use the definition

$$E(\ell) = \exp\left[-g^2/2\ell^2 U^4\right] \quad , \tag{A.3}$$

Eq. (3.2) may be written as

$$F(\ell,\phi) = \left(\frac{1}{6\pi}\right)\left(3+\left\{4\left[1-E(\ell)+3E(\ell)a_1\right]\right\}\cos 2\phi+[1-E(\ell)]\cos 4\phi\right) \quad . \tag{A.4}$$

It is known[17] that

$$J_m(x) = \frac{1}{\pi}\int_0^{\pi} \cos(m\phi - x \sin\phi)\, d\phi \qquad (m = 0,1,2,\ldots) \quad , \tag{A.5}$$

Pages 78-80 blank

From Eq. (A.5) it can be shown that

$$J_{2m} = \frac{2}{\pi} \int_0^{\pi/2} \cos 2m\phi \cos(x \sin \phi)\, d\phi \qquad (m = 0,1,2,\ldots) \quad . \quad (A.6)$$

By using the symmetry of the trigonometric functions involved, it can be shown that

$$\int_{-\pi}^{\pi} \cos 2m\phi \exp[j\ell\Delta r \cos(\phi - \theta)]\, d\phi = (-1)^m 4 \cos 2m\theta \times \int_0^{\pi/2} \cos 2m\phi \cos(\ell\Delta r \sin \phi)\, d\phi$$

$$= (-1)^m 2\pi \cos 2m\theta J_{2m}(\ell\Delta r) \quad . \quad (A.7)$$

Using Eq. (A.6), and substituting in the angular part of (A.2)

$$\int_{-\pi}^{\pi} F(\ell,\phi) \exp[j\Delta r\ell \cos(\phi - \theta)]\, d\phi = J_o(\ell\Delta r) - \frac{1}{3}\left\{4[1 - E(\ell)] + 3E(\ell)a_1\right\} \times J_2(\ell\Delta r) \cos 2\theta + \frac{1}{3}[1 - E(\ell)] \times J_4(\ell\Delta r) \cos 4\theta \quad . \quad (A.8)$$

Thus

$$R(\Delta r,\theta) = \int_0^\infty \ell S(\ell)\left(J_0 - \frac{4}{3}\cos 2\theta J_2 + \frac{1}{3}\cos 4\theta J_4\right) d\ell$$

$$+ \int_0^\infty \ell S(\ell)E(\ell)\left[\frac{1}{3}\left(4 - 3a_1\right)\cos 2\theta J_2 - \frac{1}{3}\cos 4\theta J_4\right] d\ell \quad . \quad (A.9)$$

2. Evaluation of the Spectral Moments

The $2n^{th}$ moment of the power spectral density $S(\ell,\phi)$ given by Eq. (3.16) may be rewritten as

$$M_{2n} = \int_0^\infty \ell^{2n+1} S(\ell)\left\{\int_{-\pi}^{\pi} F(\ell,\phi)\cos^{2n}(\theta - \phi)\, d\phi\right\} d\ell \quad . \quad (A.10)$$

Considering at first the integration over ϕ, we note that

$$\int_{-\pi}^{\pi} \cos 2m\phi \cos^{2n}(\theta - \phi)\, d\phi = \frac{(2n-1)!!\,n!\,2\pi}{2^n(n-m)!(n+m)!}\cos 2m\theta \quad (A.11)$$

$$\text{for } 0 \le m \le n$$

$$= 0 \quad \text{for } m > n \quad .$$

Substituting from Eq. (A.4) and using Eq. (3.18)

$$\int_{-\pi}^{\pi} F(\ell,\phi)\cos^{2n}(\theta-\phi)d\phi = \frac{(2n-1)!!}{2^n(n+2)!}\left\{\left[\frac{8}{3}n(n-1)\cos^4\theta + 8n\cos^2\theta + 2\right]\right.$$

$$+ nE(\ell)\left[a_1(n+2)(2\cos^2\theta - 1) + (n+3)\right.$$

$$\left.\left. - \frac{8}{3}(n-1)\cos^4\theta - 8\cos^2\theta\right]\right\}$$

$$\triangleq I_{1n} + I_{2n}E(\ell) \quad (A.12)$$

From Figure 6 we note that $E = \exp(-g^2/2\ell^2U^4)$ may be replaced by unity for $\ell > \ell_1$, even for the lowest wind speed (corresponding to $u_{*min} = 12$ cm/s). Thus, for $\ell > \ell_1$ Eq. (A.12) becomes

$$\int_{-\pi}^{\pi} F(\ell,\phi)\cos^{2n}(\theta - \phi)\,d\phi = \frac{(2n-1)!!}{2^n(n+1)!}\left[a_1 n\left(2\cos^2\theta - 1\right) + n + 1\right]$$

$$= I_{1n} + I_{2n} \quad \text{for } \ell > \ell_1 \quad . \qquad (A.13)$$

Using Eqs. (3.3), which define $S(\ell)$ over five separate regions, Eq. (A.10) may be written with the help of the approximation (A.13):

$$M_{2n} = I_{1n}\int_0^{\ell_1} S_1(\ell)\ell^{2n+1}\,d\ell + I_{2n}\int_0^{\ell_1} S_1(\ell)E(\ell)\ell^{2n+1}\,d\ell$$

$$\times\left(I_{1n} + I_{2n}\right)\left[\int_{\ell_1}^{\ell_2} S_2(\ell)\ell^{2n+1}\,d\ell + \int_{\ell_2}^{\ell_3} S_3(\ell)\ell^{2n+1}\,d\ell\right.$$

$$\left. + \int_{\ell_3}^{\ell_\nu} S_4(\ell)\ell^{2n+1}\,d\ell + \int_{\ell_\nu}^{\infty} S_5(\ell)\ell^{2n+1}\,d\ell\right] . \qquad (A.14)$$

These integrations over ℓ may all be performed in closed form for $n < 4$, except for the integral over $0 \le \ell \le \ell_1$ which has a series solution. However, the series converges very rapidly and the first few terms are sufficient. The integral over $\ell_\nu \le \ell < \infty$ evidently does not exist for values of $n = 4$ or higher. Thus only the moments up to the seventh are defined, and due to the symmetry of $R(\Delta r,\theta)$, only the even moments have nonzero values.

Adopting the notation

$$g_n = \int_0^{\ell_1} S_1(\ell)\ell^{2n+1}\, d\ell$$

$$h_n = \int_0^{\ell_1} S_1(\ell)E(\ell)\ell^{2n+1}\, d\ell$$

$$q_n = \int_{\ell_1}^{\ell_2} S_2(\ell)\ell^{2n+1}\, d\ell$$

$$r_n = \int_{\ell_2}^{\ell_3} S_3(\ell)\ell^{2n+1}\, d\ell \qquad \text{(A.15)}$$

$$s_n = \int_{\ell_3}^{\ell_\nu} S_4(\ell)\ell^{2n+1}\, d\ell$$

$$t_n = \int_{\ell_\nu}^{\infty} S_5(\ell)\ell^{2n+1}\, d\ell \quad .$$

we have

$$M_{2n} = I_{1n}g_n + I_{2n}h_n + \left(I_{1n} + I_{2n}\right)\left(q_n + r_n + s_n + t_n\right) \quad . \text{(A.16)}$$

Expressions for I_{1n}, $(I_{1n} + I_{2n})$, g_n, h_n, q_n, r_n, s_n, and t_n for $n = 0$, 1, 2, and 3 are presented in Table A-1. The following expressions for the first two moments are obtained from the table.

Table A-1

INTEGRALS APPEARING IN THE SPECTRAL MOMENTS

	n = 0	n = 1	n = 2	n = 3
I_{1n}	1	$\frac{1}{6}\left(4\cos^2\theta + 1\right)$	$\frac{1}{48}\left(8\cos^4\theta + 24\cos^2\theta + 3\right)$	$\frac{1}{32}\left(8\cos^4\theta + 12\cos^2\theta + 1\right)$
$\left(I_{1n} + I_{2n}\right)$	1	$\frac{1}{4}\left(2 + a_1\cos 2\theta\right)$	$\frac{1}{16}\left[6 + 4a_1\cos 2\theta + a_2\cos 4\theta\right]$	$\frac{1}{64}\left[20 + 15a_1\cos 2\theta + 6a_2\cos 4\theta + a_3\cos 6\theta\right]$
b_n	$aU^{-1}\sqrt{4g^2\hat{z}}$	$-\frac{a}{3}X_1$	$-\frac{a}{4}\ell_2^2\left(\frac{u_{*m}}{u_*}\right)^4\left[1 - b_1X_1\right]$	$-\frac{a}{8}\ell_2^4\left(\frac{u_{*m}}{u_*}\right)^8\left[1 - b_1 + b_1^2X_1\right]$
f_n	$aU^{-4}\sqrt{4g^2\left(\hat{z} + \frac{1}{2}\right)}$	$-\frac{a}{4}X_2$	$-\frac{a}{4}\ell_2^2\left(\frac{u_{*m}}{u_*}\right)^4\left[1 - b_2X_2\right]$	$-\frac{a\ell_2^4}{8}\left(\frac{u_{*m}}{u_*}\right)^8\left[1 - b_2 + b_2^2X_2\right]$
c_n	$\frac{a}{3\ell_2^2}\left(\frac{u_*}{u_{*m}}\right)\left[\left(\frac{u_*}{u_{*m}}\right)^3 - 1\right]$	$a\left[\frac{u_*}{u_{*m}} - 1\right]$	$\frac{a\ell_2^2}{5}\left[\left(\frac{u_*}{u_{*m}}\right) - \left(\frac{u_{*m}}{u_*}\right)^4\right]$	$\frac{a\ell_2^4}{9}\left[\left(\frac{u_*}{u_{*m}}\right) - \left(\frac{u_{*m}}{u_*}\right)^8\right]$
s_n	$\frac{aD}{2\ell_3^p(p-2)}\left(\ell_3^{p-2} - \ell_2^{p-2}\right)$	$\frac{aD}{2\ell_3^p p}\left(\ell_3^p - \ell_2^2\right)$	$\frac{aD}{2\ell_3^p(p+2)}\left(\ell_3^{p+2} - \ell_2^{p+2}\right)$	$\frac{aD}{2\ell_3^p(p+4)}\left(\ell_3^{p+4} - \ell_2^{p+4}\right)$
t_n	$\frac{aD}{4}\left[\frac{1}{\ell_3^2} - \frac{1}{\ell_2^2}\right]$	$\frac{aD}{2}\ln\left(\ell_2/\ell_3\right)$	$\frac{aD}{4}\left(\ell_2^2 - \ell_3^2\right)$	$\frac{aD}{8}\left(\ell_2^4 - \ell_3^4\right)$
u_n	$\frac{aD}{16}\frac{1}{\ell^2}$	$\frac{aD}{12}$	$\frac{aD}{8}\ell^2$	$\frac{aD}{4}\ell^4$

$$X_1 = \gamma + \log b_1 + \sum_1^{\infty}\frac{\left(-b_1\right)^r}{r\cdot r!} \qquad b_1 = \left(\hat{z}g^2/\ell_1^2U^4\right)$$

$$X_2 = \gamma + \log b_2 + \sum_1^{\infty}\frac{\left(-b_2\right)^r}{r\cdot r!} \qquad b_2 = \left[\left(\hat{z} + \frac{1}{2}\right)g^2/\ell_1^2U^4\right]$$

γ = Eulers constant
= 0.57722

$$M_o = \frac{a}{4}\frac{U^4}{\beta g^2} - \frac{a}{3\ell_2^2}\left(\frac{u_*}{u_{*m}}\right)\left[1 - \left(\frac{u_*}{u_{*m}}\right)^3\right] + \frac{aD}{2(p-2)\ell_3^2}\left[1 - \left(\frac{\ell_3}{\ell_2}\right)^{2-p}\right]$$

$$- \frac{aD}{4\ell_\nu^2}\left[1 - \left(\frac{\ell_\nu}{\ell_3}\right)^2\right] + \frac{aD}{16}\frac{1}{\ell_\nu^2} \qquad \text{(A.17)}$$

and

$$M_2 = \cos^2\theta\left(-\frac{a}{6}\left(X_1 + X_2\right) + \frac{aa_1}{2}\left\{-\frac{X_2}{4} + \frac{u_*}{u_{*m}}\left(1 - \frac{u_{*m}}{u_*}\right)\right.\right.$$

$$\left.\left. + \frac{D}{2p}\left[1 - \left(\ell_2/\ell_3\right)^p\right] + \frac{D}{2}\ln\frac{\ell_\nu}{\ell_3} + \frac{D}{12}\right\}\right)$$

$$+ \left(-\frac{a}{24}\left(X_1 + X_2\right) + \frac{a}{2}\left(1 - \frac{a_1}{2}\right)\right.$$

$$\left.\times\left\{\frac{-X_2}{4}\frac{u_*}{u_{*m}}\left(1 - \frac{u_{*m}}{u_*}\right) + \frac{D}{2p}\left[1 - \left(\ell_2/\ell_3\right)^p\right] + \frac{D}{2}\ln\frac{\ell_\nu}{\ell_3} + \frac{D}{12}\right\}\right) \qquad \text{(A.18)}$$

where

$$X_i = \gamma + \ln b_i + \sum_1^\infty \left(b_i\right)^r/r \cdot r! \quad , \qquad \text{(A.19)}$$

$$b_1 = \left(\beta g^2/\ell_1^2 U^4\right) \quad , \qquad \text{(A.20)}$$

and

$$b_2 = \left[\left(\beta + \frac{1}{2}\right)g^2/\ell_1^2 U^4\right] \quad . \qquad \text{(A.21)}$$

On examination of the terms in Eq. (A.18) it is evident that, if a_1 is independent of ℓ as we have assumed, the terms are functions only of wind speed or u_*. Therefore, we rewrite Eq. (A.19) as

$$M_2 = F_o\left(u_*\right)\cos^2\theta + G_o \quad . \qquad \text{(A.22)}$$

3. The Second Moment of $S'(\ell,\phi)$

The second moment of the power spectral density of the perturbation is

$$M_2 = \int_0^\infty \ell^3 S'(\ell)\, d\ell \cdot \int_{-\pi}^{\pi} F'(\phi) \cos^2(\theta - \phi)\, d\phi \quad . \qquad (A.23)$$

Using Eqs. (3.37) and (A.11), we get

$$\int_{-\pi}^{\pi} F'(\phi) \cos^2(\phi - \theta)\, d\phi = \frac{a_1' \cos 2\psi}{2} \cos^2\theta + 2\,\frac{a_1' \sin 2\psi}{4} \sin\theta \cos\theta$$

$$+ \left(\frac{1}{2} - \frac{a_1'}{4}\right) \cos 2\psi \quad . \qquad (A.24)$$

Using Table A.1, we get

$$\int_0^\infty \ell^3 S'(\ell)\, d\ell = \frac{EGAD}{2}\left\{\frac{1}{6} - \frac{1}{2}\exp X\left[\gamma + \ln X + \sum_1^\infty \frac{(-X)^r}{r \cdot r!}\right]\right\}$$

$$\triangleq I'\left(\ell_{max}, \ell_\nu', E\right) \qquad (A.25)$$

where

$$X = (3/2)\left(\ell_{max}/\ell_\nu'\right)^2 \quad . \qquad (A.26)$$

Therefore

$$M_2 = \frac{I' a_1' \cos 2\psi}{2} \cos^2\theta + 2\,\frac{I' a_1' \sin 2\psi}{4} \sin\theta \cos\theta + I'\left(\frac{1}{2} - \frac{a_1'}{4}\right) \cos 2\psi$$

$$\triangleq F_1 \cos^2\theta + 2H_1 \sin\theta \cos\theta + G_1 \quad . \qquad (A.27)$$

It is noted that F_1, G_1, and H_1 are functions of ℓ_{max}, ℓ_ν', E, a_1', and ψ.

Appendix B

REPRESENTATION OF THE ENSEMBLE AVERAGE SPATIAL COHERENCE FUNCTION

The ensemble average spatial coherence function is given by Eq. (2.30) as

$$\langle \gamma(\Delta u,\Delta v)\rangle = \exp\left[-j\,\frac{k}{R}\left(\Delta u x_o + \Delta v y_o\right)\right] \times \exp\left\{-k^2(\cos\beta + \cos B)^2[R(0,0) - R(\Delta u,\Delta v)]\right\} \quad . \quad (B.1)$$

Consider the exponent of the second exponential factor; k is the wave vector of the optical radiation. For 10.6 μm radiation k^2 has a value of 3.5×10^7. Even for angles β and B as large as 60° [when the approximations made in the derivation of Eq. (2.35) are no longer valid] the cosine factor is on the order of unity. Hence the exponential has appreciable value only for very small values of [R(0,0) - R(Δu,Δv)]. Conversely, if ε is an arbitrarily small number,

$$\exp\left\{-k^2[R(0,0) - R(\Delta u,\Delta v)]\right\} < \varepsilon \quad (B.2)$$

when

$$R(0,0) - R(\Delta u,\Delta v) > -\left(\ln \varepsilon/k^2\right) \quad . \quad (B.3)$$

Pages 89-90 blank

1. Behavior of $\langle \gamma(\Delta u, \Delta v) \rangle$ Near the Origin

Using Eq. (2.61), the condition (B.3) becomes, near $\Delta r = 0$,

$$\frac{1}{2} M_2 \Delta r^2 - \frac{1}{24} M_4 \Delta r^4 + \ldots > -\left(\ln \epsilon / k^2\right) \quad . \tag{B.4}$$

If we neglect for the moment terms in Δr of order higher than 2,

$$\Delta r > \left(-2 \ln \epsilon / M_2 k^2\right)^{1/2} \quad . \tag{B.5}$$

If we choose the smallest value for M_2 (see Figure 9), which will be the value of G_o ($\theta = 90°$) for $u_* = 12$ cm/s, and if we choose $\epsilon = 10^{-99}$,

$$\Delta r_o > 0.027 \text{ cm} \quad .$$

As discussed in Section II-C, at this small separation the contribution of the additional terms in (B.4) are negligible, which justifies disregarding those terms in this discussion and in the expression for $[R(0,0) - R(\Delta u, \Delta v)]$.

Thus the spatial coherence function $\langle \gamma(\Delta u, \Delta v) \rangle$ is a very narrow sharply peaked function near the origin and may be represented accurately for small Δr by

$$\langle \gamma(\Delta u, \Delta v) \rangle = \exp\left[-j \frac{k}{R} \left(\Delta u x_o + \Delta v y_o\right)\right]$$

$$\times \exp\left[-k^2 (\cos\theta + \cos\theta')^2 \frac{1}{2} M_2 \Delta r^2\right] \quad \text{for } \Delta r < 0.02 \text{ cm} \quad . \tag{B.6}$$

2. Behavior of $\langle Y(\Delta u,\Delta v)\rangle$ for $\Delta r_o \leq \Delta r < \infty$

We recall the integral expression for $R(\Delta r,\theta)$ given by Eq. (A.9). Since $E(\ell) \leq 1$ for all ℓ, by combining the two terms in Eq. (A.9) we may write

$$R(\Delta r,\theta) \leq \int_o^\infty \ell S(\ell)\left[J_o - a_1 \cos 2\theta \cdot J_2\right] d\ell \quad . \qquad (B.7)$$

The value of a_1 measured by different investigators varies between 0 and 0.5. The variation of cos θ is between +1 and -1. Therefore $(J_o + J_1)$ and $(J_o - J_1)$ bound the variations of $[J_o - a_1 \cos 2\theta \cdot J_2]$. The values of $[J_o(\ell\Delta r) \pm J_1(\ell\Delta r)]$ are plotted as a function of $\ell\Delta r$ in Figure B-1. It is seen that the maximum positive excursions occur for $J_o - J_2$ for $\ell\Delta r$ = 0, 6.9, 13.3, and so on. Further, the maxima at other than $\ell\Delta r$ = 0 do not attain a value greater than 0.6.

These observations mean the following in interpreting Eq. (B.7). At Δr = 0, the integrand is essentially $\ell S(\ell)$, since $(J_o \pm J_2)$ is unity for all values of ℓ. Thus $R(\Delta u,\Delta v)$ has the maximum value at the origin. As Δr increases, the oscillations in $(J_o \pm J_2)$ become important and influence the value of the integral. From Figure 4 it is seen that $S(\ell)$ is positive for all values of ℓ and has a fairly sharp maximum. As Δr increases from zero, the product $\ell S(\ell)(J_o \pm J_2)$ decreases.

It is intuitively clear that the integral will have a minimum (negative) value when the first minimum of $(J_o \pm J_2)$ approximately coincides with the maximum of the function $\ell S(\ell)$. The minimum occurs at $(\ell\Delta r)$ = 3.5 for $(J_o - J_2)$ and at $(\ell\Delta r)$ = 5.2 for $(J_o + J_2)$. If the maximum of $\ell S(\ell)$ occurs at ℓ_{max}, then the minimum values of the integral occur (for a_1 = 1) at $\Delta r_{min\ 1} = (3.5/\ell_{max})$ and $(5.2/\ell_{max})$--for the directions θ = 0 and $\pi/2$ respectively. Similarly, the integral has a maximum value of $\Delta r_{max\ 2} = (6.9/\ell_{max})$ and $(8.5/\ell_{max})$. For instance, for $u_* = 24$ cm/s,

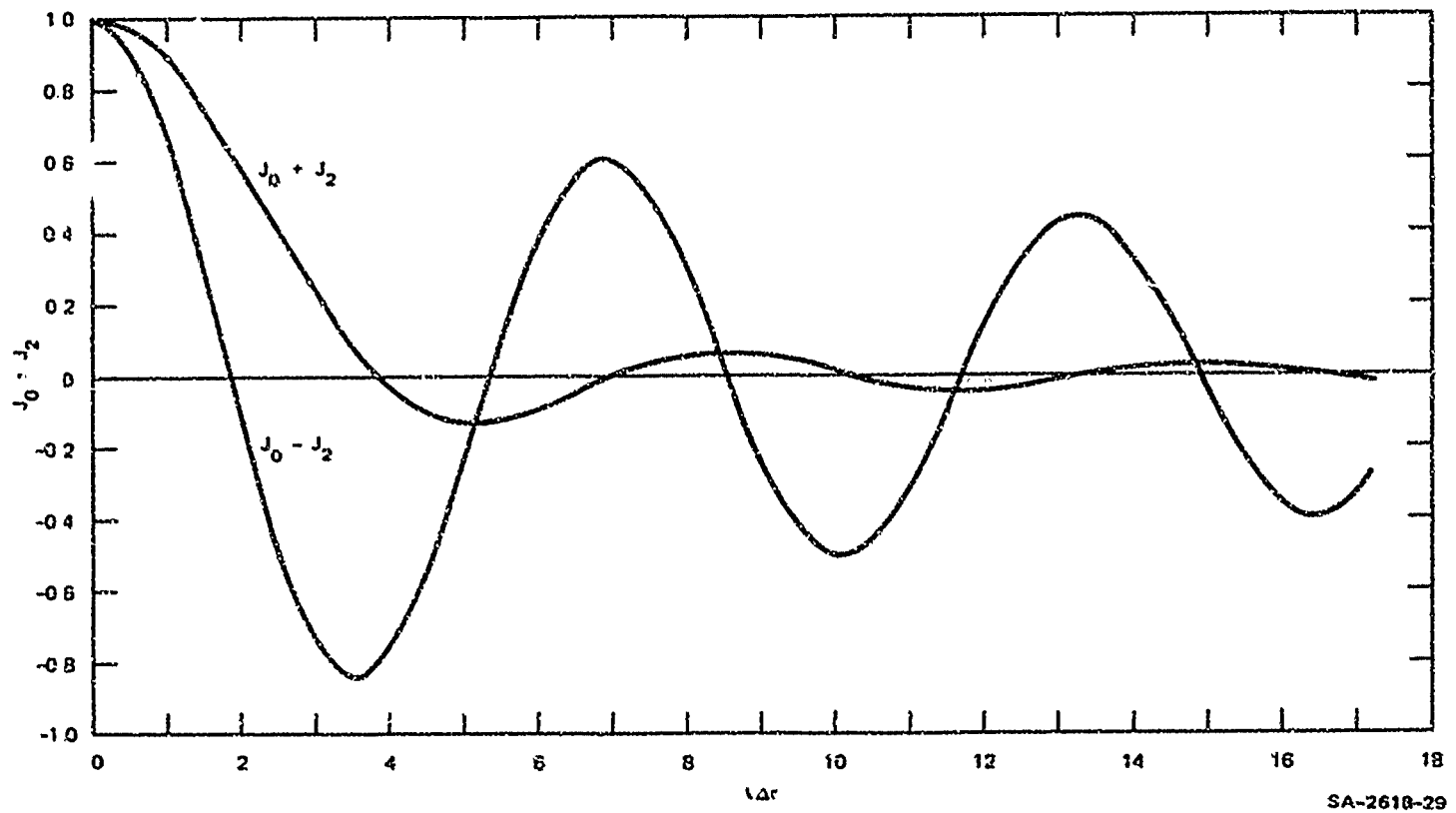

FIGURE B-1 THE FUNCTIONS $[J_0(\ell\Delta r) + J_2(\ell\Delta r)]$ AND $[J_0(\ell\Delta r) - J_2(\ell\Delta r)]$

$\xi S(\xi)$ has a maximum at $\xi = 0.0012$ cm^{-1}. Thus in the direction $\theta = 0$, the first maximum of $R(\Delta r,\theta)$ occurs at approximately 57.5 meters. Noting that the peak value of $(J_o - J_2)$ at 6.9 is 0.6, it is surmised that the value of the integral will be less than 0.6 R(0,0), and condition (B.3) is amply satisfied.

The conclusion to be made from the above discussion is that $R(\Delta u,\Delta v)$ is a function that smoothly decreases away from $\Delta r = 0$, where it has an absolute maximum, and whose further maxima are significantly less than its value at the origin. This implies that

$$\exp\left|-k^2[R(0,0) - R(\Delta u,\Delta v)]\right| < 10^{-99}$$

(or less than any other arbitrarily small value we wish to impose) over the entire $(\Delta u,\Delta v)$ plane except near the origin, where it may be approximated by Eq. (B.6).

Since Eq. (B.6) also becomes arbitrarily small over the rest of the $(\Delta u,\Delta v)$ plane, we may extend the validity of Eq. (B.6) over the entire plane. Therefore, when k is large, we may write

$$\langle \gamma(\Delta u,\Delta v)\rangle = \exp\left[-j\,\frac{k}{R}\left(\Delta u x_o + \Delta v y_o\right)\right] \times \exp\left[\left(k^2/2\right)(\cos\beta + \cos B)^2 M_2 \Delta r^2\right] \quad . \quad \text{(B.8)}$$

Similar arguments may be made in the case of the spatial coherence function of the perturbed ocean surface.

REFERENCES

1. Willard J. Pierson, Jr. and Robert A. Stacy, "The Elevation, Slope, and Curvature Spectra of a Wind Roughened Sea," Contribution No. 132, Geophysical Sciences Laboratory, Department of Meteorology and Oceanography, New York University (June 1972).

2. J. D. Rigden and E. I. Gordon, "The Granularity of Scattered Optical Maser Light," Proc. IEEE, Vol. 50, p. 2367 (1962).

3. B. M. Oliver, "Sparkling Spots and Random Diffraction," Proc. IEEE, Vol. 51, p. 220 (1963).

4. J. W. Goodman, "Statistical Properties of Laser Sparkle Patterns," Stanford Electronics Laboratory Report, Stanford, California (December 1963).

5. L. I. Goldfischer, "Autocorrelation Function and Power Spectral Density of Laser-Produced Speckle Patterns, J. Opt. Soc. Am., Vol. 55, p. 247 (1965).

6. J. W. Goodman, "Some Effects of Target-Induced Scintillation on Optical Radar Performance," Proc. IEEE, Vol. 53, p. 1688 (1965).

7. S. Lowenthal and A. A. Arsenault, "Image Formation for Coherent Diffuse Objects: Statistical Properties." J. Opt. Soc. Am., Vol. 60, p. 1478 (1970).

8. R. B. Crane, "Use of a Laser-Produced Speckle Pattern to Determine Surface Roughness," J. Opt. Soc. Am., Vol. 60, p. 1658 (1970).

9. H. H. Arsenault, "Roughness Determination with Laser Speckle," J. Opt. Soc. Am., Vol. 61, p. 1425 (1971).

10. J. W. Goodman, "Comparison of Various Theories Concerning Laser Speckle." Appendix B in Ref. 11. A summary of this appendix is expected to be submitted for publication in the Journal of the Optical Society of America (1973).

11. P. Beckmann and A. Spizzichino, The Scattering of Electro-Magnetic Waves from Rough Surfaces (The Macmillan Company, New York, New York, 1963).

12. B. Kinsman, Wind Waves (Prentice-Hall Inc., Englewood Cliffs, New Jersey, 1965).

13. John H. Mackay, "On the Gaussian Nature of Ocean Waves," Internal Technical Note No. 8, Engineering Experiment Station, Georgia Institute of Technology, Atlanta, Georgia (1959).

14. K. S. Krishnan and N. A. Peppers, "Remote Techniques for Capillary Wave Measurement," Technical Report, Stanford Research Institute, Menlo Park, California, AD 762 453 (1973).

15. R. T. Frost and F. C. Jackson, "Measurement of Ocean Surface Parameters by Means of Scattered Electromagnetic Radiation," Space Sciences Laboratory Report, General Electric Company, Valley Forge, Pennsylvania (June 1972).

16. J. V. Evans and T. Hagfors, Radar Astronomy (McGraw-Hill Book Company, Inc., New York, New York, 1968).

17. R. V. Churchill, Fourier Series and Boundary Value Problems (McGraw-Hill Book Company, Inc., New York, New York, 1941).